



Hydrogen-related defects in crystalline semiconductors: a theorist's perspective

Stefan K. Estreicher

Physics Department, Texas Tech University, Lubbock, TX 79409, USA

Received 17 November 1994; accepted in final form 5 January 1995

Abstract

Hydrogen is a common impurity in all semiconductors. Although it is sometimes deliberately introduced, hydrogen often penetrates into the crystal during device processing. It interacts with broken or weak covalent bonds, such as those found at extended and localized defect centers. The main results of these covalent interactions are shifts of energy levels out of (or into) the gap and new optical activity (infrared absorption and Raman scattering). The shifts in energy levels lead to the passivation (or activation) of the electrical activity of various centers. Hydrogen can also interact with the perfect crystal and with itself, sometimes leading to the formation of extended structures known as platelets. Finally, H also acts as a catalyst, dramatically enhancing the diffusivity of interstitial oxygen in Si. The consequences of these interactions are substantial changes in the electrical and optical properties of the crystal, and in the lifetime of charge carriers. The thermal stability of the complexes containing hydrogen varies from room temperature up to several hundreds of degrees Celsius, and the diffusion of H is trap-limited up to rather high temperatures. Hydrogen normally exists in more than one configuration and charge state in semiconductors. A range of experimental and theoretical techniques have been used to investigate the rich properties of hydrogen in semiconductors, and several extensive reviews focusing mostly on the experimental side of these issues have been published in the past five years. The present review focuses mostly on the theoretical work performed in this field. However, the most recent experimental results are also discussed, and the current understanding of hydrogen interactions in semiconductors summarized.

Keywords: Defects; Hydrogen; Semiconductors

1. Introduction

Everything has already been said. However, since no one listens, it is necessary to begin again.

A. Gide

1.1. Scope of this review

Hydrogen is a very common impurity in all semiconductors. It can be incorporated during the growth of the crystal but, more importantly, it is present at virtually every stage of the processing of devices. This makes it an unavoidable impurity even in devices fabricated with the most perfect single crystals. Indeed, H is found in the chemicals used for wet etching, solvent cleaning, and in organic masks, as an OH species in oxides, in water vapor in vacuum systems, and so on. Hydrogen may also be deliberately introduced. For example, hydrogenation is sometimes performed as the last step of polycrystalline-silicon solar-cell processing. This boosts the performance of these cells by a substantial amount.

At high temperatures, hydrogen diffuses readily through most semiconductors. At low temperatures, it is attracted to any strained region of the crystal where it traps, often

binding to an imperfect host atom bond. Hydrogen can also self-trap, for example by bridging a covalent bond, forming largely immobile molecules, or precipitating into aggregates that extend over hundreds of ångströms.

Strained regions of the crystal occur at lattice defects (localized or extended) as well as at any impurity, interstitial or substitutional, including deliberately introduced dopants (Figs. 1 and 2 indicate interstitial sites; see Appendix). The result is the formation of complexes containing hydrogen, which have very different electrical and optical properties than the original defect center. Hydrogen allows strained bonds to relax toward a less-strained configuration. This shifts the energy levels, often removing them from the forbidden gap (passivation), occasionally introducing new levels into the gap (activation), or otherwise altering the electrical activity of the unhydrogenated center. Further, a variety of infrared (IR)- (or Raman-) active hydrogen-related vibrational modes appear following hydrogenation. They correspond to various stretch and wag modes of hydrogen. But hydrogen does more than interact in an essentially static manner with strained regions of the crystal. At least in Si it also enhances the diffusivity of interstitial oxygen, leading to the formation of thermal donors at temperatures much lower than can be achieved without the presence of hydrogen. Further, some hydrogenation techniques lead to the formation near the surface of extended structures known as platelets, able to trap enormous amounts of hydrogen. A number of reviews of these properties have been published in the past few years [1–5].

The interactions involving hydrogen are very diverse and often affect the properties of a semiconductor in a macroscopic way. For example, nearly 100% of boron dopants are easily passivated in Si around room temperature, leading to an increase in the resistivity of the sample by several orders of magnitude. Annealing above 200 °C restores the sample to its pre-hydrogenation state. Because H is such a common impurity and affects devices in so many ways, various aspects of its interactions have been studied for over a dozen

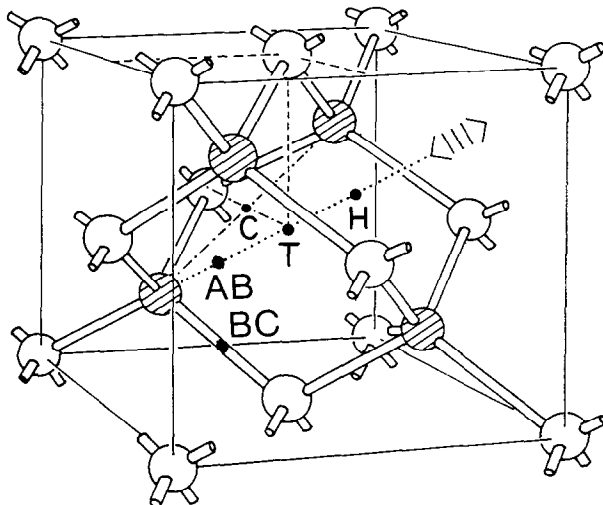


Fig. 1. Most important interstitial sites in the diamond or zinc-blende lattices. Along the $\langle 111 \rangle$ axis are the antibonding (AB), tetrahedral interstitial (T), and hexagonal (H) sites. In compounds, a subscript refers to the nearest neighbors (NNs) to a particular site. In elemental semiconductors, no subscripts are needed. The bond-centered (BC) site is at (or near) the center of a covalent bond. Some interstitials form puckered bonds, which we also refer to as BC sites. Note that an impurity is stable at the BC site only after a substantial relaxation of the bond. Two interstitial sites which are not on a $\langle 111 \rangle$ axis are the C site, at the center of the rhombus formed by three adjacent host atoms and the T site, and the M site (not shown), midway between two adjacent C sites.

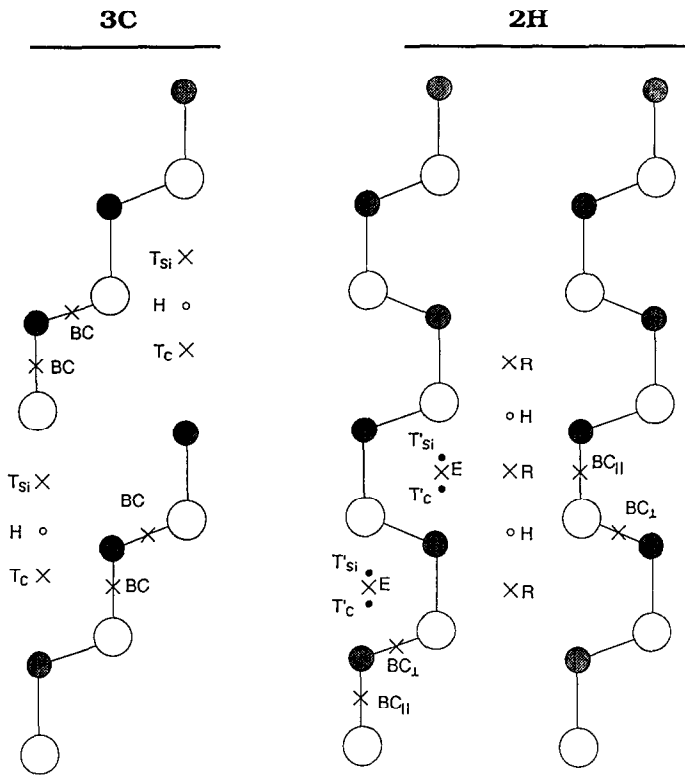


Fig. 2. Comparison of the interstitial sites in the $\{110\}$ plane for the zinc-blende and wurtzite structures. The example used is that of the 3C (zinc-blende) and 2H (wurtzite) polytypes of SiC. Except for the use of subscripts to denote the NN atom(s) to a given site, the notation is the same as in Fig. 1. In the wurtzite structure, the angle between any atom and two of its NNs is not exactly the tetrahedral angle. Further, there are two inequivalent BC sites, one along the stacking direction (BC_{II}) and one approximately perpendicular to it (BC_1). Finally, there are two additional interstitial sites, labeled R and E.

years. Note that it has been known for much longer that hydrogen ties up dangling bonds, for example at vacancies, dislocations, or grain boundaries, which improves the electronic properties of the material. This originated the use of hydrogenated amorphous silicon [6]. However, the role of hydrogen in other interactions was not immediately recognized. The first observation of H altering the electrical activity of an impurity in a crystalline semiconductor occurred in 1974, with the activation of the normally inactive substitutional Si in high-purity Ge [7–9]. However, it is the report of the passivation of the shallow boron acceptor in Si in 1983 [10–13] that really set a large number of experimentalists and theorists into motion. Several thousand papers later, many interactions involving hydrogen have been observed and a number of them are now at least qualitatively understood.

Many experimental and theoretical techniques have been a part of the brief history of hydrogen in crystalline semiconductors. The most important experimental tools include IR and Raman spectroscopy, secondary-ion mass spectrometry (SIMS), deep-level transient spectroscopy (DLTS) and other capacitance measurements, transmission electron microscopy (TEM), channeling, spreading resistance profiling, electron paramagnetic resonance (EPR), electron nuclear double beam resonance (ENDOR), etc. A very important tool which uses positive muons rather than protons, muon spin rotation (μ SR), provides critical information on isolated hydrogen in almost all crystalline semiconductors. In a few cases, similar experiments involving hydrogen and muons have been performed, and the results match

very closely. It is now accepted that muon spectroscopy does provide important clues on the behavior of isolated hydrogen in many hosts. However, because its mass is only about one-ninth that of a proton, the muon has a large zero-point energy and experiences smaller activation energies. Its diffusion properties are therefore different. Further, the lifetime of the muon is of the order of two microseconds, and μ SR allows the observation of metastable states but not necessarily of equilibrium configurations.

Theoretical interest in hydrogen in semiconductors arose from the unexpected results from early muon spin rotation studies [14]. Among other unexpected features, these data showed that, in Si, the Fermi contact density at the muon, $|\Psi(0)|^2$, is about half the free atomic value. This shows a 1s-type wavefunction that is delocalized when compared with free atomic H, but localized when compared with the hydrogenic wavefunctions of shallow impurities. As is discussed in Ref. [15], the effective Bohr radius predicted by effective mass theory for this species is 1.8 \AA_B as compared, for example, with 18 \AA_B for the P acceptor in Si. This suggested that interstitial H is a deep donor in Si. Modifications to effective mass theory needed to understand the early μ SR data were first discussed by Wang and Kittel [16].

The first total energy calculations dealing with H in a finite molecular cluster, performed in 1978, were based on extended Hückel theory (EHT) [17,18]. These highly parameterized calculations predicted that, when no dangling bonds are present, interstitial H goes off the tetrahedral site along a $\langle 111 \rangle$ direction to an anti-bonding (AB) site. Since then, a number of semiempirical Hartree–Fock (HF) techniques have been used to address a variety of H-related issues in diamond and silicon. More recently, approximate ab-initio and ab-initio HF techniques have been employed, sometimes followed by post-HF treatments which include the effects of electron correlation. Important contributions of density-functional (DF) theory to this area began in 1988, complemented by a few molecular dynamics (MD) simulations. As algorithms and software become more sophisticated, computers faster (and cheaper), large memories more affordable, and disk space abundant, some of the uncertainties associated with the use of small clusters or cells to mimic the host crystal are being removed. Many authors now use more complete basis sets and larger clusters or cells. As a result, the calculations are more accurate today than just a few years ago. Undoubtedly, some of today's questions will be answered by more refined calculations and by the new experiments they will suggest.

Until a few years ago, the key questions regarding H in semiconductors dealt with the nature of the complexes involving hydrogen. When it became clear that, for example, shallow impurity passivation is due to the formation of a covalent bond rather than to direct compensation, the equilibrium geometries, electronic structures, and vibrational modes of hydrogen–shallow dopant pairs were calculated. Predictions of reorientation kinetics and metastability were made. Today, the basic features of many small hydrogen–impurity complexes are understood, especially in Si and GaAs. These include H-acceptor and H-donor pairs, H-vacancy complexes, or H interacting with isoelectronic impurities such as C in Si. Information is also being published on complexes involving H and some transition metal (TM) impurities. Theoretical and experimental studies are also beginning to address issues related to more extended complexes. However, puzzling fundamental questions remain in a number of areas. In random order, let me mention the following.

First, the difficult issue of the *diffusion* of hydrogen has yet to be resolved to everyone's satisfaction. It is apparent that interstitial hydrogen in semiconductors generally can be found at two sites and in three charge states (H^+ , H^0 , and H^-), with only H^0 being

metastable (two configurations coexist in the same charge state). The various states have different diffusion paths and/or activation energies. Further, the abundance and stability of each species vary with the Fermi level, the temperature, and perhaps specific properties of a sample. In addition, the vacancy–hydrogen pair in Si has been predicted to also be mobile at moderate temperatures. As a result, the observed diffusivity of hydrogen varies greatly from one sample to the other, and from one experimentalist to the other.

Second, experimental observations dealing with the *reactivation* of H-passivated donors in Si and in GaAs are not fully understood. Reports of the partial reversibility of the passivation/reactivation reactions suggest that the complexes formed may be bistable (different charge states exist with different geometrical configurations). The neutral complex is electrically inactive, but the charged (+1) complex would be a donor.

Third, new experimental information is being published on the interactions between hydrogen and selected *TM impurities* such as Pt in silicon. Little is known about H-TM complexes. Theory lags behind experiment in this area.

Fourth, except for hydrogen dimers (H_2^T and H_2^*), little is known about complexes involving more than one hydrogen. Some evidence of *multiple trapping* of H at dopants exists. Further, the nature of hydrogen platelets is not known, and we are at the very early stages of the understanding of their nucleation mechanisms. These disk-shaped structures appear in the sub-surface region of plasma-exposed Si samples and extend over hundreds of angströms. The platelets trap most of the H trying to penetrate into the bulk, and are tremendous gettering centers. They are therefore of great practical interest.

Fifth, there is abundant experimental evidence that atomic hydrogen substantially *enhances the diffusivity* of interstitial oxygen (O_i) in Si. The evidence, however, is not microscopic, and little is known experimentally about the details of the interactions taking place. Two theoretical models exist, both suggesting a mechanism for a single hop of O_i , assuming that H is nearby. However, the experimental features reported are far from being explained. Interestingly enough, this hydrogen-related question touches a very long-standing problem, that of oxygen-related thermal donors in Si (see, for example, Refs. [19–21]).

Sixth and finally, the amount of knowledge (experimental and theoretical) gathered in the case of crystalline Si far exceeds that in any other semiconductor, with the possible exception of GaAs. Hydrogen interactions appear to be far simpler in some hosts (diamond) than in others (Si), but there is too little information about most other semiconductors to assume that we are even aware of unusual properties of H in less-commonly used hosts. For example, μ SR experiments in copper halides show that a behavior of hydrogen qualitatively distinct from that observed in Si or GaAs is to be expected. In particular, neutral muonium is metastable at the same interstitial site (T_{Cu}).

The present review focuses on the theoretical work done, the μ SR results, the experimental data obtained since the last reviews, and discusses the current understanding of the behavior of hydrogen in elemental and compound semiconductors. Although I will make every effort to present other authors' views, the tone of this review will unavoidably be affected by my understanding. My perspective has evolved over the years, sometimes changed in the light of new experimental information or of calculations performed by other theorists, in particular in those areas where existing models predict conflicting properties, do not fully explain the available data, or where predictions have not yet been confirmed by experiment. My aim is not to repeat and discuss at length the results already reviewed elsewhere. Instead, I will use the most recent experimental and theoretical results to paint as broad a picture as possible, and emphasize those areas which are controversial.

The various parts of this review are shown in the Contents. The present introductory section continues with some details of the theoretical techniques applied to the study of hydrogen in semiconductors. It also contains an overview of the μ SR techniques and of the μ SR centers that are observed. The actual μ SR results are in Section 2 which discusses isolated H and H pairs. Section 3 contains the description of the interactions between H and impurities and defects. Section 4 concludes with some comments, personal remarks, and a short list of 'hot' issues.

1.2. Theoretical techniques

Theory has played a key role in the understanding of hydrogen-containing defects in semiconductors (see Ref. [22] and the theory sections in Refs. [2,3,5]). Theoretical studies are crucial because experiment gives only part of the information needed to understand the properties of a defect. In the more favorable situations, IR spectroscopy provides the identity of the species involved in a complex, some vibrational modes, the symmetry of the defect, and its thermal stability. This is the case for many hydrogen–shallow dopant complexes. If the defect has a non-zero spin and exists in high enough concentrations, techniques such as EPR can also provide a wealth of microscopic information. More often, however, experiment provides only indirect information. For example, the dramatic increase by atomic H of the diffusivity of O_i in silicon around 350 °C has been suggested, not because of any direct information on H–O_i interactions but because an increase in the formation rate of O-related thermal donors was observed. The current understanding of this phenomenon is incomplete and relies mostly on theoretical descriptions.

Nowadays, most calculations are performed at or near the ab-initio or first-principles levels, which essentially means that none of the parameters used are adjusted to experimental data (more precise definitions are given below). However, many approximations remain, both in the way the host crystal is approximated and in the way the Schrödinger equation is solved. The quality of the calculations is continuously improving. This is owing in part to the availability of powerful workstations, in part to advances in software packages, and in part to theoretical developments. However, as will be detailed below, uncertainties remain regarding the size of the clusters or supercells used, the basis sets, and other ingredients of the calculations.

The aim of theory is to link all the experimental observations, provide as complete a picture as possible and, of course, make reliable and verifiable prediction(s) about as yet unobserved features. The calculated quantities include the equilibrium geometries at the various minima of the potential energy surface, the electronic structures, the spin and charge densities, the diffusion paths and activation energies, the IR- or Raman-active vibrational modes, and in some cases, the dynamic behavior at various temperatures. Not all quantities are predicted with the same accuracy. In particular, the positions of energy levels in the gap are only obtained qualitatively at best. A precise determination of defect energy levels requires the knowledge of the excited states (conduction band (CB)) of the system. Only some excited states (those that have a different symmetry from the ground state) can in principle be calculated at the DF level, and post-HF calculations which include many-electron excitations are only feasible for small molecules. There are far too many such excitations to render the problem computationally tractable.

However, while some quantities are not reliably predicted by theory, a lot of useful information is available and reliable. For example, the equilibrium geometry of a defect is

often accurately predicted by both HF- and DF-based techniques, with only small disagreements between the various techniques. DF calculations tend to predict accurate charge and spin densities, and the calculated vibrational frequencies are increasingly closer to the measured ones. HF calculations also provide a lot of chemical information (such as the covalent overlap or the population in a specific orbital), which is not always quantitative, but helps develop a deeper understanding of the interactions taking place.

The level of accuracy varies with the species involved in the defect, their charge and spin state, the technique used, the way the host crystal is approximated, and many technical details of the calculations. For example, DF calculations using plane-wave basis sets have difficulties dealing with elements such as O, F, or 3d TM, which have strong potentials. On the other hand, HF techniques neglect electron correlation, which affects different configurations of a given defect unequally.

As concerning the modeling of the host crystal, some authors prefer hydrogen-saturated molecular clusters while others use periodic supercells. In the first case, the presence of the surface may affect the calculated properties of a defect. In the second case, interactions between defects in neighboring cells creates rather wide defect bands. Further, variations in the predictions may result from the choice of basis set or other technical aspects of the calculations which are not always detailed in the finished publication. In any case, the quality of the predictions is also a function of the know-how of the theorist involved.

Other difficulties are related to an incomplete understanding of the physics of a problem. For example, calculating the barrier for diffusion of H⁰ in a semiconductor involves guessing how much the crystal responds to the diffusing interstitial. The barrier separating the tetrahedral interstitial (T) and the bond-centered (BC) sites cannot be calculated without explicitly including the relaxations of the host crystal. Assuming that the crystal relaxes instantaneously for intermediate positions of H grossly underestimates the barrier, while assuming a frozen crystal never allows the BC site to become a minimum of the energy. Such problems have to be addressed by MD simulations.

1.2.1. Molecular clusters and supercells

Two methods have been developed to approximate the host crystal. In both cases, one begins with a rather small number of host atoms at their regular lattice sites, forming a cluster (or cell). The number of atoms included is usually varied to check for size effects. Typical sizes are in the range of about 8–70 host atoms. For compound semiconductors, the clusters generally have the same number of atoms of each type to guarantee that, in the absence of a defect, the average number of valence electrons at each atomic site equals four, i.e. that there are no holes in the valence band (VB) or electrons in the CB. If a different number of atoms of each species is used, the cluster must carry a net charge. The clusters have dangling bonds on their surface, and these can be handled in two ways. *Molecular clusters* (or simply clusters) use hydrogen atoms to saturate the surface. The host atom–H bond length must be energy-optimized in order to minimize the effects of the surface on the calculated properties of a defect. The advantages of using H saturators are many. First, H is well described with a single 1s orbital and thus does not increase substantially the total number of orbitals. Second, H forms strong covalent bonds, and the bonding and antibonding levels associated with the surface host atom–H bonds are far below the top of the VB and far above the bottom of the CB, respectively. Finally, the corresponding wavefunctions are highly localized on the surface, and do not overlap significantly with atoms beyond their immediate nearest neighbor (NN).

In the case of interstitial H in Si, cluster-size studies [23,24] made at and near the ab-initio HF level have shown that potential-energy surfaces of the neutral interstitial rapidly become independent of the way the surface is terminated when the cluster size increases from 10 to 44 host atoms. This is illustrated in Fig. 3 in the case of H^0 moving along a T–H path in diamond. The curves labeled with Roman numbers are obtained in clusters in which the C–H bond length at the surface is optimized (1.09 \AA) while the curves labeled with Arabic numbers have $C-H=C-C=1.55\text{ \AA}$. It is clear that large differences occur only in the small clusters in which C–H is not optimized.

Questions remain as to the cluster-size dependence of other properties of H^0 (such as the wavefunction) or that of other defects, which may be less localized, or exhibit a dipole moment which is likely to interact more strongly with the surface of the cluster. The surface host atom–H bond is always somewhat polar. This results in a small dipole layer on the surface, which varies with the host. However, for symmetric configurations of a defect, the total dipole moment of the cluster+defect system is most often either zero or very small. In compound semiconductors, an additional issue needs to be considered: the long-ranged part of the Madelung potential is not included in the calculation because the cluster is finite. This is expected to affect the potential energy surface of charged defects the most. In principle, one could sum the Madelung energy for an infinite distribution of point charges outside the cluster, which would mimic the entire host crystal. Such calculations have not been carried out to date. Ongoing studies (preliminary results were published in the monthly journal of the Swiss Center for Scientific Computing [25]) are aimed at resolving these issues. Thanks to recent software developments in the partial retention of diatomic differential overlap (PRDDO) methodology (see below), molecular clusters ranging in size up to 504 host atoms have been calculated. Fig. 4 shows the $C_{44}H_{42}$ and $C_{504}H_{210}$ clusters. Preliminary results indicate that geometries converge much faster than eigenvalues or wavefunctions.

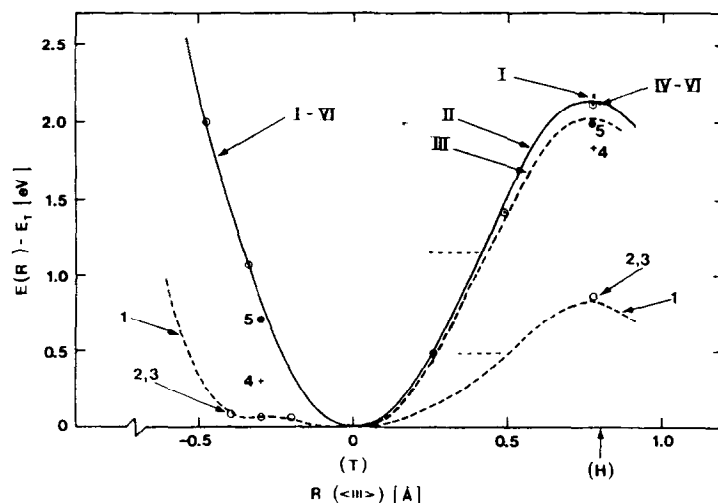


Fig. 3. Potential energy surface for H^0 moving along the $\langle 111 \rangle$ direction in various diamond clusters. The Roman numerals corresponds to clusters with surface C–H bond lengths optimized (1.09 \AA) while the Arabic numerals have $C-H=C-C=1.55\text{ \AA}$. The curves labeled I, II, and III are ab-initio HF results, the other numbers are approximate ab-initio ones. Increasing numbers correspond to increasingly larger clusters, in the range $C_{10}H_{16}$ – $C_{30}H_{40}$. The T and H sites are marked. The clusters with $C-H=C-C$ show large cluster-size effects, but converge toward the results obtained in even the smallest cluster with the optimized surface. The figure is from Ref. [23] with permission.

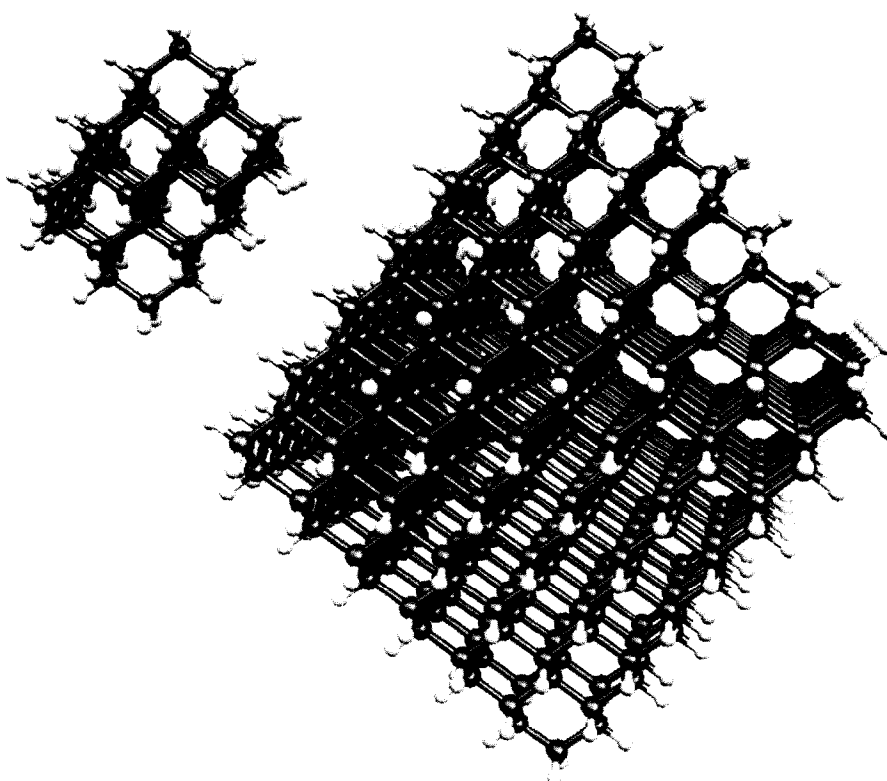


Fig. 4. Comparison of the $C_{44}H_{42}$ and $C_{504}H_{210}$ diamond clusters. The largest cluster has only been used in test runs, but routine calculations in clusters containing some 200 host atoms should become the norm in the next few years.

While cluster size effects may be monitored with approximate methods such as PRDDO, high-level calculations will continue to be restricted to rather small clusters and to suffer from some uncertainties related to size effects. However, it has been shown by various authors that, if the clusters are correctly saturated, the chemical bonds are not affected by cluster size except for the smallest clusters. Lattice relaxation and distortions as well as energetics are more sensitive to the size of the system. Eigenvectors and wavefunctions may be even more sensitive, depending on the nature of the defect under study.

Supercells (or cyclic clusters) periodically repeat the cluster or cell in all directions of space, thus preserving the periodicity and bypassing the surface problem. Properties of perfect crystals are remarkably well reproduced using this technique. However, in the case of defects in semiconductors, supercells have drawbacks as well. The most important one is that the periodic repetition of the cell results in a periodic defect. This transforms defect energy levels into defect bands, the width of which reflects the strength of defect-defect interactions in neighboring cells. Even in the case of isolated H^0 hydrogen in Si, this band is quite wide: it is 1.2 eV in a 16-atom cell, and 0.5 eV in a 32-atom cell [26,27]. The band width varies with the defect, its location within the cell, and the amount of distortion around it. Similar cell-size effects have been reported in compound semiconductors [28]. Note that in compound semiconductors, the contribution to the Madelung energy of an infinite crystal is present, in contrast to the case of molecular clusters. However, it corresponds to a crystal which contains a periodic defect, which affects the charge distribution.

Recent systematic cell-size studies have been carried out [29,30] in the case of dopant-H pairs in Si. Cell sizes were varied in the range 8–64 atoms (before the inclusion of the

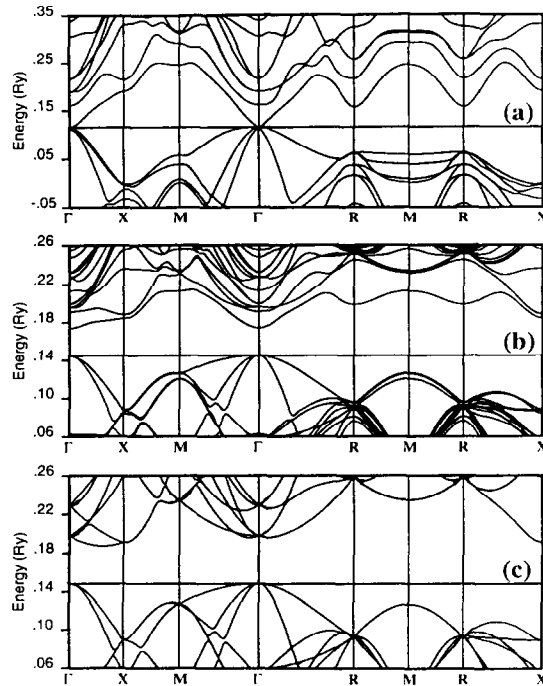


Fig. 5. Calculated band structure as a function of cell size for the {B, H} pair in Si. (a), (b), and (c), contain 7, 15, and 63 Si atoms in addition to the {B, H} pair. The horizontal line is aligned to the top of the VB. The smallest cell shows a metallic behavior. The figure is from Ref. [30] with permission.

dopant–H pair). As can be seen in Fig. 5, the band structure shows a metallic behavior in the 8 Si-atom cell. For a fixed cutoff energy (see below), the results show that the geometries vary considerably in cells of different sizes. For example, in the case of the {B, H} pair in Si, the H–B internuclear distance increases from 1.351 Å (8-atom cell) to 1.473 Å (16-atom cell) to 1.551 Å (64-atom cell). Such variations are much greater than those observed in molecular clusters. They affect considerably some calculated properties of the defect. For example, the calculated Si–H stretching mode of the {P, H} pair in Si is shown as a function of cell size in Fig. 6.

In summary, molecular clusters and periodic supercells have both advantages and disadvantages. Systematic studies of size effects show that molecular clusters exhibit smaller size dependencies than periodic supercells. The problems are being addressed and calculations in large supercells (64 atoms and more) and huge clusters (so far, up to 504 host atoms) will undoubtedly resolve many of the uncertainties.

1.2.2. Hartree–Fock-based calculations

The HF method attacks the many-body problem up front. The Hamiltonian contains the kinetic energy of the electrons, the electron–nuclear attraction, and the electron–electron and nuclear–nuclear repulsion terms. In atomic units, it is given by

$$\mathcal{H} = -\frac{1}{2} \sum_i \nabla_i^2 - \sum_{A,i} \frac{Z_A}{r_{Ai}} + \sum_{i < j} \frac{1}{r_{ij}} + \sum_{A > B} \frac{Z_A Z_B}{r_{AB}} \quad (1)$$

where A and B number the nuclei, i and j the electrons, Z are the nuclear charges, and $r_{xy} = |\mathbf{r}_x - \mathbf{r}_y|$. The many-electron wavefunction $|\Psi\rangle$ is constructed as one (or several) Slater

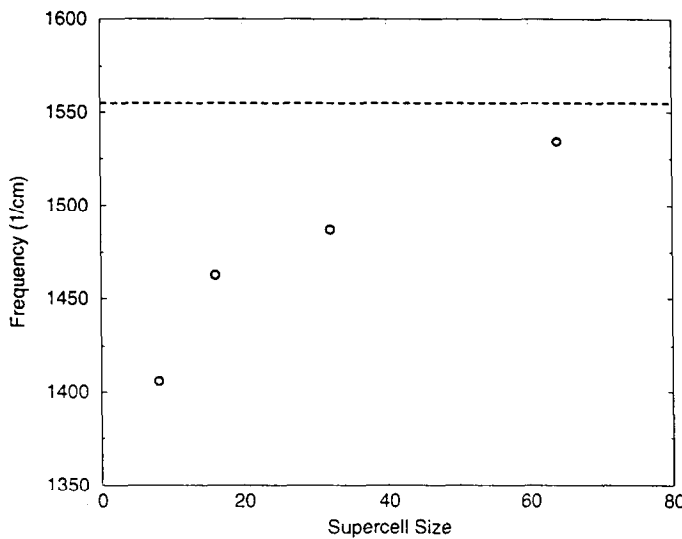


Fig. 6. Calculated stretching vibrational frequency vs. number of atoms per cell in a supercell scheme. Large variations in optimized geometries result in large changes in calculated frequencies. The numbers appear to converge nicely toward the experimental value (dotted line) for large cells. The figure is from Ref. [30] with permission.

determinant of one-electron molecular orbitals (MOs) ϕ_μ , which are linear combinations of (known [31]) atomic orbitals (AOs) χ_i

$$\phi_\mu = \sum_i c_{\mu i} \chi_i \quad (2)$$

where the variational coefficients $c_{\mu i}$ may be spin dependent [32,33]. The atomic orbitals χ_i are Slater orbitals, often expanded in terms of Gaussians for computational convenience. Finally, the expectation value of the Hamiltonian $\langle \Psi | \mathcal{H} | \Psi \rangle$ is calculated. Self-consistency is achieved as follows. One first guesses an initial set of expansion coefficients $c_{\mu i}^{(0)}$, constructs the total wavefunction $|\Psi^{(0)}\rangle$, and diagonalizes the Hamiltonian. The eigenvectors are a new set of coefficients $c_{\mu i}^{(1)}$, which are used to obtain the next wavefunction $|\Psi^{(1)}\rangle$, and the cycle continues to self-consistency. The most time-consuming part of the calculation is the evaluation of the four-center integrals, which have the form

$$\langle i, j | k, l \rangle = \int d^3r_1 \int d^3r_2 \frac{\chi_i(\vec{r}_1)\chi_j(\vec{r}_1)\chi_k(\vec{r}_2)\chi_l(\vec{r}_2)}{|\vec{r}_1 - \vec{r}_2|} \quad (3)$$

Note that electron exchange integrals are all calculated, but that no electron correlation is included, except for the antisymmetry of the wavefunction. The number of such integrals is proportional to $N^{4/8}$, where N is the total number of orbitals. A reduction in this number can be achieved by using pseudopotentials (see, for example, Ref. [34]) or frozen cores [35]. The HF calculations which calculate all the required integrals are called ab initio. Such calculations are restricted to small clusters and/or high-symmetry situations. Today, on a state-of-the-art workstation, single-point calculations at the ab-initio HF level with split-valence polarized basis sets can be made in clusters containing 26 host atoms (without core orbitals). Ab-initio HF predicts very good equilibrium geometries and electronic structures, but overestimates barriers for diffusion and vibrational frequencies, especially if small basis sets are used.

A variety of basis sets and different types of wavefunctions can be employed [33]. Minimal basis sets use a single Slater orbital per occupied orbital (e.g. 1s, 2s, three 2p,

3s, and three 3p for each Si atom). Split-valence basis sets use one Slater orbital per core orbital, but two independent orbitals for each valence state (i.e. two 3s and two sets of 3p orbitals for Si). Finally, polarized basis sets include a set of orbitals with an orbital quantum number higher than the highest one occupied (e.g. a set of five 3d orbitals in the case of Si). In most cases, each Slater orbital is fitted to a fixed linear combination of Gaussians. The many-electron wavefunctions can also be of several types. Only the simplest ones are computationally tractable for the large systems under consideration here. The most commonly used wavefunctions are the following.

- (i) Restricted closed shell (RHF), where each MO has an occupation number of 0 or 2 and the spin is zero everywhere.
- (ii) Unrestricted open shell (UHF), where each spin direction is independent from the other. The spin MOs have occupation number 0 or 1. This wavefunction is an exact eigenfunction of S_z but not of S^2 . Because the two spin directions are independent, the expectation value of the spin operator S^2 is almost always larger than $s(s+1)$. This ‘spin contamination’ is usually very small (e.g. 0.76 instead of 0.75 for a net spin of 1/2), but needs to be monitored in every calculation, especially when dealing with high spin multiplicities or configurations far from a local minimum of the potential surface (see, for example, Ref. [36]). Note that UHF and RHF energies are not directly comparable.
- (iii) Restricted open shell (ROHF) [37], where each MO has an occupation number of 0 or 2 except for one or more open shells, orthogonal to each other, which may have *fractional* occupancies. This type of wavefunction must be used to describe an orbitally degenerate state, high spin multiplicities, or multiple spin systems. The wavefunction is equivalent to a multi-determinant wavefunction, but only the open shell(s) are treated separately. The ROHF wavefunction is an eigenfunction of S_z and S^2 , but is computationally more cumbersome. The RHF and ROHF energies are directly comparable, thus allowing the calculation of the energy difference, e.g. between the singlet (RHF) and triplet (two open-shell ROHF) states of a system with an even number of electrons.
- (iv) Generalized valence-bond (GVB) [37], where selected pairs of orbitals (typically one or two pairs) are described in terms of overlapping singly occupied orbitals: $\phi_\mu(1)\phi_\mu(2) \rightarrow \{\phi_{\mu a}(1)\phi_{\mu b}(2) + \phi_{\mu b}(1)\phi_{\mu a}(2)\}$. The pairs have different orthogonality restrictions from the original orbitals and the GVB approach allows the incorporation of optimal ionic and covalent characters in the wavefunction which behaves properly at all internuclear distances. GVB calculations are complicated and their use for defects in semiconductors has been limited [38].

In order to add electron correlation, one must include the unoccupied states, which are the excited states of the system. So far, only one type of treatment has been used in the case of defects in semiconductors. It is a perturbation expansion [39] developed by Møller and Plesset (MP). One starts with a large basis-set ab-initio HF calculation. The converged wavefunction consists of the optimized occupied states and of a large number of unoccupied states. Excitations are constructed by taking one, two, three, or more electrons in occupied states and promoting them into all the possible unoccupied states. The set of combinations involving 1 up to n electron excitations is referred to as MP _{n} (n th-order Møller–Plesset expansion in electron correlation, a post-HF treatment). There are of course a very large number of such excitations, and even a MP₂ expansion must be restricted to a small number of allowed initial and final states. Each excitation forms a new determinant,

and the total wavefunction contains the original HF determinant and the sum of all the possible excitations. The coefficients of this linear combination of determinants are optimized. The resulting corrections to the energy (for MP_n , $n > 2$) and to the wavefunction (for MP_n , $n > 3$) affect the various configurations of a defect center differently (see Refs. [40,41]). These calculations are computationally intensive, especially regarding disk space. They are therefore limited to single-point calculations in small clusters, using geometries optimized at lower levels of theory.

Note that post-HF correlation corrections involve excited states while in DF calculations the exchange-correlation potential V_{xc} is a function of the ground-state density alone (see next section). According to DF theory, the exact properties of the ground state can be obtained without any knowledge of or reference to excited states. Within HF theory, excitations provide correlation corrections as well as some excited-state properties. The limiting situation, in which all the possible excitations of all possible electrons are included (a full configuration interaction (CI) calculation [37]) gives all the ground- and excited-state properties.

Because of the expense associated with routine calculations at the ab-initio HF level with large basis sets, a number of approximations have been developed. They fall into two categories: semiempirical methods and the approximate ab-initio method of PRDDO. It is necessary to use such methods in the case of defects in semiconductors because one must perform geometry optimizations in little or no symmetry in the largest possible molecular clusters or periodic supercells in order to monitor the size effects and to allow for the inclusion of lattice relaxations and distortions. Optimized geometries can subsequently be used to perform single-point high-level calculations in the smallest cluster which is meaningful for a given defect.

The most approximate method based on linear combinations of atomic orbitals (LCAO) is EHT (see, for example, Refs. [17,18]). In addition to introducing semiempirical parameters, this method uses a product wavefunction rather than a Slater determinant. Thus, the electrons do not obey Pauli's principle, and the calculation cannot be carried out to self-consistency (this would lead to a solution in which all the electrons are in the same ground state orbital). EHT no longer seems to be in use.

Many semiempirical approximations to ab-initio HF theory have been developed. In these methods, only a few of the two-electron integrals are actually calculated, and from 3 up to some 50 parameters are introduced. They are adjusted so that the calculation reproduces selected experimental data, such as ionization energies or heats of formation. When applied to situations for which they are parameterized, semiempirical HF techniques can produce remarkably good results [42]. However, they are not necessarily parameterized for all of the unusual chemistry that sometimes results from H interactions in semiconductors. Further, parameterizations exist only for selected elements or pairs of elements, which further restricts the applicability of the methods. Finally, they are always limited to minimal basis-set RHF and UHF wavefunctions.

Three semiempirical HF methods have been applied to the study of H in semiconductors. They are complete neglect of differential overlap (CNDO) [43], modified intermediate neglect of differential overlap (MINDO) [44], and modified neglect of diatomic overlap (MNDO) [45,46]. CNDO is the most approximate of these methods and is rarely used today. MINDO was originally designed for the calculation of bonding energies, and the parameterization was developed for pairs of elements. It contains about 10 parameters per element plus 2 parameters per pair of elements. MNDO contains fewer parameters (about

7 are optimized per element) but a more refined version [42] uses up to 18 parameters per element.

An alternative to semiempirical approximations to ab-initio HF was developed by the Lipscomb group at Harvard [47–49]. The method of PRDDO contains no semiempirical parameters (hence ab initio) but introduces mathematically well-defined approximations which allow a reduction of the number of two-electron integrals from N^4 to N^3 (hence approximate) with little loss of accuracy. The trick is to orthogonalize the initial atomic basis set in such a way that the four-center integrals (Eq. (3) with i, j, k , and l on different centers) are exceedingly small and can be neglected. This introduces small and systematic errors relative to ab-initio (minimal basis-set) calculations. These errors are corrected when building the Fock matrix.

Because of the relatively small number of integrals that must be calculated, PRDDO uses Slater orbitals rather than the usual linear combinations of Gaussians. This guarantees that the wavefunctions have correct cusps and tails. As a result, PRDDO predicts reliable equilibrium geometries. The most recent version of the code is designed to handle very large systems. It introduces refinements in the way orbitals on distant centers are orthogonalized, allowing for the use of sparse matrix techniques. Further, almost all the integrals are calculated analytically, and frozen core options are introduced [50]. Average errors in bond lengths and atomic charges (relative to ab-initio HF calculations) are only 0.010 Å and 0.016 e, respectively. Tests on the C₅₀₄H₂₁₀ molecular cluster (see Fig. 4) have been conducted [25].

PRDDO is a very flexible approach which allows the study of a wide range of impurities and complexes in intrinsic and compound semiconductors at a uniform level of theory. It provides reliable equilibrium geometries, and approximate energetics and electronic structures. It is restricted to small basis sets and includes no correlation. The calculated energy differences are often too high. However, PRDDO provides excellent inputs for single-point calculations at higher levels of theory, such as large basis-set ab-initio HF calculations followed by MP corrections in electron correlation.

1.2.3. The density-functional approach

Hohenberg, Kohn, and Sham [51–53] have shown that the ground state of the interacting electron gas can be obtained by solving the one effective particle Schrödinger equations (in atomic units):

$$\left\{ -\frac{1}{2} \nabla^2 + V_{\text{eff}}[n] \right\} \psi_i(\vec{r}) = \epsilon_i \psi_i(\vec{r}) \quad (4)$$

The effective potential contains the Hartree potential $V_H[n]$, an external potential $V_{\text{ext}}[n]$, and an exchange-correlation potential $V_{\text{xc}}[n]$, which are all functionals of the ground-state density $n(\mathbf{r}) = \sum_i |\psi_i(\mathbf{r})|^2$. One starts with a guess density $n^{(0)}(\mathbf{r})$, constructs $V_{\text{eff}}[n^{(0)}]$, and solves the Schrödinger equation. The eigenvectors provide a new density $n^{(1)}(\mathbf{r})$ which is used to calculate a new effective potential $V_{\text{eff}}[n^{(1)}]$, and the cycle continues to self-consistency.

The self-consistent solution would give the exact ground-state density, were V_{xc} known. This potential is written as the functional derivative of the exchange-correlation energy E_{xc} , which itself is not known. The local density approximation (LDA) consists of expanding E_{xc} in the Taylor series

$$E_{\text{xc}}[n] \approx \int d^3r n(\vec{r}) \epsilon^{(1)}(n(\vec{r})) + \frac{1}{2} \int d^3r |\vec{\nabla} n(\vec{r})|^2 \epsilon^{(2)}(n(\vec{r})) + \dots \quad (5)$$

and neglecting all but the first term of this expansion. Several parameterizations exist [54–57] (a parameterization of the exchange-correlation potential in Ref. [56] is in Ref. [57]) for $\epsilon^{(1)}$. The DF calculations using the LDA are often referred to as local-density functional (DF with LDA) (LDF) calculations. Note that although electron correlation is included, electron exchange is approximated. On the other hand, HF techniques include exchange exactly, but neglect correlation. A hybrid approach was recently proposed [58]. It consists of calculating a large basis-set HF wavefunction, using it to construct the density, then calculating the correlation part of V_{xc} , thus obtaining a correction to the HF energy.

In order to avoid having to recalculate all the energy integrals and their functional derivatives at each iteration, the densities and potentials are expanded in terms of N basis functions. The integrals are evaluated once, and the coefficients of the expansion are varied to self-consistency. The most time-consuming part of the calculation is the diagonalization of the effective Hamiltonian matrix, a procedure which scales as N^3 . The type of basis set depends on how the crystal is represented.

If supercells are used [26,27], the basis set normally consists of plane waves included up to a fixed kinetic energy E_c , typically 12 Ry. The low-energy waves are treated exactly, and the high-energy ones are treated in perturbation theory. Very large numbers (thousands) of plane waves are required [59] to describe, for example, atomic H⁰. Mixed basis sets consisting of plane waves and Gaussians can also be used. In molecular clusters [60,61], the basis set of choice consists of Gaussians with s, p, and d symmetry. These Gaussians may be centered at atomic sites or at BC sites. In the case of a charged defect, the basis set must be selected with care [61].

If plane waves are used, the cutoff energy E_c determines the basis set size. E_c should be as small as possible to minimize the computational effort, but large enough to produce accurate energies and densities. Systematic tests of LDF calculations in supercells have been conducted [29,30]. The total energies of the 8-, 16-, 32-, and 64-atom supercells with and without a {B, H} pair have been calculated as a function of E_c . In order to allow a comparison of the total energies, the total energy of pure Si with the largest value of E_c was subtracted. The results (Fig. 7) show that convergence is achieved in this case for

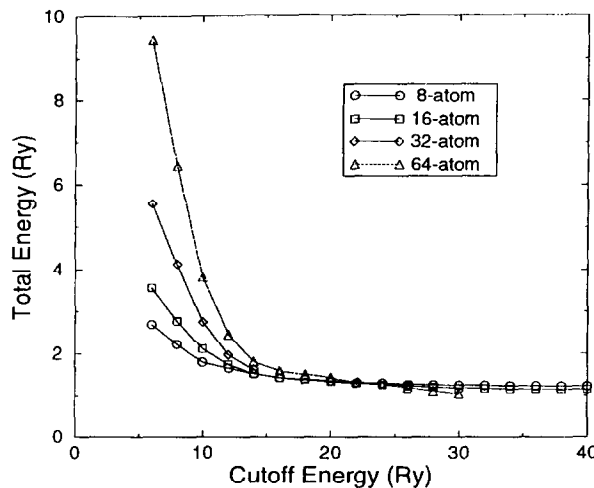


Fig. 7. Normalized total energies of 8-, 16-, 32-, and 64-atom Si supercells containing the {B, H} pair vs. plane-wave cutoff energy E_c (see text). The figure is from Ref. [29] with permission.

$E_c > 15$ Ry, a value larger than that typically used in such calculations. The converged value of E_c is likely to be defect dependent.

The core states are removed from the calculation by the use of ab-initio pseudopotentials [62,63]. This not only reduces the basis-set size, but also avoids the core region where the true potentials vary rapidly. These pseudopotentials are non-local, norm-conserving, and contain no semiempirical parameters. The pseudowavefunctions are nodeless, normalized, and constructed in order to match the exact eigenfunction of an atom in a particular electronic state beyond a given core radius. Inside the core, the nodeless wavefunctions bear no resemblance to the true atomic eigenfunctions. The corresponding pseudopotential is obtained by direct inversion of the Schrödinger equation. Ab-initio pseudopotentials are strong for the valence functions of atoms which have no core functions of the same symmetry, such as 2p for O or 3d for Ti. This causes problems when plane-wave basis sets are used.

The use of pseudopotentials prevents the study of core-polarization effects. However, Van de Walle and Blöchl [64] have developed a method to reconstruct valence wavefunctions in the core region of atoms starting with the pseudowavefunctions generated from ab-initio pseudopotentials. This has allowed them to use spin-dependent LDF theory with pseudopotentials to calculate hyperfine (hf) parameters quite accurately, even though core polarization effects were not included.

The applications of LDF with ab-initio pseudopotentials are often called first-principles DF, in the sense that no semiempirical parameters are present. The quality of such calculations depends on a number of factors, such as the basis set used (plane waves, gaussians, or mixed), the basis-set size (energy cutoff for plane waves, number of gaussians with different symmetry, etc.), cell size (defect-defect interactions in neighboring cells) or cluster size (surface effects), species under study (strength of the pseudopotential) and, to a lesser extent, the choice of parameterization for the exchange-correlation potential [54–56]. Including the spin doubles the size of the calculation. As a result, most LDF calculations are spin averaged, meaning that the net spin is zero everywhere.

LDF predicts good equilibrium geometries and excellent densities. Further, the vibrational frequencies are more reliable than those predicted at the ab-initio HF level. On the other hand, since only the total density is meaningful, the one-electron wavefunctions cannot be obtained. As a result, much of the chemical information is not provided (population analysis, bond indices, etc.).

LDA is responsible for the gap problem: the calculated bandgap is about half the experimental one. The reasons for this are well understood [65], and the conduction bands are usually simply shifted upward to resolve the problem. Calculations beyond the LDA require many-body techniques [66–68] and are impractical for the study of defects in semiconductors.

1.2.4. Molecular dynamics simulations

In an MD simulation, the electronic problem is solved quantum mechanically (usually with the DF approach) and the nuclear motion is calculated classically. The electronic and nuclear coordinates are still decoupled via the Born–Oppenheimer approximation, but nuclear motion is explicitly included. Further, the kinetic energy of the nuclei determines the temperature of the system, and various quenching techniques can be used to converge the system toward a local or global minimum of the potential energy. Finally, diffusion or dissociation processes can be monitored at various temperatures. Note that the temperature of the electrons remains zero regardless of the temperature of the ions. The reasons for

this are first the bandgap problem (see above) leading to incorrect thermal occupation of excited states, and second the fact that LDF is not strictly applicable to excited states. Only those excited states that have a symmetry different from the lower-lying states are accessible.

The basic equations were derived by Car and Parrinello [69]. All MD simulations use the same basic equations to calculate the nuclear motion (integration of Newton's second law). Differences between the various methods occur in the actual calculation of the forces. These depend on the way the electronic problem is solved, which is where most of the computing time is spent. Forces are obtained from the gradient of the total energy which, within LDF theory, is obtained from (in atomic units)

$$\begin{aligned} E_{\text{tot}} = & 2 \sum_i \langle \psi_i | \frac{\vec{p}^2}{2} | \psi_i \rangle + 2 \sum_{i,A} \langle \psi_i | V_{\text{ps}}(\vec{r} - \vec{R}_A) | \psi_i \rangle + \frac{1}{2} \int d^3 r_1 \int d^3 r_2 \frac{n(\vec{r}_1)n(\vec{r}_2)}{|\vec{r}_1 - \vec{r}_2|} \\ & + \int d^3 r n(\vec{r}) \epsilon_{\text{xc}}(n) + \frac{1}{2} \sum_{A \neq B} \frac{Z_A Z_B}{|\vec{R}_A - \vec{R}_B|} \end{aligned} \quad (6)$$

where V_{ps} is the appropriate ionic potential. The densities are calculated approximately, since a fully self-consistent solution for every set of atomic coordinates would be computationally prohibitive. Note that the same classical equations of motion could be solved with forces obtained from a HF total energy. In practice, however, the MD simulations performed so far have all used DF-based total energies.

The Car–Parrinello approach [69] is based on first-principles DF theory, as described in the previous section. It uses periodic supercells with plane-wave basis sets. Its only assumptions are the validity of classical mechanics to describe ionic motion, the Born–Oppenheimer approximation, as well as the validity of the approximations involved in LDF and the use of supercells (see above). Because the approach is computationally intensive, approximate methods were developed. A slightly approximated but much faster approach was developed by Stumpf and Scheffler [70].

A simplified ab-initio approach was developed by Sankey and Niklewski [71]. They used a tight-binding scheme to systematically simplify the electronic interactions, also using periodic supercells. The basis set consists of a small number of localized pseudo-atomic orbitals with s and p symmetry. These functions have a cutoff radius in order to reduce or eliminate the interactions between atoms located far from each other. Note that this method is not self-consistent, but uses the Harris functional scheme [72].

Two semiempirical MD approaches have recently been proposed to study the dynamics of hydrogen in Si. The first is a tight-binding method [73] based on the approximations developed by Wang et al. [74]. The second [75] uses semiempirical functionals fitted to a database of selected experimental data and ab-initio calculations. Such semiempirical schemes use much less computational time than ab-initio ones, which allows for MD simulations to be performed in supercells containing hundreds or thousands of atoms (rather than dozens, as in ab-initio simulations) and to consider much longer simulation times (see below). The accuracy of the results, of course, diminishes as approximations are added.

In practical calculations, a temperature is chosen and the electronic problem is solved at each time step. Typical time steps range from 0.1 fs (for a very light atom such as H) to 1 fs for heavier nuclei. Hundreds or thousands of time steps must be considered to either converge the system to a minimum of the potential energy by rapid quenching (this

may consist of the removal of a fraction of the kinetic energy every few time steps) or monitor the diffusion of an impurity at a fixed temperature.

1.3. Muon spin rotation

The μ SR technique [76] is a tool analogous to EPR which allows the observation of hf and superhyperfine (shf) structures in addition to a Zeeman frequency. The observed quantity is an energetic positron, resulting from the parity-violating muon decay (for reviews, see Refs. [77–80]). Spin-polarized positive muons are injected into a crystal where they thermalize within a few picoseconds. The muon may remain a bare μ^+ , trap one electron and form a paramagnetic center ($\text{Mu} = \mu^+ e^-$), trap two electrons (Mu^-), or perhaps even form a covalent bond, e.g. with a dangling bond such as Si–Mu. Unless a single electron is involved, only the Zeeman precession of the muon spin in the local magnetic field is seen.

Within some 2.2 μs , the muon decays into a positron and two neutrinos. The positron is preferentially emitted in the direction of the spin of the muon. In traditional μ SR experiments, millions of muons are sequentially implanted, and the time and angular dependencies of the emitted positrons are detected. The depolarization rate (loss of the initial muon spin polarization) can also be monitored. It provides information on the diffusion of the muon. Alternative experiments involve positron channeling (from muon decay) or muon channeling (from pion decay). Recent developments in μ SR techniques include muon level-crossing resonance (μ LCR) [81–83] (analogous to ENDOR) and radio frequency μ SR (r.f.- μ SR) [84,85] (analogous to continuous wave nuclear magnetic resonance (cw NMR)). The former method allows the measurement of contact spin densities on nuclei other than the muon itself, and perhaps even the spectroscopic identification of muonium–impurity pairs. The latter allows the monitoring of the concentration of a given muonium state as a function of temperature, and the determination of reaction-rate parameters for the muonium site and charge-change reactions.

The mass of the muon is only one-ninth that of the proton. Thus, the zero-point energy of the muon in a given potential is much larger than that of a proton, and a muon experiences smaller activation energies than a proton. Therefore, it diffuses much faster than a proton. In a number of instances, quantum tunneling has been observed. Further, because of its short lifetime, the muon does not come to full equilibrium with its surroundings, and metastable states can be seen. In most cases, only a single muon is in the sample at any given time, and the consequences of muon–muon interactions are not recorded. Recent developments in the technique (integral measurements) allow the simultaneous implantation of pulses of muons. Note that the details of the muon-stopping process have yet to be fully understood. However, μ SR has provided a wealth of information on isolated hydrogen-like centers in semiconductors, and there is no doubt that much less would be understood today were μ SR not available.

A paramagnetic state of isolated hydrogen, the AA9 center, has been observed by EPR in Si [86,87]. Once scaled by the ratio of the muon to proton nuclear moments, the hf tensor of AA9 is virtually identical [87,88] to that of bond-centered muonium (Mu^* or Mu_{BC}^0). This provides convincing evidence that μ SR does indeed provide direct information on hydrogen and hydrogen-related centers. Note that muonium centers have been seen in all the alkali halides. A comparison [89] of the μ SR to EPR data (U centers) is another confirmation that the muon truly behaves like a light isotope of the proton.

In insulators such as quartz, the μ SR spectrum consists of the non-paramagnetic μ^+ signal and of a single paramagnetic species, very similar to free atomic muonium. However, μ SR experiments [14] in silicon revealed the presence of three centers, two of which had unexpected features. In addition to μ^+ , which could be owing to any non-paramagnetic defect, two paramagnetic centers were observed. The first one was labeled normal muonium because its hf tensor is (on the average) isotropic and therefore reminiscent of an atomic-like species. However, its Fermi contact density is about half the free atomic value, showing an unexpectedly large delocalization of the 1s wavefunction. The second one was labeled anomalous muonium and remained unexplained for over 10 years. It corresponds to a highly anisotropic center with trigonal symmetry and is characterized by a very small (almost zero) Fermi contact density at the muon.

The correct identification of this center as neutral bond-centered muonium was proposed in 1984 by Symons on the basis of chemical arguments [90] and again by Cox and Symons [91,92] in 1986. The first calculations confirming their prediction were performed that same year, in the case of diamond [93–95] and silicon [94,96]. Other authors later confirmed the calculated structure and performed further studies (see the next section). After it was realized that interstitial muonium (or hydrogen) can force the covalent bonds in hosts such as diamond or silicon to relax by nearly 40% and form bridged bonds, the importance of including lattice relaxations and distortions when studying defects was established. It is now common to consider atomic displacements of several tenths of an angström when hydrogen interacts with a host crystal, with itself, or with impurities or defects in a semiconductor.

To date, muonium centers have been seen in 17 semiconductors with the diamond (c-C, Si, Ge), and zinc-blende (3C- or β -SiC, GaP, GaAs, GaSb, InP, InAs, InSb, ZnS, ZnSe, CdS, CdTe, CuCl, CuBr, CuI) structures, as well as in the hexagonal 6H polytype of SiC. Not all these hosts have been studied at the same level of detail. The most data are available on Si, but quite a few details are known about several other hosts, in particular c-C, GaP, GaAs, and the copper halides. The results will be discussed later in the relevant sections. Below is a summary of the general features of the various muonium centers.

- (a) Normal muonium or $Mu_T^0 = \mu^+e^-$ is atomic-like and corresponds to neutral interstitial muonium at the T site or diffusing rapidly among sites of lower symmetry in such a way that its hf interaction is isotropic, even at very low temperatures. In Si and Ge, measurements of the depolarization rate show that Mu_T^0 is very mobile at all temperatures [77]. It is less mobile in GaP and GaAs [97], and it is localized at (or around) a single T site in c-C [77,79]. The Fermi contact density is a substantial fraction of the free atom value, indicating that the unpaired electron resides primarily in a 1s-type orbital. Its value ranges from 83% of the free atom value in c-C down to 45% in Si, except for copper halides where it is unusually low (about 30%). In a few hosts, two or even three Mu centers are seen. In compound semiconductors, the hf parameters are nearly independent of the anion [80].
- (b) Anomalous muonium or Mu_{BC}^0 (initially labeled Mu^*) is also paramagnetic and corresponds to a muon bridging a substantially relaxed host atom bond. The structure is reminiscent of hydrogen-bridged bonds, e.g. in diborane. The hf tensor has axial ($\langle 111 \rangle$) symmetry, and the contact density at the muon is very small. In elemental semiconductors, the odd electron resides primarily in a non-bonding orbital, symmetrically located on the two NNs and the six second NNs to the muon. The situation is different in compound semiconductors. The muon forms unequal bonds with its two NNs, resulting in one of two configurations: A $\cdots \mu$ -B or A- $\mu \cdots$ B. In the former case, most of the odd electrons

reside on atom A and, in the latter case, on atom B. The stronger bond involving the muon is almost a two-center two-electron bond, not the three-center two-electron bond that occurs in elemental hosts. Which of the two possible configurations is realized depends on the relative stability of the odd electron on atom A or B (electronegativity), and on the relative strength of the A–H and B–H bonds. Mu_{BC}^0 is seen only in the less ionic compounds, and then only one center is observed (i.e. of the two a priori possible configurations, only one is realized). Note that since the odd electron never participates in the bonding, Mu_{BC}^0 is easily thermally ionized, except in the case of diamond where it is stable up to at least 1 000 K.

- (c) Non-paramagnetic muonium or μ^+ or diamagnetic muonium could, a priori, be a positive ion (Mu_{BC}^+), a negative ion (Mu_T^-), or belong to any closed-shell muon–impurity or muon–defect pair, for example μ^+ trapped at a shallow acceptor, Mu trapped at a substitutional C in Si, etc. How many distinct centers contribute to the μ^+ signal is not known. It probably depends on the host, the temperature, the Fermi level, and the concentration of defects and impurities.

Note that the (0/+) energy level associated with Mu_T is buried in the valence band (the ionization energy of the neutral T-site, atomic-like, species is high). Further, trapping a second electron on Mu_{BC}^0 (i.e. forming Mu_{BC}^-) is unlikely. Indeed, this electron cannot participate in the bonding and weakens the covalent configuration. Therefore, Mu (or H) has at most two energy levels in the gap: (0/+) for Mu_{BC} and (−/0) for Mu_T .

Recent r.f.- μ SR data [98,99] show that in Si and GaAs, most of μ^+ is either Mu_{BC}^+ or Mu_T^- , depending on the position of the Fermi level and the temperature. In p-type Si, there is evidence that Mu_{BC}^0 and at least some of μ^+ are at the same site [84,88]. Further, positron channeling experiments confirm [100] that the μ^+ signal originates mostly from BC sites.

The fraction of incoming muons forming Mu_T , Mu_{BC} , and μ^+ varies with the host, the donor and acceptor concentrations, the temperature, and other factors related to the impurity content. For example, substantial differences in the μ SR spectra have been reported [77] between CZ-Si, where the concentration of O_i is of the order of 10^{16} cm^{-3} , and FZ-Si in which $[\text{O}_i] \sim 10^{14} \text{ cm}^{-3}$. Further, some fraction of the incoming muons is not accounted for. This missing fraction is almost zero in high-resistivity c-C, Si, or GaAs, but may be quite large in other hosts. This can be owing, for example, to rapid charge exchanges between different states or other factors resulting in fast depolarization rates. Further, thermally induced transitions between the various muon states are sometimes observed and provide essential information as to the relative stability of the various muonium species.

Table 1 contains a summary of the μ SR species observed in high-resistivity semiconductors, at low temperatures. It also lists the thermally-induced transitions reported between muon states. More details about the results in various hosts will be discussed in Section 2. Note that Mu_{BC}^0 has been seen only in c-C, Si, Ge, GaP, and GaAs. It has not (yet?) been observed in SiC, GaSb, InP, InAs, InSb or in the more ionic compounds (II–VI and I–VII compounds). A thermally induced transition from Mu_T^0 to Mu_{BC}^0 in c-C shows that the latter is the stable species. A $\text{Mu}_T^0 \rightarrow \text{Mu}_{\text{BC}}^0$ transition in irradiated Si suggests that Mu_{BC}^0 is more stable than Mu_T^0 in Si as well. Recent r.f.- μ SR studies in non-irradiated Si confirm the stability of the BC site in this host. In Ge, GaP, and GaAs, no clear evidence exists as to the relative stability of the T and BC sites. More about these transitions is in the next section. For details about μ SR and a complete set of references, the reader is referred to the recent reviews of the topic [77–80,84].

Table 1

Fraction of incoming muons forming the various muonium centers and the missing fraction in high-resistivity semiconductors at low temperatures ($T < 30$ K)

Group	Host	% Mu*	% Mu	% μ^+	% missing	Transitions
IV	c-C	22.7(8)	68.9(1)	8.1(3)	0.3(3)	$\text{Mu} \rightarrow \text{Mu}^*$
	Si	36.8(2)	61.0(8)	7.5(4)	–5.3(8)	$\text{Mu}^* \rightarrow \mu^+$
	Ge	8(4)	72(10)	10(2)	10(11)	$\text{Mu} \rightarrow \mu^+$
IV–VI	3C-SiC		30(5)	65(12)	5(19)	$\mu^+ \rightarrow \text{Mu}$
	6H-SiC ^a		56(13)	11(2)	33(13)	$\text{Mu}^{\text{A}I} \rightarrow \text{Mu}^{\text{A}}$ $\text{Mu}^{\text{A}II} \rightarrow \text{Mu}^{\text{A}}$
III–V	GaP	18(3)	72(10)	11(1)	–1(11)	
	GaAs	35(5)	63(6)	9(1)	–7(8)	$\text{Mu}^* \rightarrow \mu^+$
II–VI	ZnS		19(3)	20(1)	61(3)	
	ZnSe		11(2)	36(1)	53(2)	
I–VII	CuCl	66(3) ^I 9.9(8) ^{II}	16(4)	8(5)		$\text{Mu}^{\text{I}} \rightarrow \text{Mu}^{\text{II}}$ $\rightarrow \mu^+$
	CuBr	66(5) ^I 5.8(8) ^{II}	23(4)	5(6)		$\text{Mu}^{\text{I}} \rightarrow \text{Mu}^{\text{II}}$
	CuI	72(3)	18(8)	10(9)		$\text{Mu} \rightarrow \mu^+$

In 6H-SiC, the fractions were obtained at room temperature, and %Mu refers to the sum of all the Mu species. The missing fraction is a lower limit and the μ^+ fraction is an upper limit. Missing in the tables are GaSb, InP, InAs, InSb, CdS, and CdTe, in which only μ^+ has so far been observed. The (confirmed) transitions between muon states are also given. The tables comes from Ref. [77]. It differs slightly from the table found in Ref. [78] (which is reproduced in Ref. [5]) because of sample dependencies. The most recent results are shown.

^a Refs. [101] and [102].

2. Isolated H and H dimers

Hydrogen is the simplest element of the Periodic Table.

(*unknown, often quoted, and incorrect source*)

Studies related to H in semiconductors have been carried out for a long time. The first (unsuccessful) attempt [103] at detecting H in diamond crystals dates back to 1849. However, the present story begins with the first microscopic observation which led to our current understanding of the properties of H in semiconductors. This is the first complete μ SR spectrum [14] obtained by Brewer et al. in Si. This spectrum (taken at 77 K) is compared with that in quartz (at room temperature) in Fig. 8. In both hosts, the non-paramagnetic μ^+ signal is present and can be assigned to a variety of defects, as discussed in the previous section. However, two paramagnetic centers are present in Si. The expected one corresponds to an atomic-like muonium species, characterized by an isotropic hf interaction. This center was labeled normal muonium (Mu) even though it has one peculiarity: in quartz, the splitting of the two lines corresponds to a Fermi contact density identical to that in the free atom (zero-field splitting of 4463.3 MHz). In Si, the splitting of the two Mu lines is more than twice as large as in SiO_2 , indicating a contact density equal to only 45% of the free atom value. The unexpected center, showing up as a bunch of lines below 50 MHz, could not be identified and was labeled anomalous muonium (Mu*).

In the following 11 years, further experiments showed that Mu* has trigonal symmetry and is found in germanium [104] and diamond [105] as well. Theoretical models included a muonium-exciton molecule [14], a muonium at an AB site [106], and a charged vacancy-muonium pair [107] (see also the Comment and Reply to Ref. [107] in [108]), none

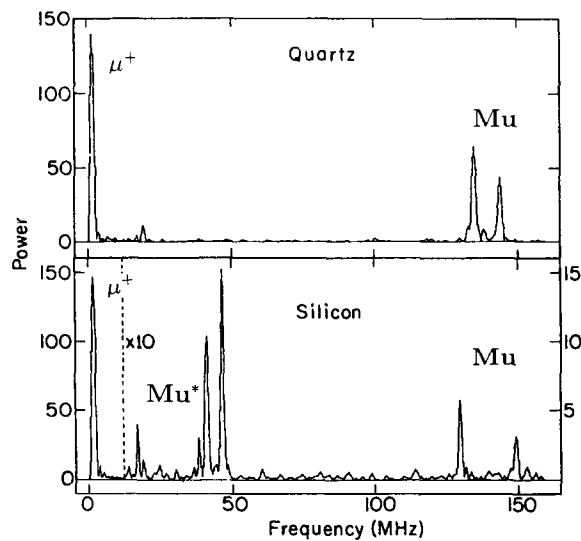


Fig. 8. Comparison of the first complete μ SR spectrum in c-Si to the much simpler one seen in SiO_2 (see text). The figure is from Ref. [14] with permission.

of which was fully satisfactory. In 1984, Symons [90] suggested, on the basis of chemical arguments, that the mysterious Mu^* center should be associated with the BC site. The first ab-initio calculations were published two years later for diamond [93,94] and silicon [94]. They were rapidly followed by a number of other calculations at various levels of theory, first in elemental, then in compound semiconductors.

The possible configurations of isolated H and hydrogen pairs in elemental and compound semiconductors are shown in Fig. 9. The sites are uniquely defined in elemental hosts, but there are two possible configurations for each site in compounds. With a few exceptions, only one of them is actually realized. Note that H at the BC site forms a true three-center two-electron bond only in elemental hosts. In compounds, H forms a bond much more like a two-center two-electron bond with one of its NNs and overlaps only weakly with the other. Note also that the notation H_T does not imply that H is at the tetrahedral interstitial site, but refers to the isotropic μ SR center. It has tetrahedral symmetry (on average), i.e. the local minimum of the potential energy could be at the T site or at a site of lower symmetry, provided that H moves rapidly among such sites in a way that averages the interactions to T_d symmetry. Finally, note that the H_2 molecule is shown in Fig. 9 as having a $\langle 111 \rangle$ orientation. There is no agreement among theorists as to the lowest energy orientation (see below).

2.1. Elemental semiconductors

The relative stabilities of H_T and H_{BC} as well as H_2^T and H_2^* in c-C, Si, Ge, and α -Sn have been calculated in molecular clusters at the ab-initio HF level [109,110]. The total energy differences are shown in Fig. 10. The calculations were performed in the neutral charge state (the ionization energy to form H_{BC}^+ or H_T^- is of the order of a few tenths of an electronvolt). As will be discussed below, different theoretical approaches differ in many details of their predictions. Thus, the position of the zero of the energy and the exact shapes of the curves are probably theorist-dependent. However, the trends shown below should be valid.

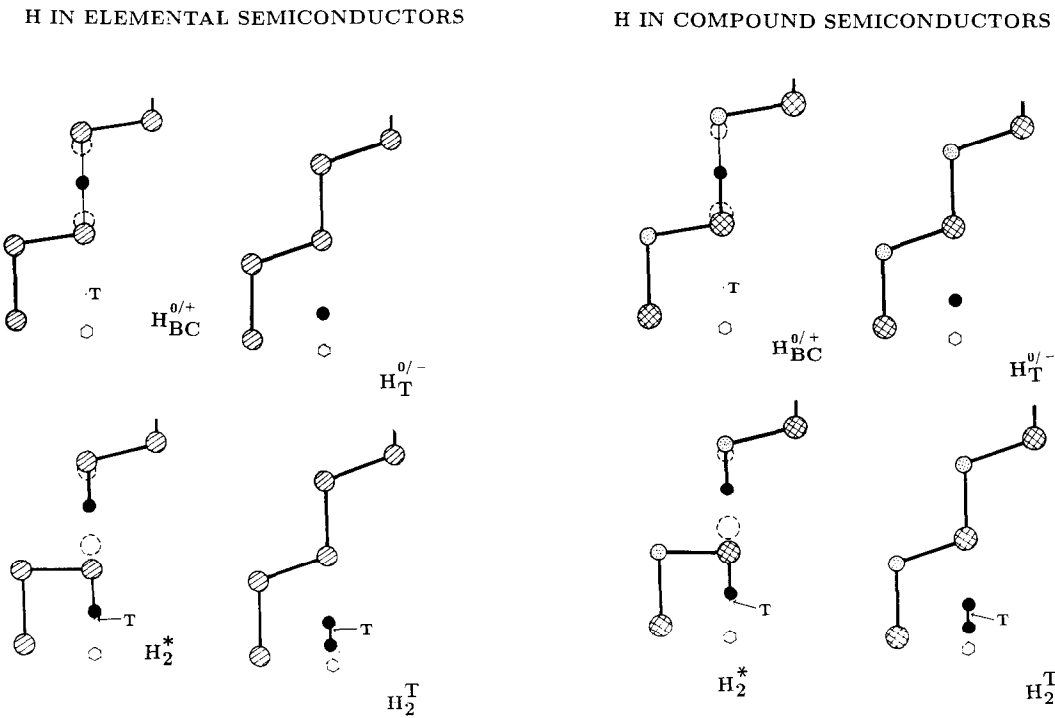


Fig. 9. Possible configurations in the {110} plane for isolated H and hydrogen pairs in elemental and compound semiconductors (see text). Note that in compounds, the T site needs an index to specify which of the two sites is involved. The possible charge states are indicated, except for the pairs which are always neutral. The dashed and dotted circles are host atoms, and the filled circle is H. The dashed circles show the unrelaxed lattice sites. T shows the location of the tetrahedral interstitial site, and the hexagonal interstitial site is marked with a small hexagon. The thick lines represent strong bonds (essentially 2-electron bonds), and thinner lines show weaker (covalent) overlap, such as one-electron bonds.

The two main features of these trends are the following. First, as one goes down the Periodic Table, the lattice constant increases. Thus, the free volume available at (near) the T site increases, which stabilizes H_T and H_2^T . This also makes it easier to relax the lattice and form H_{BC} , but this is a major factor only when going from c-C to Si. In Si and beyond, near-optimal bond lengths in the bridged bond seem to be easily realized. Second, as one goes from diamond to tin, the bond strengths involving H decrease. Compare for example the bond strengths in molecules [111]: H-CH₃, 4.54 eV; H-SiH₃, 3.98 eV; H-GeH₃, 3.60 eV; and H-Sn(n-C₄H₉)₃, 3.20 eV. These numbers suggest that the stability of both H_{BC} and H_2^* decreases as one goes down the Periodic Table.

2.1.1. Diamond

The behavior of H appears to be simpler in diamond than in any other semiconductor. All the direct experimental evidence comes from μ SR, and the results have a rather straightforward interpretation. At low temperatures (see Table 1), most muons form either Mu_T^0 ($\sim 70\%$) or Mu_{BC}^0 ($\sim 23\%$). The non-paramagnetic fraction (μ^+) does not play a dominant role, even at high temperatures. Mu_T^0 must be localized at the T site (or rapidly rotating around a single T site [112]) because its hf tensor is isotropic and the low depolarization rate implies a non-diffusing impurity. In the range 500–700 K, it converts to M_{BC}^0 with an activation energy [77] of the order of 0.5 eV. This is the energy difference between the top of the barrier separating the T and BC sites and the vibrational energy

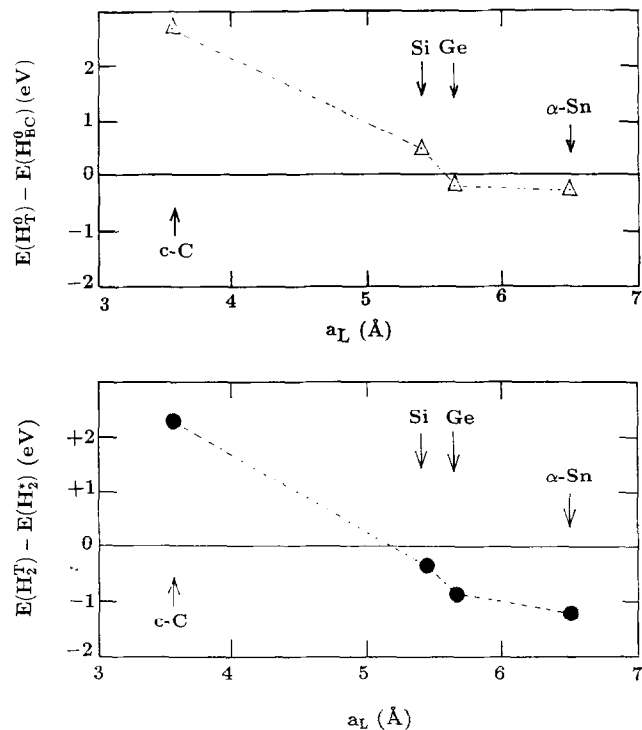


Fig. 10. Relative stability of H_T and H_{BC} , and H_2^T and H_2^0 in elemental semiconductors vs. the lattice constant. The trends shown are the results of ab-initio HF calculations in molecular clusters (see text). The figures are from Refs. [109,110] with permission.

of the muon in the potential well at the T site. For a muon, this vibrational energy may be far above the actual minimum, especially since the curvature of the potential well is large (large energy differences combined with a small lattice constant). Thus, a heavier impurity such as a proton will experience a higher barrier.

The anisotropic Mu_{BC}^0 center is seen up to 1 080 K, the highest temperature at which the Zürich group dared to study the 46 carat ‘Maltese Cross’ diamond [105]. This indicates that the (+/0) level associated with H at the BC site is sufficiently deep below the CB to prevent thermal ionization. Further, Mu_{BC}^0 does not diffuse in the microsecond time scale at these temperatures (this would result in a reduction in the anisotropy). There is no indication that either Mu_{BC}^+ or Mu_T^- are abundant at any temperature. However, this result is only relevant for short-lived species in undoped samples. The equilibrium state cannot be obtained from μ SR experiments. A dependence of the Mu_T^0 relaxation rate on the nitrogen content was reported [77].

The early theoretical work [23,113–115] did not include the BC site which was first identified in 1986, and the potential energy surfaces obtained before then were incomplete. The T site was proposed to be a local minimum of the total energy at the ab-initio UHF level [23,113,115] and the H site with the semiempirical method of CNDO [114].

The first total energy calculations that included a relaxed BC site were obtained independently by Claxton et al. [93] in a small cluster with ab-initio UHF, and by Estle et al. [94] in larger clusters with the PRDDO method. The predictions of both groups are similar. A relaxation of the C–C bond by about 40% allows H to form a bridged bond. This is the stable configuration for isolated H in diamond, and has all the features required

to explain the anomalous muonium data. There is a large barrier separating the T and BC sites.

A summary of the results of total energy calculations obtained by various groups is in Table 2. There is general agreement that H_{BC}^0 is stable and much lower in energy than any other state of isolated H^0 . There is also agreement that the activation energy for diffusion is very high, making H^0 a slow diffuser at best. The main disagreement deals with the mechanism for diffusion.

In Refs. [23,115,117], the diffusion involves H_T^0 and T–H–T paths, while Ref. [118] predicts a comparable activation energy but for direct BC to BC migration of H_{BC}^0 via a site near C. Using the atomic superposition and electron delocalization molecular orbital (ASED-MO) method in large clusters, Mehandru et al. [119] also studied the migration properties of H^+ and H^- . They find that all the charge states of H are stable at the BC site only, with little difference in the equilibrium configurations. The C–H bond lengths in the C–H–C bond are 1.07 Å, 1.11 Å, and 1.13 Å for H_{BC}^+ , H_{BC}^0 , and H_{BC}^- , respectively. All three species diffuse directly from BC site to BC site in the {110} plane, via a site near C, with activation energies of 0.1 eV (for H^+), 1.9 eV (for H^0), and 2.5 eV (for H^-). The very low activation energy for H^+ suggests a highly mobile impurity, and assumes that the C–C bonds in the diamond lattice are able to relax fast enough to allow adjacent BC sites to become minima of the potential energy as H^+ jumps. This issue will need to be settled by MD simulations at high temperatures. If the MD simulations in Si (see below) are any guide for c-C, the diffusion mechanism may involve both (T and BC) configurations.

It is worth mentioning that even though the C–C bond relaxes by some 40% to accommodate H, the resulting C–H bond length in the bridged bond is not longer than 1.10 Å, i.e. virtually equal to that of a normal two-electron bond. When bridged bonds occur in free radicals, the bond lengths in the bridged bond are substantially longer (typically 15%) than in the corresponding two-center bonds. Thus, in diamond, H barely fits in the C–C bond. It is therefore not surprising to see how much energy is needed to insert H^{free} into diamond at the BC site: this energy is estimated at 7.4 eV in Ref. [95] (see Fig. 10) but only at 1.7 eV in Ref. [118].

As discussed in Refs. [94,95], the force constant for H_{BC}^0 along the C–H–C bond is about six times larger than perpendicular to it, suggesting the H_{BC}^0 vibrates primarily in the nodal plane. The vibrational frequencies of H_{BC}^0 have been calculated at the LDF level

Table 2
Potential energy surface calculations for H^0 in diamond

Author [Ref.]	Relax. (%)	$E(H_T^0)$	$E(T \rightarrow BC)$	Diffusion	
				Path	E_a
Claxton et al. [93] ^a	39	1.0	1.9		
Estle et al. [94,95] ^b	41	2.7	<2.4	T–H–T	2.1
Briddon et al. [116] ^c	43	1.9			
Mehandru et al. [118] ^d	43	no min.	5.3	BC–BC	1.9

Relax., the relaxation of a C–C bond needed to form H_{BC}^0 . The zero of the energy is for the relaxed BC configuration. All the energies are in eV.

^a Ab-initio HF, $C_{10}H_{16}$ cluster.

^b PRDDO, $C_{44}H_{42}$ cluster; 1st and 2nd NNs to the BC and T sites relaxed; E_a is from Refs. [23,115]; $E(H_T^0)$ calculated at the ab-initio level also gives 2.7 eV (see Refs. [109,110]); see also Ref. [117].

^c LDF, $C_{26}H_{30}$ cluster; 1st and 2nd NNs to the BC site relaxed.

^d Semiempirical ASED-MO method, $C_{46}H_{48}$ cluster.

Table 3

Hyperfine and superhyperfine contact (ν_c) and dipolar (ν_{dip}) frequencies at Mu_{BC}^0 and at a neighboring ^{13}C nucleus in diamond compared with the experimental data. The frequencies are in MHz

Author [Ref.]	Hyperfine		Superhyperfine	
	ν_c	ν_{dip}	ν_c	ν_{dip}
Hoshina et al. [120] ^a	-137	400		
Vogel et al. [121] ^b	-1030	130		
Casarini et al. [122] ^c	-154	483	50	117
Paschedag et al. [123] ^d	-215	280	92	52
	-145	194	90	51
Experiment [124] ^e	-206	187	127	46

^a Local spin DF/Green's function with an (assumed) 42% relaxation of the C-C bond.

^b Ab-initio UHF calculation int he C_8H_{18} cluster with a double-zeta basis set and polarization functions on selected atoms.

^c Local spin DF in the C_8H_{18} cluster. The numbers shown are the ones obtained at the highest level of theory.

^{d,e} Ab-initio UHF calculation with a polarized double-zeta basis set followed by a limited CI treatment in the C_8H_{18} cluster. The values obtained before ^d and after ^e averaging over the spread of the muon wavefunction are given.

by Briddon et al. [116]. They determined 3132 cm^{-1} and 1230 cm^{-1} for the stretch and wag modes, respectively. The high value of the stretch mode is consistent with an unusually stiff bridged bond.

The contact and dipolar hf (at the proton or muon) and shf (at a ^{13}C NN) frequencies have been calculated at various levels of theory. Table 3 gives the calculated and experimental values. The large basis set ab-initio ROHF calculations followed by a limited configuration interaction (CI) expansion predict [123] values remarkably close to the experimental ones, despite the use of the small $\text{MuC}_8\text{H}_{18}$ cluster. This is because, in diamond, 92% of the odd electron resides [124] on the NN to the muon. In Si, this electron is substantially more delocalized.

Theorists have also predicted the consequences of H-H interactions. Briddon et al. [116] were the first to suggest, on the basis of LDF calculations, that the H_2^T molecule dissociates and forms a new defect (Fig. 9) at a gain of 3.32 eV. This dimer, labeled H_2^* by Chadi a year later [125], was predicted to be more stable than two H_{BC}^0 dimers by some 3.5 eV (if on adjacent sites) and 2.0 eV (if on second-adjacent sites). Using the semiempirical ASE-MO method, Mehandru et al. [118] obtained a similar value, 1.5 eV, for the energy difference between H_2^* and two isolated H_{BC}^0 centers. The greater stability of H_2^* over H_2^T by about 2.2 eV is also predicted by ab-initio HF (as well as PRDDO) calculations [109,110], as shown in Fig. 10. Note that the H_2^* pair should be IR active, but has not yet been observed in diamond.

2.1.2. Silicon

Fig. 10 shows that the situation is much less clear in Si than in diamond. Indeed, H_T and H_{BC} are within a few tenths of an eV of each other, as are H_2^T and H_2^* . Many of the approximations in total-energy calculations can affect the result by such an amount: cluster or cell size, basis set (size and quality), amount of relaxation allowed, weather, etc. Further, the question of charge states is critical because ionization energies are of the order of a few tenths of an electronvolt as well. As a result, theorists agree to disagree on the existence and nature of metastable and charged states, diffusion paths, activation energies, and other properties of hydrogen in Si. However, a consensus has been reached on a number of issues.

Much more experimental information is available in silicon than any other semiconductor. Data were obtained from EPR, DLTS, μ SR, and IR spectroscopy. Indirect information is also extracted from changes caused by H in the electrical activity of dopants. As will be discussed in Section 3, these experiments do not always have a unique interpretation. After discussing the most recent experimental information, I will summarize the theoretical predictions.

2.1.2.1. Overview of the experimental situation

Conventional μ SR experiments [77] (see Table 1) show that at low temperatures and in high resistivity Si, 61% of incoming muons form Mu_T^0 , 37% Mu_{BC}^0 , and the rest μ^+ . The rapid depolarization rate of Mu_T^0 implies that this species is highly mobile, even at very low temperatures. Around 200 K, Mu_{BC}^0 ionizes and the μ^+ intensity increases correspondingly. A $\text{Mu}_T^0 \rightarrow \text{Mu}_{BC}^0$ transition was first reported in irradiated samples [126]. More about the thermally-induced transitions between muon states and the nature of the non-paramagnetic μ^+ state(s) in high resistivity and doped samples has recently been obtained from integral μ SR measurements and is discussed below.

A critical confirmation that muonium experiments are indeed relevant to hydrogen was provided by the observation in 1987 of an EPR center [86] labeled AA9. Once scaled by the ratio of the hydrogen to muon nuclear magnetic moments, the hf tensors of AA9 and Mu_{BC}^0 match very closely [87,88], even though the EPR center was observed under intense illumination in samples implanted with rather high-energy protons (~ 20 MeV).

The identity of AA9 was later confirmed [127], and a combination of EPR and DLTS experiments have shown [127,128] that AA9 can be associated with a DLTS donor center [129] labeled E3'. It has a (zero-field) level at $E_c - 0.16$ eV, which is the (0/+) level of isolated H_{BC} . The experiments were carried out in high-resistivity n-type (P-doped) FZ-Si. These are not only the first direct observations of interstitial H in a semiconductor, but also the first demonstration of its electrical properties.

Isochronal annealing studies [127,128] of E3' exhibit a number of interesting features. Zero-bias annealing at 100 K for 5 min makes the E3' signal disappear. The rate, $3 \times 10^{12} \exp\{-0.29 \text{ eV } (kT)^{-1}\} \text{ s}^{-1}$, suggests an atomic jump. This reaction is reversible by cooling while injecting minority charge carriers. A possible interpretation for the disappearance of the DLTS signal is the sequence $\text{H}_{BC}^0 \rightarrow \text{H}_T^0$ (thermally induced) followed by $\text{H}_T^0 + e^- \rightarrow \text{H}_T^-$. The reverse reaction would involve hole capture: $\text{H}_T^- + h^+ \rightarrow \text{H}_T^0 \rightarrow \text{H}_{BC}^0$. The time scale is sufficient to insure that the barriers between the T and BC sites can be overcome. After the first cycle, only two-thirds of the E3' center are recovered and a new donor appears, called E3''. This new center is likely to be a bistable {X, H} complex, which saturates after the first cycle, since subsequent cycling does not affect the intensity ratios of the E3' and E3'' defects.

The identity of the E3'' center is not known. However, it is possibly associated with either the dopant or substitutional C, since both form pairs with H and both pairs could be bistable (see Refs. [130–132] for {P, H} and Refs. [133,134] for {C, H}). In any case, the fact that the {X, H} trap saturates after the first cycle suggests that neither H_{BC}^0 nor H_T^- are very mobile, since centers located further away from H would become traps as well, resulting in a continuous decrease of the E3' intensity with the number of anneal/recovery cycles. A second and irreversible anneal of the E3' center occurs at 200 K. The rather slow rate, $\sim 10^8 \exp\{-0.44 \text{ eV } (kT)^{-1}\} \text{ s}^{-1}$, implies that H is diffusing.

There is a strong correlation between the properties of the E3' center and those of bond-centered muonium observed by r.f.- μ SR [85]. This technique allows one to monitor the intensity of the various μ SR centers and their transitions as a function of temperature, as long as they do not undergo charge and site changes at the sub-microsecond time scale [98,99]. The reader should consult Refs. [85,99] for details. The main results are the identification of the non-paramagnetic μ^+ centers, their thermally induced transitions, and several energy and capture parameters. Fig. 11 shows the temperature dependence of the μ^+ intensity in intrinsic, p-type (B-doped, $\sim 10^{14} \text{ cm}^{-3}$) and n-type (P-doped, $\sim 10^{15} \text{ cm}^{-3}$) FZ-Si.

In intrinsic Si, the low T fractions are 0.46 (Mu_T^0), 0.40 (Mu_{BC}^0), and 0.03 (μ^+). The fractions quoted do not add up to 100% because of muons lost in the cryostat and of the error bars on each number. A sharp increase in the initial ($T=0$) μ^+ fraction near 135 K corresponds to the thermal ionization $\text{Mu}_{\text{BC}}^0 \rightarrow \text{Mu}_{\text{BC}}^+ + e^-$. There is no more Mu_{BC}^0 at 200 K (the shoulder around 180 K is caused by the anisotropy of the center, as shown in the Appendix in Ref. [99]). The best-fit energy value for this process is 0.22 eV. Since there is little difference in the relaxation of the crystal upon ionization of hydrogen at the BC site [117], this value should be very close to the total energy difference between Mu_{BC}^+ (with an electron in the CB) and Mu_{BC}^0 , i.e. the (0/+) energy level associated with Mu_{BC} should be near $E_c - 0.22$ eV. The gradual increase in the μ^+ intensity in the 200–300 K range is owing to the sequence $\text{Mu}_T^0 \rightarrow \text{Mu}_{\text{BC}}^0$ followed by the immediate ionization of the

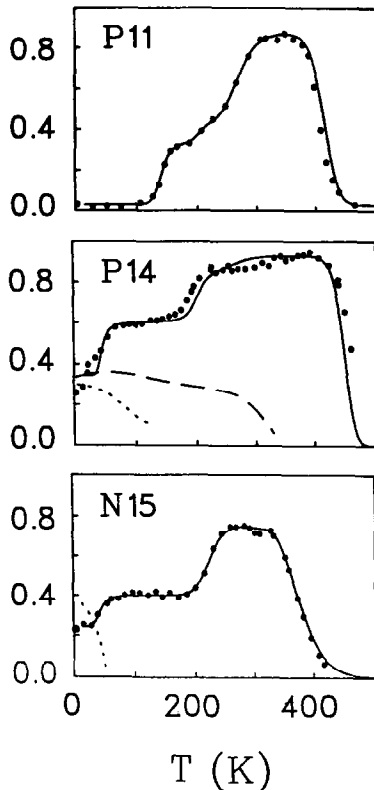


Fig. 11. Experimental r.f.- μ SR data (points) and fits (lines). The (normalized) amplitude of the non-paramagnetic μ^+ signal vs. temperature in intrinsic (B-doped, 10^{11} cm^{-3} , labeled P11), p-type (B-doped, 10^{14} cm^{-3} , labeled P14), and n-type (P-doped, 10^{15} cm^{-3} , labeled N15) silicon (see text). The figures are from Ref. [99] with permission.

BC species. The best fit for the T-to-BC barrier is 0.39 eV. This is the energy difference between the top of the potential barrier and the zero-point energy of the muon in the Mu_T^0 state. Because of the difference in mass between the muon and the proton ($m_p \approx m_\mu/9$), the zero-point energy of a proton in the same potential well is below that of a muon. As a result, a proton experiences a higher potential barrier than a muon, by an amount (at least 0.1 eV) which depends on the shape of the potential surface.

The drop in the μ^+ intensity which begins near 380 K can be modeled by a site and charge cycle involving Mu_{BC}^+ and Mu_T^0 . Longitudinal-field μ SR studies [135] above 450 K confirm that the rapidly-relaxing species is Mu_T^0 . The data imply an activated capture process, $\text{Mu}_{\text{BC}}^+ + e^- \rightarrow \text{Mu}_T^0$, with energy 0.38 eV.

In p-type material, the fractions at low T are 0.07 (Mu_T^0), 0.50 (Mu_{BC}^0), and 0.33 (μ^+). The increase in the μ^+ fraction below 50 K is caused by an interaction between Mu_T^0 and the B dopant. While the details are unknown, the candidates include the charge exchange process $\text{Mu}_T^0 + B^0 \rightarrow \text{Mu}_{\text{BC}}^+ + B^-$ and the formation of the {Mu, B} pair. The sharp increase in the μ^+ amplitude at 50 K coincides with the thermal ionization of the dopants and is caused by the hole capture process $\text{Mu}_{\text{BC}}^0 + h^+ \rightarrow \text{Mu}_{\text{BC}}^+$. The gradual increase near 200 K is owing to the remaining Mu_T^0 species converting to Mu_{BC}^+ . However, since the increase in the low-temperature μ^+ fraction comes at the expense of Mu_T^0 , there are few of them left at 200 K. Above room temperature, the loss of the non-paramagnetic signal is owing to the same site and charge cycle as in intrinsic samples, except that the onset temperature slightly increases with the acceptor concentration.

In n-type material, the low T fractions are 0.17 (Mu_T^0), 0.69 (Mu_{BC}^0), and 0.24 (μ^+). The increase in the μ^+ fraction is again caused by interactions between the donor and Mu_T^0 , possibly Mu_T^- near a P⁺, or a {Mu, P} pair. The step near 50 K coincides with the ionization of the donor and corresponds to the electron-capture process $\text{Mu}_T^0 + e^- \rightarrow \text{Mu}_T^-$. The temperature at which this step occurs always coincides with the temperature at which the donor ionizes (P, As, and Sb have been tried). The increase in the μ^+ intensity corresponds to a decrease in the Mu_T^0 intensity, while the Mu_{BC}^0 intensity remains unchanged. Above 100 K, all the Mu_T^0 has converted to Mu_T^- . The Mu_{BC}^0 center remains present up to 200 K, but the muon spin is depolarized by electron scattering. The sharp increase just above 200 K is caused by the activated process $\text{Mu}_{\text{BC}}^0 + e^- \rightarrow \text{Mu}_T^-$, which has the prefactor $1.6 \times 10^{13} \text{ s}^{-1}$ and the energy parameter 0.34 eV. Above 350 K, this process competes with the T-to-BC site change and subsequent ionization to form Mu_{BC}^+ . The loss of the signal above 400 K is again owing to the site and charge-change cycle reported for intrinsic and p-type samples.

Fig. 12 contains the various energy parameters relevant to the transitions observed. These energies can be compared with those obtained from the DLTS studies [129] discussed above. Small differences could be owing to the difference of mass between the proton and the muon. The energies identified by r.f.- μ SR (with the corresponding DLTS energies in parentheses) are $E_{\text{BC}}^{0/+} = 0.22 \pm 0.01$ eV (0.16 ± 0.01), $E_{\text{T/BC}}^0 = 0.39 \pm 0.04$ eV, $E_{\text{BC/T}}^{+/0} = 0.38 \pm 0.06$ eV (0.44 ± 0.01), and $E_{\text{BC/T}}^{0/-} = 0.34 \pm 0.01$ eV (0.29 ± 0.01). No solid number has yet been obtained for the (-/0) gap level associated with Mu_T . A crude estimate places this level somewhat deeper than $E_c - 0.4$ eV, which would support the predicted [26] negative-U property of hydrogen in Si.

Note that for both p- and n-type samples, the initial Mu_T^0 fraction is reduced and the Mu_{BC}^0 fraction increased. This is most likely related to a decreased mobility of Mu_T^0 caused by the presence of dopants in the sample, and resulting in Mu_T^0 having more time to access

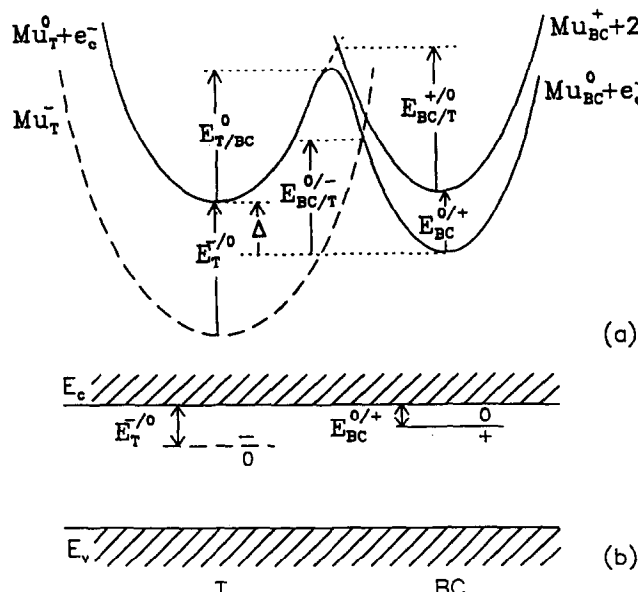


Fig. 12. Schematic potential-energy diagram for the various states of isolated muonium in Si, (a) and energy levels in the gap associated with the BC and the T sites (b). Mu_T^- is only seen in n-type samples, but the other three centers exist for any type of doping. The energies shown are listed in Table 4. The figures are from Ref. [99] with permission.

a BC site. Further, these experiments clearly show that the diffusion of hydrogen-like species in Si above room temperature always involves more than one site and more than one charge state. In intrinsic and p-type Si, the states are Mu_{BC}^+ , Mu_{BC}^0 , and Mu_T^0 . The three dominant states in n-type Si are Mu_T^- , Mu_T^0 , and Mu_{BC}^0 below 320 K (the crossover temperature depends on the concentration of dopants), while the ionized state is Mu_{BC}^+ above that temperature, just as in the p-type samples.

Recent longitudinal field μ SR experiments [136] confirm the results of the above-mentioned r.f.- μ SR studies, that in P-doped Si crystals ($\sim 5 \times 10^{14} \text{ cm}^{-3}$), Mu_{BC}^0 does not convert to Mu_T^- up to at least 200 K.

Finally, lattice location experiments based on the nuclear reaction $D(^3\text{He}, p)^4\text{He}$ were performed. Picraux and Vook [137] found a unique position of the implanted deuterium at the AB site, 1.6 Å from a Si atom along a $\langle 111 \rangle$ direction, which could be owing to a secondary minimum of the potential surface, to a D-impurity pair, to a D_2 molecule, or be damage-related. A subsequent channeling study by Bech Nielsen, [138] with more control over implantation damage, found over 80% of the deuterium slightly off the BC site (0.2 Å in a $\langle 110 \rangle$ direction), the rest originating 0.2 Å away from the T site. Note that a fraction of the signal could have originated from D_2^* centers, a possibility not considered in the initial interpretation of the data.

2.1.2.2. Theoretical predictions for isolated H

Prior to the first calculations which included the relaxed BC site, [94,96] theoretical work on hydrogen in Si was limited to the unbound H_T species and the H_2^T molecule. Approximate total energy studies placed H_T^0 at the T site (EHT [17,18]), the AB site (pseudopotential Green's functions [139] and tight-binding approximation [140]), and the M site (MNDO in clusters [141]). Very shallow profiles were reported at the CNDO level [114].

The predictions for potential surfaces which include the BC site are summarized in Table 4. Consensus has been reached that H^+ can only be stable at the BC site, and that H^- is in the low electron density region of the crystal, most likely at the T site. There is (almost) uniform agreement that H^0 is metastable, with the stable state being H_{BC}^0 . Note that this is unambiguously implied by the μ SR results discussed above. A number of areas of disagreement remain. The precise location of the metastable state (H_T^0) is not agreed upon, except that it must be rapidly diffusing in the low-density region of the crystal, and that it is only a few tenths of an electronvolt less stable than H_{BC}^0 (at 0 K). More importantly, there is no consensus (to say the least) regarding the diffusion paths and activation energies of the various charge states of hydrogen in Si. This does not come as a surprise because: (i) all the methods used to obtain static potential energy surfaces are designed to calculate minima rather than saddle points of the energy; and (ii) one can only guess how much the host crystal is able to relax while the light H interstitial moves through it.

The stretching frequency has been calculated for H_{BC} . The values 2203 cm^{-1} [148] and 2210 cm^{-1} [27] have been obtained for H_{BC}^+ , and 1708 cm^{-1} [148] and 1945 cm^{-1} [27] for H_{BC}^0 . The latter value is close to the (preliminary) result of a tight-binding MD simulation [149]. These frequencies are high for hydrogen in a bridged bond, indicating that the crystal cannot relax around H_{BC} as much as it would in a free radical. Note that removing the odd electron from H_{BC}^0 strengthens the bond as one would expect, since the odd electron resides primarily in an antibonding sp^2 -type orbital (populating an antibonding

Table 4
Potential energy surface calculations for H in silicon

Author [Ref.]	H^0		H^+	H^-	Diffusion	
	Stable	Metastable (ΔE)			Path	E_a
Estle et al. [94] ^a	BC	T (0.3)				
Estreicher [96,117] ^b	BC	T (0.3)	BC		H^0 : T-H-T	0.59
Deák et al. [142–144] ^c	BC	AB (0.9)	BC	AB	H^0 : BC-M-BC	0.8
						0.43
Van de Walle et al. [26,27] ^d	BC	none	BC	T	H^{+0} : BC-C-BC	<0.2
					H^- : T-H-T	0.25
DeLeo et al. [145] ^e	BC	—	BC		H^0 : BC-BC ⁺	1.0
Chang et al. [125,146] ^f	T	BC (0.25)	BC	T	H^+ : BC-C-BC	
					H^- : T-H-T	
Jones [147], Briddon et al. [148] ^g	BC	AB (0.1)	BC	T	H^+ : BC-M-BC	0.4
					H^0 : BC-C-BC	0.28
					H^0 : AB-C-AB	<0.1

ΔE is the energy difference (eV) between the stable and the metastable states. The activation energy for diffusion, E_a , is also in eV. The calculated relaxation of the NN to H_{BC} are always around 35–40%.

^a PRDDO in the $Si_{44}H_{42}$ cluster. The first and second NNs to the BC and T sites are relaxed.

^b Ab-initio HF (SV* basis set) and PRDDO in clusters. The BC \rightarrow T barrier is <0.89 eV. The prediction for H^+ is from Ref. [117].

^c MINDO/3 in a 32-atom cyclic cluster. The H^- prediction is from Ref. [144], in which the authors find that H^0 is the stable state in a narrow range of Fermi level positions.

^d LDF, 32-atom supercells. The atoms are fully relaxed for all positions of H. H^+ is stable in intrinsic and p-type Si and H^- is stable in n-type material.

^e MNDO in small clusters containing no high-symmetry interstitial site other than BC. H_{BC}^0 is found to have two degenerate minima along the bond, just off and on either side of the center of the bond.

^f LFD, 180-atom supercell. H^+ is stable in intrinsic and p-type Si and H^- is stable in n-type material.

^g LDF in a $Si_{51}H_{52}$ cluster, Gaussian basis set.

orbital always weakens the bond index). The H_{BC}^0 center is (weakly) IR active for asymmetric oscillations of the Si NNs to H.

Experimentally, the diffusion properties of H and the state of the diffusing species are also unknown. The μ SR data imply that Mu_T^0 is highly mobile (rapid depolarization of the muon spin) and that Mu_{BC}^0 is not (anisotropic hf tensor). The latter comment holds for H_{BC}^0 as well, since the AA9 center is also highly anisotropic. This suggests that even though the BC species is easily kicked out of the BC site by phonons at or above room temperature, direct BC-to-BC motion is an unlikely event for both H_{BC}^0 and H_{BC}^+ , except perhaps at very high temperatures. This is intuitively consistent with the fact that a Si-Si bond must relax by 35–40% to accommodate H_{BC} , and a relaxation is likely to occur in a time scale longer than one would associate with the jump of a particle as light as a proton.

Three MD simulations have examined the high-temperature diffusion properties of hydrogen in silicon. The first [150] was a first-principles LDF treatment of H^+ in a 128-atom supercell in the range 1 000–1 950 K. The other two [73,151] were tight-binding MD simulations of H^0 in a 64-atom supercell (in Ref. [73], cell-size effects have been checked up to 512 atoms), in the temperature range 1050–1675 K [73] and 800–1800 K [151]. Both tight-binding MD simulations were extended to over 100 000 time steps. Despite using different techniques and involving a different charge state of hydrogen, the qualitative predictions of all three calculations are very similar and in full qualitative agreement with the picture emerging from the recent r.f.- μ SR experiments.

The authors in Refs. [73,150] describe the diffusion as jump-like, with H vibrating at the BC site for many time steps, then suddenly jumping to the low-density region of the crystal and diffusing rapidly, then self-trapping again at another BC site. Direct diffusion between adjacent BC sites occurs at high temperatures. This is illustrated in Fig. 13, which shows a trajectory for H^0 at 1 050 K. The calculated activation energies are 0.33 ± 0.25 eV [150] and 0.45 eV [73] with prefactors 9.4×10^{-3} and $6.9 \times 10^{-3} \text{ cm}^2 \text{ s}^{-1}$, respectively. Both numbers are quite close to the diffusivity measured at high temperatures by Van Wieringen and Warmoltz [152], $2 \times 10^{-4} \exp\{-0.48 \text{ eV } (kT)^{-1}\} \text{ cm}^2 \text{ s}^{-1}$. The activation energy should be interpreted as the barrier to overcome to leave the BC site rather than the T \rightarrow H \rightarrow T potential barrier. Note that this number is conspicuously close to that deduced for the BC \rightarrow T activation energy from the r.f.- μ SR and DLTS experiments discussed above.

The results of the third MD simulation [151] are qualitatively similar, with the unexpected result that at low temperatures, the BC and H sites are minima of the potential surface,

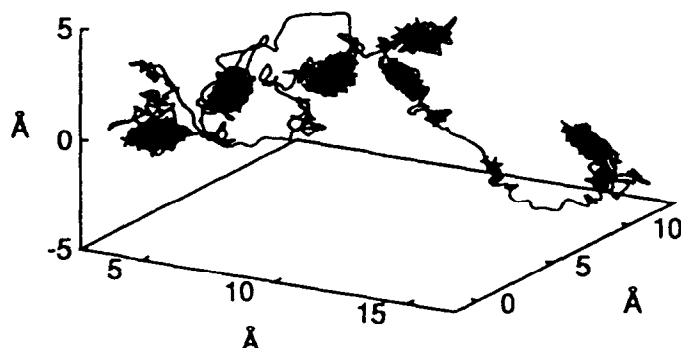


Fig. 13. H trajectory calculated at 1 050 K by Boucher and DeLeo [73]. The picture shows that H^0 self-traps for long times at BC sites, and occasionally jumps to the low-density region of the crystal where it diffuses rapidly.

within less than 0.1 eV of each other. The M, T, and C sites are reported to be several tenths of an electronvolt higher. With the exception of a CNDO calculation [114], no author has found the H site to be a minimum of the energy. This site is in conflict with the μ SR data.

MD simulations as well as μ SR experiments suggest that the diffusion of H at high temperatures involves more than one state: very rapid diffusion in the low-density region of the crystal (H_T) interrupted by self-trapping in the high-density region of the crystal (as H_{BC}^0 and/or H_{BC}^+), with the possibility of direct BC-C-BC hopping at high T. The net diffusivity at a given temperature would correspond to an average over the amount of time spent in each state. One would expect a dependence on the dopant concentration, especially in n-type material, since the greater availability of free electrons would favor H_T^- formation, which has a larger ionic radius than H_T^0 and therefore could diffuse slower. A first-principles calculation of the diffusion coefficient of H^+ based on a static potential surface has been proposed [153]. The calculation involves direct $BC \rightarrow C \rightarrow BC$ motion, and produces a diffusivity comparable to the high-temperature experimental number.

Experiments illustrating electric-field enhanced diffusion of hydrogen, especially well documented in p-type Si (see, for example, Ref. [154]), can be interpreted in terms of H_{BC}^+ alone. However, if more than one state of H is involved in the diffusion, an alternative picture is possible: H_{BC}^+ jumps off a BC site along field lines, captures an electron and diffuses as H_T^0 , self-traps at another BC site where it ionizes, and experiences the field again.

As the temperature decreases, the diffusivity of hydrogen is reduced because trapping at impurities or defects occurs. These reactions depend on the concentration of impurities and probably on the history of the sample. The trapping of hydrogen at various impurities and defects will be discussed in the next section. As concerning the diffusion of hydrogen in various types of Si samples, the topic has been the subject of an extensive and excellent review in a recent book [4] which includes a detailed discussion of diffusion equations.

In addition to the complicated diffusion of interstitial H, two different mechanisms have been suggested, and each of them might play a role under particular circumstances. First, Chang and Chadi proposed [125] that the H_2^* dimer is mobile. As will be discussed below, there is direct experimental evidence [155] that this defect exists, but no direct evidence that it is mobile (or immobile). It is likely that MD simulations will prove or disprove the mobility of this pair. Second, Corbett et al. [156] and, more recently, Sopori et al. [157–160] have proposed that vacancy-hydrogen complexes might be mobile. This suggestion was based on the modeling [156] of SIMS profiles after (deuterium) plasma exposure, and to explain the enhanced diffusivity of H in (vacancy-rich) poly-Si [157–160]. A recent static potential energy calculation [41] supports the mobility of the {V, H} pair in the 0 and +1 charge states, but there is no direct evidence of this happening. Ongoing MD simulations [161] indicate that this process is more complicated than initially claimed [41].

Table 5 compares the results of the calculations of hf and shf parameters with experiment for both H_{BC}^0 and H_T^0 (assumed to be at the T site). The agreement is sufficiently convincing as to leave little doubt that the defect centers studied by theory and experiment are indeed one and the same. Note that ab-initio HF and PRDDO calculations for Mu_T^0 [96] predict Fermi contact densities larger than the free atomic value. The wavefunction associated with a localized Mu_T^0 (or H_T^0) has a node between the muon and its Si NNs, resulting in the electron piling-up on the nucleus. A decrease in the spin density results from the rapid

Table 5

Hyperfine and superhyperfine contact (ν_c) and dipolar (ν_{dip}) frequencies for Mu_{BC}^0 , its first and second ^{29}Si nearest neighbor, and for Mu_T^0 (assumed to be at the T site), in silicon, compared with the experimental data. The frequencies are in MHz.

Author [Ref.]	Mu_{BC}^0		Si_{NN}		Si_{NNN}		Mu_T^0
	ν_c	ν_{dip}	ν_c	ν_{dip}	ν_c	ν_{dip}	ν_c
Katayama-Yoshida et al. [162] ^a							1812
Estreicher [96] ^b	−624						4597
Kuten et al. [163] ^c	−661	52					3827
Vogel et al. [121] ^d	−670	47					
Casarini et al. [122] ^e	−104	117	−127	−57			3043
Van de Walle et al. [64] ^f	−35	22.3	−85	−21.5	−23	−0.6	2187
Experiment [88]	−67.3	25.3	−95.1	−21.2	−22.4	−0.9	2006

^a Green's function LCAO.

^b Ab-initio HF and PRDDO in clusters.

^c CNDO and INDO calculations in clusters.

^d Ab-initio UHF calculation with a polarized double-zeta basis set in small clusters. The frequencies are averaged over the spread of the muon wavefunctions.

^e Spin LDF in small clusters.

^f Local spin DF in supercells.

motion of the impurity, especially toward AB sites, allowing the 1s wavefunction to overlap positively with the host crystal. This possibility, first proposed by Cox and Symons [91,92], has been investigated theoretically [164]. However, the results of recent spin LDF calculations [64] of hf and shf parameters with Mu_T^0 localized at the T site reproduce remarkably well the experimental results, suggesting that any corrections owing to the rapid diffusion of the muon are very small. This also suggests that the 1s wavefunction of H has a positive (bonding) overlap with the Si host.

Additional theoretical work related to isolated H in Si includes the mass-dependent quantum effects [165] arising when going from muonium to hydrogen and deuterium. The interactions of H with imperfect Si–Si bonds have also been studied [166,167].

2.1.2.3. The negative-U question

Interstitial hydrogen has been predicted to exhibit negative-U properties on the basis of first-principles LDF calculations [26,125]. This implies that, in equilibrium, two isolated H interstitials in otherwise perfect Si would form H_{BC}^+ and H_T^- rather than both remain neutral. An equivalent statement in the present context is that H must have an acceptor as well as a donor level in the gap, with the acceptor level lying below the donor level. Note that the existence of a donor level associated with H has been suggested early by a number of authors [16,168].

The evidence for the existence of the positive charge state, H_{BC}^+ has never been disputed. The non-paramagnetic μSR state, μ^+ , has historically been assumed to be a bare positive muon [77]. The ionization of Mu_{BC}^0 has since been observed in Si and other semiconductors as well. Further, the DLTS studies of the E3' center [129] also detect the ionization of H_{BC}^0 . Indirect evidence which points to the existence of a positively charged species exists as well. It includes the ease with which shallow acceptors such as B^- are passivated by hydrogen (see next section), the field-enhanced diffusion of hydrogen in p-type Si which has been reported by several groups (see, for example, Ref. [154]), or the

modeling of passivation profiles [169]. As discussed above, the donor level ($H_{BC}^{0/+}$) is at $E_c - 0.16$ eV (DLTS [129]) or $E_c - 0.22$ eV (r.f.- μ SR [99]).

On the other hand, there have been many arguments in favor and against the existence of the negative charge state. There is no direct evidence for H_T^- , although indirect evidence is mounting. The earliest donor-passivation experiments [170,171] resulted in much smaller passivation fractions than was the case for acceptors. The Coulomb attraction between a positively charged donor and a rapidly diffusing H_T^- species should result in easily achieved and complete passivation. However, since the donor-hydrogen pair has H bound to a Si atom at the AB side, a bond weaker than the BC-like configuration of acceptor-hydrogen pairs, it is also possible that the lower passivation fraction results from the weaker bond. The modeling of the μ^+ intensity distribution vs. temperature in n-type material implies [98,99] the existence of Mu_T^- , although many details remain to be established. An estimate of the (-/0) level of Mu_T is deeper than $E_c - 0.4$ eV.

Field-enhanced diffusion of hydrogen reported in Sb-doped [172] and P-doped [173] silicon is a strong indication that H is negatively charged at least some of the time. Note that it is a priori also possible to interpret these data assuming that the debonding of donor-hydrogen pairs occurs more readily in the depletion region than elsewhere in the sample [174].

More complicated experiments use the light-enhanced reactivation of hydrogen-passivated, P-doped diodes. It is known [175,176] that donor-hydrogen pairs are thermally debonded near 100 °C. However exposure to light greatly enhances the reactivation rate of shallow donors [177,178], which can occur even at room temperature. Johnson and coworkers have assumed that the reactivation is caused by the break-up of the passivated {P, H} pair into P^+ and H^- . In a series of measurements of capacitance transients interpreted using the break-up assumption [179,180], they obtained an acceptor level for interstitial H at the midgap ($E_c - 0.56$ eV) which, according to them, corresponds to the H_T^-/H_{BC}^0 level. Combined with the $E_c - 0.2$ eV donor level, this would make H a strong negative-U center.

However, there is disagreement [181] on the interpretation of the data and on the very existence of some transients. The key source of contention is the break-up assumption. Indeed, it has been observed that the light-induced reactivation of {P, H} (and {As, H}) pairs is to a large extent reversible [132]. After light exposure, the charge density in the sample increases dramatically, and the applied bias (sometimes left on for several days) should sweep out all the charged H. However, leaving the sample at zero bias in the dark for a day or so results in the recovery of 30–80% of the passivated centers, without additional exposure to H. This implies that a substantial fraction of H remains at or near the donor, regardless of the applied field, which contradicts the break-up hypothesis. A possible interpretation of this remarkable recovery is the conversion of the passivated {P, H}⁰ pair into an electrically active {P, H}⁺ donor state under exposure to light [131,182,183]. More on donor-hydrogen centers is discussed in the next section.

2.1.2.4. Hydrogen dimers

Two kinds of H dimers exist in crystalline silicon, H_2^T and H_2^* (Fig. 9), although direct experimental evidence only exists for the IR-active H_2^* pair [155]. This type of configuration was first proposed in diamond by Briddon et al. [116], then in Si by Chang and Chadi [125,146] and Déak and coworkers [142,143]. The experimental identification, obtained in high-resistivity (n-type) Si, includes the IR stretch and wag modes of the two H's (with all

the D substitutions) and the determination of the symmetry. The defect anneals out at 200 °C. Table 6 contains a comparison of the calculated and measured IR active modes.

It has been suggested that the H_2^* pair easily dissociates under illumination [185] and that it is mobile [125]. The latter prediction relies on a path calculated by moving each H in succession while keeping the other one fixed. However, since the two Si-H bonds involved have different strengths, a competing suggestion might be that the H in the AB position breaks up first, leaving H_{BC}^0 , which may jump out of the BC site independently from the first H. There is no experimental evidence regarding the mobility of H_2^* , except that the IR spectrum indicates trigonal symmetry up to 200 °C, which suggest that the pair does not diffuse up to that temperature.

The existence of molecular hydrogen in Si (H_2^T , Fig. 9) has first been suggested by Corbett et al. [186] in 1983. Since then, many authors have included this species in their calculations and estimated its stability relative to other possible configurations, such as H_2^* or two isolated H_{BC}^0 . The results of these calculations are summarized in Table 7. There is general agreement that H_2^T exists, is at (or very near) the T site, that its barrier for rotation is very small, its activation energy for diffusion (via the H site) is large and, with one exception, that it is marginally (substantially) more stable than H_2^* (than two isolated H_{BC}^0). The areas of disagreement include the lowest-energy orientation of H_2^T and its bond

Table 6
Calculated and measured IR active modes of the H_2^* pair in Si. The frequencies are in MHz

Author [Ref.]	H_{BC}		H_{AB}	
	Stretch	Wag	Stretch	Wag
Chang et al. [184] ^a	2070	220	1480	690
Holbech et al. [155] ^b	2164	612	1844	1002
Experiment [155]	2062		1838	817

^a LDF, 18 atoms supercell.

^b LDF, $Si_{51}H_{52}$ cluster.

Table 7
Theoretical predictions for H_2^T in c-Si. The lowest-energy orientation, barrier for rotation (E_{rot} (eV)), activation energy for diffusion (E_a (eV)), bond lengths (H-H (Å)), and stability relative to H_2^* and to two isolated H_{BC}^0 's are given

Author [Ref.]	Orientation	E_{rot}	E_a	H-H	$\Delta E(H_2^*)$	$\Delta E(2H_{BC}^0)$
Corbett et al. [186] ^a	$\langle 111 \rangle$			2.7		
Mainwood et al. [114] ^b	$\langle 100 \rangle$	<0.1	0.95	0.75		2.0
Deák et al. [142,143,187] ^c	$\langle 111 \rangle$	~0	0.56		-0.49	-0.24
Van de Walle et al. [26,27,188] ^d	$\langle 100 \rangle$		1.1	0.86	0.54	1.74
Chang et al. [146] ^e	$\langle 111 \rangle$	~0		0.85	0.4	2.1
Briddon et al. [148] ^f	$\langle 100 \rangle$		>1	0.85	0.2	3.3
Jones [147], Maric et al. [109], Estreicher et al. [110] ^g	$\langle 111 \rangle$	≤ 0.1	<2	0.70	0.25	

^a MNDO, $Si_{14}H_{20}$ cluster.

^b CNDO, $Si_{30}H_{40}$ cluster.

^c MINDO/3, 32-atom supercell.

^d LDF, 32-atom supercell.

^e LDF, 18-atom supercell. In this calculation, H_{T0} is more stable than H_{BC}^0 , and $E(2H_{T0}) = 1.6$ eV.

^f LDF, $Si_{51}H_{52}$ cluster.

^g Ab-initio and PRDDO calculations in various clusters.

length, predicted to be from 15% longer to 7% shorter than the free molecule value, 0.75 Å.

Note that possible reactions leading to the formation of H_2^* include $H_{BC}^+ + H_T^- \rightarrow H_2^*$ and $H_{BC}^0 + H_T^0 \rightarrow H_2^*$ (other reactions require a change of charge state). In any case, H_{BC} is a likely precursor, since there is a barrier between the T and BC sites. The easiest reactions for molecule formation are $H_T^0 + H_T^0 \rightarrow H_2^T$ and $H_{BC}^+ + H_T^- \rightarrow H_2^T$ (with an activation energy to leave the BC site). Since the BC and T site species are abundant in Si, both dimers could occur in all but heavily doped samples. In the strong doping cases, a single-charge state of H could dominate, resulting in a Coulomb repulsion between like species and preventing pair formation.

Molecular hydrogen has never been observed in c-Si, in contrast to hydrogenated amorphous silicon [189–192]. A recent report of the EPR signal [193] that could be interpreted as a charge state of H_2^T , the NL-52 center, is most probably associated with the P_b center, a defect believed to be related to a dangling bond, and which is common at Si–SiO₂ interfaces [194,195]. While a charge state of H_2^T has been rejected as a candidate for NL-52 on a theoretical basis [110,196], the precise identification of NL-52 is not agreed upon [196,197].

2.1.3. Germanium

Ultra-pure Ge used for radiation detectors was the first material in which H was observed to alter the electrical activity of substitutional impurities [7–9]. The highest-quality crystals must be grown in a H₂ ambient which, it is believed, passivates the majority of residual deep traps in the material. As-grown, high-purity Ge has a H concentration of some 10¹⁴ cm⁻³. The most abundant substitutional impurities is C. Hydrogen interacts with it, and the {C, H} pairs are shallow acceptors. Despite the fact that Ge was the first material in which such effects were detected, much less experimental and theoretical information is available for it than Si.

However, the experimental data show qualitative differences in the behavior of H in Ge vs. Si. This is a priori surprising because not only the properties of the two semiconductors are very similar (crystalline structure, lattice constant, gap, etc.), but also the chemistry of the Si–H compounds is at least qualitatively similar to that of Ge–H compounds (type of configurations, bond strengths, etc.).

Muon spin rotation studies in Ge show that, at low temperatures, the μ_{T^0} species dominates (~72%) relative to μ_{BC}^0 (~8%) and μ^+ (~10%). Thus, far fewer of the injected muons form a BC species in Ge than in Si, despite the fact that the Ge–Ge bond is softer than the Si–Si bond and therefore should be easier to stretch. Further, no thermally-activated $\mu_{T^0} \rightarrow \mu_{BC}^0$ or $\mu_{BC}^0 \rightarrow \mu_{BC}^+$ conversion is observed. On the contrary, the rapidly diffusing μ_{T^0} species dominates the spectrum, and the μ^+ fraction is much less abundant than in Si, especially above 200 K. Muon dynamics at high temperatures in Ge are qualitatively different [198] from those in Si. Here, high refers to the onset of rapid charge and site exchanges processes, which begins around 400 K in Si (see Fig. 11) and around 200 K in Ge. The precise temperatures vary with the electron density and the electron capture rates. Details are not understood, but the processes used in the Si case cannot be applied directly to Ge.

There have been no EPR observations of paramagnetic H in Ge, and much less IR absorption data is available in Ge than in Si. However, the H_2^* pair has recently been seen [128] in proton-implanted intrinsic Ge. The implantation at room temperature produced

a H concentration in the sample of the order of 0.05 at.% at depth of 10–60 μm . The IR lines, about half as intense as in comparably treated Si samples, show the two H stretching vibrations at 1774 and 1989 cm^{-1} .

Further, the passivation of shallow acceptors or donors in Ge is not achieved under conditions that lead to almost complete passivation in Si. Only two reports of (partial) passivation of the boron acceptor in Ge have been reported [1,199], and donor passivation has never been achieved.

Finally, systematic thermal effusion (TE) experiments have been conducted in similarly doped Si, Ge, and GaAs [200]. The various samples were exposed to a deuterium plasma for 20 h at the temperature T_{pl} , then D was extracted from the crystal in a TE chamber. In addition to the information that can be extracted from the various TE peaks, one striking feature is apparent when comparing the results for similarly doped Si and Ge samples. As seen in Fig. 14, the total amount of D that can be extracted from Ge is not only one order of magnitude smaller than from Si, but also sharply decreases with T_{pl} while it increases with T_{pl} in the case of Si.

Few total energy calculations have been published for H in Ge. A semiempirical HF study at the CNDO level [201] in large clusters did not include the BC site. It was found that H_T^0 is at the AB site, and readily diffuses through the crystal with an activation energy of the order of 0.17 eV. A possible configuration for H^+ is suggested off the T site in the $\langle 001 \rangle$ direction. This calculation also finds that H_2^{T} (with an H–H bond length of 0.73 Å) is energetically more stable than two isolated H_T^0 by 2.5 eV. The activation energy for H_2^{T} diffusion is 0.73 eV.

A first-principles LDF study of H in Ge in supercells [202] concluded that H should behave in Ge in a manner very similar to that predicted at the same level of theory for H in Si [26,27]. In particular, H should exhibit negative-U properties, with H_{BC}^+ the stable species in p-type Ge, and H_T^- in n-type Ge. Both charge states are highly mobile. This implies that hydrogen passivation of dopants is not observed because the H-dopant pairs are unstable even at room temperature, since the Coulomb attraction between oppositely charged dopants and (highly mobile) H species should result in pair formation. This calculation does not explain the TE data.

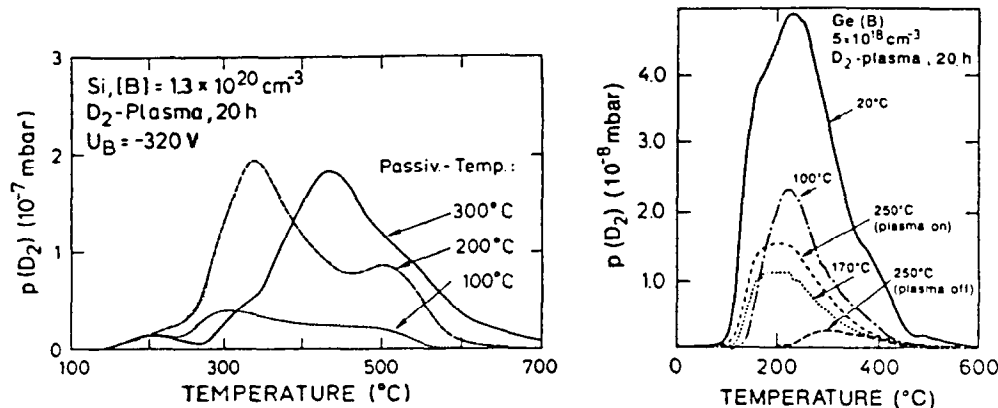


Fig. 14. Typical results of thermal effusion experiments [200] for comparably doped Si and Ge samples exposed to a D_2 plasma for 20 h at the temperature $T_{\text{pl}}=100, 200$, or 300 °C (in the case of Si) and $T_{\text{pl}}=20, 100$, or 250 °C (in the case of Ge). Not only is the vertical scale one order of magnitude larger for Si than for Ge, but the total D extracted increases with T_{pl} in the case of Si while it decreases with T_{pl} in the case of Ge.

A very different picture emerges from PRDDO and ab-initio HF calculations in various clusters [109,110,203]. As shown in Fig. 10, the T site is found to be more stable than the BC site in Ge, in contrast to silicon or diamond. This simple result has the following consequences.

- (i) Since there is a barrier to overcome to get from the T to the BC site, and since the energy at the BC site is higher than at the T site, both BC species (H_{BC}^0 and H_{BC}^+) should be much less abundant at low temperatures in Ge than in Si. Further, when the thermal energy becomes comparable with the $T \leftrightarrow BC$ barrier, the increase in population should favor the T site in Ge, instead of the BC site (as it does in Si). This is at least qualitatively consistent with the μ SR observations.
- (ii) Since the BC site is not very populated, $H^+ = H_{BC}^+$ should not be abundant, and acceptor (A) passivation must result from a reaction such as $A^- + H_T^0 + h^+ \rightarrow \{A, H\}$, which does not involve a Coulomb capture radius and is more complicated than the straightforward $A^- + H^+ \rightarrow \{A, H\}$ reaction which is believed to dominate in Si. This is consistent with a much lower acceptor passivation efficiency in Ge than in Si.
- (iii) The H_2^T molecule dominates in Ge not only because it is energetically preferred over H_2^* (see Fig 10) but also because the H_{BC} precursor is rare. When a sample is exposed to a plasma, one would expect the following. In Si, most of H is in the H_{BC}^+ state which prevents the formation of immobile H_2^T species. Further, in p-type Si, the ionized acceptors pull H^+ deeper into the bulk, and the amount of H should increase with T as the diffusivity of H increases. However, in Ge, most of the H in the sub-surface region will be H_T^0 . The formation of mostly immobile H_2^T molecules results, making it more difficult for H to penetrate. Further, the Coulomb attraction to charged acceptors in the bulk is not present. As the temperature increases, so does the mobility of H_T^0 and the probability of H_2^T formation. Thus, one would expect the formation of a sub-surface barrier of H_2^T molecules, preventing the penetration of H into the bulk. This qualitative argument does not explain the TE data, but is consistent with them.

The HF calculations [109,110,203] did not include H_T^- because of the low diamagnetic fraction observed in μ SR experiments and because of the absence of reports of donor passivation. It would be of interest to perform high-temperature MD simulations of H in Ge in order to verify some of these conclusions.

In addition to these total-energy calculations, several groups have calculated the hf parameters for Mu_{BC}^0 , with at least qualitative agreement with experiment. A summary is in Table 8.

2.2. Compound semiconductors

There are a number of important differences between elemental and compound semiconductors that need to be considered when studying interstitial H. The two (or more) different host atoms always have a different electron affinity, which has two major consequences.

First, the electronic charge is not distributed equally on two covalently bound NN host atoms, which implies an uneven charge distribution, i.e. a partly ionic interaction. The total energy must now include the long-ranged Madelung term. This contribution to the total energy has never been included when calculating potential energy surfaces for interstitial H in compound semiconductors. Its importance depends on the ionicity of the host, the site of H and, of course, on the charge state of H under consideration. Clusters neglect the fraction of the crystal that is beyond its surface, and the dipole layer on the H-saturated

Table 8

Hyperfine and superhyperfine contact (ν_c) and dipolar (ν_{dip}) frequencies for Mu_{BC}^0 and its ^{73}Ge nearest neighbor, and for Mu_T^0 (assumed to be at the T site) in germanium, compared with the experimental data. The frequencies are in MHz

Author [Ref.]	Mu_{BC}^0		Ge_{NN}		Mu_T^0
	ν_c	ν_{dip}	ν_c	ν_{dip}	ν_c
Vogel et al. [121] ^a	-848	84			
Sahoo et al. [204] ^b	-66	3			
Casarini et al. [122] ^c	-87	128	-85	-48	3977
Experiment [77]	-96	69			2360

^a Ab-initio UHF calculation in the cluster Ge_8H_{18} . The frequencies are averaged over the spread of the muon wavefunction.

^b Ab-initio UHF calculation in the cluster Ge_2H_6 .

^c Spin LDF in small clusters.

surface is larger in compounds than it is in elemental semiconductors. The optimal way to terminate such a surface has been discussed in Ref. [205]. On the other hand, periodic supercells have in each cell a charge distribution which is affected by the presence of the impurity, and does not correspond to that of the perfect crystal. Note that each cell is electrically neutral with a zero net dipole moment and that, in practice, the charges are screened by neighboring atoms. The amount to which these additional errors affect the theoretical predictions is not known. With the exception of IV–IV compounds, both clusters and supercells should have exactly the same number of each type of atoms in order to make sure that the average number of electrons on each site is four. If one includes more group V than group III atoms, for example, each excess group V atom contributes one electron to the CB. An alternative choice is to add or remove the necessary number of electrons in order to fill the VB or empty the CB.

Second, the interstitial sites are different. For example, there are two inequivalent T, AB, C, M, and BC sites. The two T sites differ not only by the net volume available (the covalent radii of the four NNs at each T site are different), but also by the field that the outer electrons of an impurity will feel when surrounded by oppositely charged NNs at each site. At AB sites, H tends to overlap covalently with its NN host atom, and that overlap is different for different atoms. At a BC site, H will not be symmetrically located between two different atoms and form a bridged bond (three-center, two-electron bond), but will form a much stronger bond with one host atom (almost a two-center, two-electron bond) and overlap much more weakly with the other (see Fig. 9). The new factors that influence the stability of H at a given site include the ionic character of the host, the relative electronegativity of each type of atom involved, and the relative bond strengths. The least electronegative (le) atom is usually listed first (such as Ga in GaAs), and the most electronegative (me) one second (such as As in GaAs). The le atom is positively charged and the me atom negatively charged. Note that the ionicity of a compound is not uniquely defined, because there are many ways to calculate the effective charge associated with a given atom. The bond strengths depend not only on the type of atoms involved but also on their coordination, and on what other atoms they may be bound to. Thus, one should beware of rules of thumb when predicting the stable configurations of H in compounds.

A final comment is appropriate here. While group IV elements naturally tend to be four-fold coordinated, the elements in other columns of the Periodic Table in general do

not. For example, in free radicals, both Ga and As much prefer to be three-fold (or five-fold) coordinated than four-fold. Forcing them into a four-fold coordination in a crystal containing defects and impurities often results in metastabilities and bistabilities resulting from a defect or impurity allowing a host atom to pick between two geometrically and electrically inequivalent configurations, one of which often has a three-fold coordinated host atom [206].

Experimental and theoretical work has been carried out on some compound semiconductors, but not on all, and not to the extent at which Si has been studied. One or more theoretical papers have been published on H in two polytypes of SiC, in GaAs, AlGaAs, GaP, c-BN, BP, and AlP. A few H-containing complexes in selected hosts have also been calculated. Muon spin rotation results exist for many compounds (see Table 1), but for some of them, only one or a few samples have been used, or only a limited range of temperatures considered. Except for GaAs, the total amount of information is much less complete than in the case of silicon. The theoretical and (direct) experimental work published to date is reviewed below. Note that this part of the review is based on a chapter written recently in Ref. [5].

2.2.1. IV-IV compounds

The only IV-IV compounds for which theoretical and μ SR studies have been published are polytypes of SiC. A very large variety of polytypes of SiC exist with cubic, hexagonal, rhombohedral, and other structures [207,208]. The most common ones include the cubic (zinc-blende) structure (3C- or β -SiC) and several of the hexagonal structures such as 6H-SiC (the most stable structure), 2H- (wurtzite) and 4H-SiC. The hexagonal structures differ in the way the {Si-C} pairs are stacked in the *c* direction. This is illustrated in Fig. 2 which compares the {110} planes of the 3C and 2H polytypes. One easily recognizes the familiar zig-zag arrangement characteristic of the zinc-blende structure, with the ABC ABC... vertical sequence. In 2H-SiC, the third layer is shifted exactly above the first one, leading to an AB AB... sequence. The 6H polytype has the sequence ABCACB ABCACB... and is therefore a hybrid of 3C and 2H, which are the two most different of the hexagonal and cubic polytypes. Note that the notation α -SiC is used for any hexagonal polytype, but often refers to 6H.

As can be seen in Fig. 2, there is a single BC site in 3C-SiC, but two inequivalent T sites (T_{Si} and T_C) separated along the $\langle 111 \rangle$ direction by H sites. The 2H polytype has two T sites (T_{Si}' and T_C'), which are distinct from the ones in 3C-SiC. It also has two inequivalent BC sites, as well as two new sites which are labeled R (one of the most important interstitial sites in the wurtzite lattice) and E [209]. The other hexagonal polytypes have a combination of interstitial sites which are locally equivalent to the ones found in 3C- or 2H-SiC (for details, see Ref. [209]).

2.2.1.1. μ SR in SiC

μ SR data are available in 3C- and 6H-SiC [102]. The low-temperature fractions and the observed transitions are summarized in Table 1. In 3C-SiC, Mu_T^0 is the only paramagnetic center, and μ^+ has not been identified. A thermally-induced $\mu^+ \rightarrow Mu_T^0$ transition shows that Mu_T^0 is more stable. In 6H-SiC, three Mu_T^0 centers are observed at low temperatures: Mu^{A1} , Mu^{AII} , and Mu^B . The hf parameters of Mu^{A1} and Mu^{AII} are within 1% of each other. At room temperature, Mu^{A1} and Mu^{AII} convert to a single center, Mu^A , so that only two paramagnetic centers remain.

2.2.1.2. Theory of H in SiC

A theoretical study [209,210] at the PRDDO level has been published for H in the 3C and 2H polytypes of SiC, using the clusters $\text{Si}_{13}\text{C}_{13}\text{H}_{26}$ (3C), $\text{Si}_{22}\text{C}_{22}\text{H}_{42}$ (3C), $\text{Si}_{24}\text{C}_{24}\text{H}_{46}$ (2H), and $\text{Si}_{26}\text{C}_{26}\text{H}_{50}$ (2H). In 3C-SiC, the lowest energy is found for H_{TSi}^0 , which is lower than H_{BC}^0 by 0.15 eV and lower than H_{TC}^0 by 1.11 eV. This is consistent with a single Mu_T^0 signal (corresponding to T_{Si}), as observed experimentally. The μ^+ signal could correspond to Mu_{BC}^+ , to Mu_T^- , or to muonium bound at a defect. Note that if it is Mu_{BC}^+ , the $\mu^+ \rightarrow \text{Mu}_T^0$ transition is consistent with the T_{Si} site being more stable than the BC site. The $\text{T}_{\text{Si}} \rightarrow \text{BC}$ barrier is estimated to be less than 1.5 eV, a value comparable with that obtained in c-C at the same level of theory, and the $\text{T}_{\text{Si}} \rightarrow \text{T}_{\text{C}}$ barrier along the $\langle 111 \rangle$ direction is less than 2 eV, a number also comparable with that calculated in c-C with PRDDO. Since Mu_T^0 does not diffuse at low temperatures in diamond, it is expected that it would not diffuse in 3C-SiC either.

In 2H-SiC, the lowest energy occurs at the R site (see Fig. 2), which is found to be 0.39 eV lower than BC_{\perp} and 1.15 eV lower than BC_{\parallel} . The large difference in energy between the two BC sites is caused by the much smaller amount of lattice relaxation that can be realized along the two inequivalent directions. A very shallow minimum of the potential surface exists at the E site, but the energy is some 2.5 eV above R. The barrier for diffusion between R sites is less than 2 eV, a little higher than the $\text{R} \rightarrow \text{BC}_{\perp}$ barrier. These results suggest that a single, isotropic μ SR signal should be observed in 2H-SiC, corresponding to an immobile Mu_T^0 at the R site.

The results obtained for 2H- and 3C-SiC can be combined to predict μ SR spectra in 6H-SiC since all the energies have been calculated relative to a common zero corresponding to H_{free}^0 far outside the undisturbed clusters. The lowest energy site in 6H-SiC is the R site, followed by the two slightly inequivalent T_{Si} sites ($\sim \text{R} + 0.6$ eV), the BC, BC_{\perp}' and BC_{\parallel}'' ($\sim \text{R} + 0.7$ eV to 1.2 eV), then T_{C} ($\sim \text{R} + 1.7$ eV) and finally E ($\sim \text{R} + 2.5$ eV). The μ SR signals and transitions observed in this polytype are assigned as follows. Mu^B corresponds to the R site, $\text{Mu}^{A\text{I}}$ and $\text{Mu}^{A\text{II}}$ to the two slightly inequivalent T_{Si} sites. The thermally induced transition of $\text{Mu}^{A\text{I}}$ and $\text{Mu}^{A\text{II}}$ to Mu^A could correspond to thermally-assisted tunneling between these two T_{Si} sites [211]. Finally, the small μ^+ signal is assigned to Mu_{BC}^+ . A $\mu^+ \rightarrow \text{Mu}^B$ (or $\mu^+ \rightarrow \text{Mu}^A$) transition is predicted to occur at higher temperatures.

2.2.2. III-V compounds

All the direct experimental information on hydrogen-like interstitials in III-V compounds comes from μ SR. Data related to changes in the electrical and optical activity upon hydrogenation are presented in Section 3.

2.2.2.1. μ SR in GaP and GaAs

The low-temperature [77,97,100] fractions of Mu_T^0 , Mu_{BC}^0 , and μ^+ in GaP and GaAs are shown in Table 1. 98% of the muons that stop in high resistivity GaAs form Mu_T^0 or Mu_{BC}^0 , and most of the muons responsible for the non-paramagnetic signal stop in the cryostat, not in the crystal [212].

The hf parameters for Mu_T^0 as well as those for Mu_{BC}^0 are almost identical in GaP and GaAs suggesting that it is the Ga atom that dictates the spin distribution and that Mu_T^0 is predominantly at the T_{Ga} site. As for Mu_{BC}^0 , μ LCR experiments [213] in GaAs have shown that 38% of the odd electron resides on the Ga NN to the muon, and 45% on the As NN. This corresponds to a configuration where the muon is somewhat more

strongly bound to its Ga than to its As NN (Ga–Mu⁺–As). On the other hand, μ LCR in GaP [214] finds 43% of the unpaired spin density on Ga and only 35% on P, suggesting that the reverse configuration is realized (Ga \cdots Mu–P). Note that the spin density fractions are rather close to each other in both cases, so that the difference in bond strength should not be very large. The electronegativity of P and As are almost the same, as are the bond strengths (e.g. in diatomics). Therefore, the details of the configurations realized cannot be deduced from qualitative arguments. A high-field μ SR spectrum of GaAs is shown in Fig. 15.

Recent μ LCR [215–217] experiments in heavily n-type GaAs (doped with Si or Te) provide the best evidence yet for the presence of Mu⁻. The evidence is consistent with the replacement in heavily doped material of the mobile Mu_{T_{Ga}}⁰ center by a much less mobile, charged, species which is most likely Mu_{T_{Ga}}⁻. The μ LCR signal appears in the 50–150 K range, which is interpreted as the onset of the Mu_{T_{Ga}}⁰ \rightarrow Mu_{T_{Ga}}⁻ conversion. Note that this conversion has little effect on the other paramagnetic center, Mu_{BC}⁰. A number of details in the temperature dependence have yet to be fully understood.

The magnitude of the muon level-crossing resonances and the static line broadening seen in transverse-field experiments imply that Mu⁻ in GaAs is confined to a single T_{Ga} site during its lifetime, even at temperatures as high as 500 K. Measurements [217] of the linewidth associated with Mu⁻ show a sharp drop near 550 K, an indication that diffusion occurs. The shape and onset of this drop are donor-independent and lead to an estimate [218] of the activation energy for diffusion of Mu⁻ in GaAs near 0.71 eV. The activation energy for H⁻ must be higher because of the difference in zero-point energies.

Another feature of the depolarization rates in the μ LCR data [217] is an onset of motion occurring for Mu_{BC}⁺ around 200 K. This is interpreted as the breaking of the weaker of the two bonds in Ga–Mu⁺–As, with Mu⁺ beginning to rotate around the host atom to which it is bound the strongest.

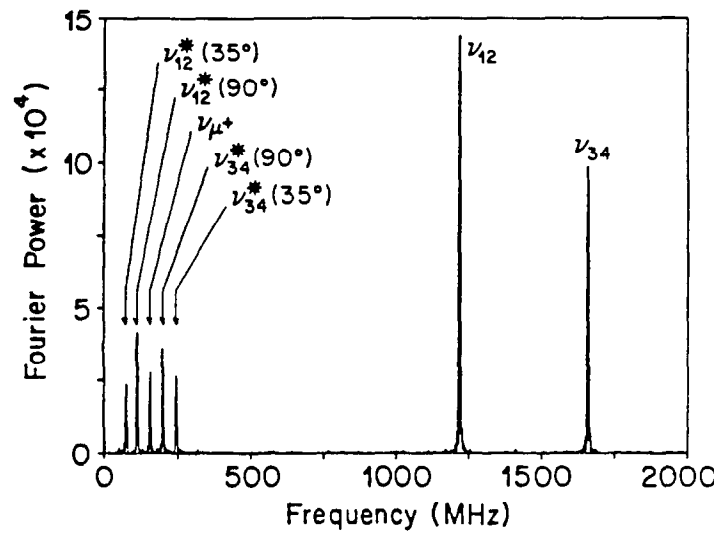


Fig. 15. Experimental transverse-field time-differential μ SR spectrum of GaAs [97] at 1.15 T. The Mu_T⁰ transitions are labeled ν_{12} and ν_{34} , and the Mu_{BC}⁰ ones, marked with an asterisk, are on both sides of the μ^+ (ν_μ^+) line with splitting varying with the angle between the field and the trigonal axis of Mu_{BC}⁰ (in this case, the field is along $\langle 110 \rangle$). The μ^+ line is mostly due to muons stopping in the cryostat.

Finally, longitudinal-field μ SR experiments [136] show that Mu_{BC}^0 is present at low temperatures in highly doped n-type GaAs ($\sim 9 \times 10^{16}$ Si cm $^{-3}$), demonstrating that more than one state of muonium exists. This result is consistent with the coexistence of several states of muonium in p- and n-type Si reported above.

2.2.2.2. Theory of H in GaAs

The equilibrium geometries and electronic structures of interstitial H in GaAs have been calculated by several groups. Briddon and Jones [219,220] used LDF theory in 26 host-atom molecular clusters. They find two minima of the potential energy, corresponding to $H_{T_{Ga}}^0$ and H_{BC}^0 . The stable state corresponds to $H_{T_{Ga}}^0$, where H has a partially filled level at $E_V + 0.9$ eV. Their result that the T_{Ga} site is more stable than the T_{As} site is consistent with the interpretation of μ SR data [97] and with the trends obtained at the PRDDO level in four compound semiconductors (see below). The metastable state at the BC site is 0.2 eV higher, with a 42% expansion of the Ga–As bond.

Pavesi and coworkers [28,221,222] studied H^+ , H^0 , and H^- at the LDF level in 16-atom periodic supercells. The (spin-averaged) H^0 calculations were repeated for H^0 in a 32-atom cell. Two sets of results were obtained in each case, corresponding to the unrelaxed and fully relaxed cell, respectively. In the former case, the bonds in the host crystal are not affected by the presence of H, which renders the BC site unreachable. In the latter case, the crystal always adjusts instantaneously to all positions of H.

In the relaxed 16-atom cell, the potential energy surface is very flat for H^0 at the C_{Ga} (0 eV), AB_{As} (0.03 eV), M (0.04 eV), and H (0.10 eV) sites. The T_{Ga} site is at +0.38 eV and the BC site at +0.46 eV. In the relaxed 32-atom cell, H^0 prefers the AB_{As} (0 eV), M (0.11 eV), and C_{Ga} (0.11 eV) sites. The BC site is at +0.19 eV and the T_{Ga} site at +0.29 eV. The relaxation at the BC site is 40%. In the unrelaxed 32-atom cell, the H and T_{As} sites have the same energy, the T_{Ga} site is 0.07 eV higher, and the BC site is not accessible. The picture for H^0 is that of a rapidly diffusing interstitial in the low charge-density region of the crystal (Mu_T^0), with the BC site much higher in energy. It is difficult to compare these results with those obtained by other groups who generally allow lattice relaxations where H is localized (i.e. at the BC site) but no (or little) relaxation where the potential surface is sufficiently flat for H to diffuse rapidly. Further, these calculations find T_{Ga} to be the highest (16-atom cell) or second highest (32-atom cell) energy site, which conflicts with earlier predictions [219,220].

Results for H^+ and H^- are available only in the 16-atom cell. In the relaxed cell, H^+ diffuses between the M (0 eV), BC (0.09 eV) and C_{As} (0.17 eV) sites, while H^- moves easily between the C_{As} (0 eV), AB_{Ga} (0.07 eV), H (0.07 eV), and T_{Ga} (0.10 eV) sites. The low barriers for diffusion of H^- are not compatible with the μ LCR data, which see Mu^- to be frozen at a single T_{Ga} site [215,217] up to 550 K. The authors predict that H has negative-U properties in GaAs.

Thermal dissociation kinetics [223–225] of hydrogen–donor pairs under reverse bias in GaAs are consistent with the existence of H^- . Clerjaud et al. [226] find the donor level of H to be 0.2–0.3 eV above the VB maximum. However, much of these data can also be explained [227] if the hydrogen–donor pair is bistable, and can be promoted into its charged state by the applied field. Further, SIMS studies [228] in p- and n-type GaAs show the existence of H^+ and H^0 , but not of H^- . On the other hand, μ LCR data clearly show that Mu^- exists. In a recent review [229], Chevallier and Pajot argue that the acceptor level lies above E_c in GaAs, but drops below E_c in the alloy, contradicting the negative-U model

for GaAs. They suggest that H^0 governs the diffusion of hydrogen in n-type GaAs and that H^- begins to play a role in $Al_xGa_{1-x}As$ only for $x > 0.06$. Thus, the situation regarding H^- is still heavily debated.

Ab-initio HF calculations [217] for H in GaAs find that H^+ is stable at the BC site, with $Ga-H = 1.50 \text{ \AA}$ and $H-As = 1.62 \text{ \AA}$. H^0 is metastable. The stable configuration corresponds to H_{BC}^0 , and $H_{T_{Ga}}^0$ is only 0.25 eV higher in energy. The T_{As} site is at +0.33 eV and the activation energy for $T_{Ga}-H-T_{As}$ diffusion is 0.65 eV. The AB_{Ga} site is only slightly less stable than the T_{Ga} site. Note that the energy difference between the T_{le} and T_{me} sites favors the le site and is in qualitative agreement with the trends shown later in Fig. 17. Finally, H^- is found to be localized at the T_{Ga} site, while $H_{T_{As}}^-$ is 1.59 eV higher, at about the same energy as the H site. The T_{As} site repels H^- because of the effective negative charge on As, the more electronegative element of Ga and As. The result is not only a large potential barrier for diffusion in the low density region of the crystal, but a very broad one as well. This result explains the absence of diffusion observed for Mu^- in GaAs [215].

In summary, the potential surface calculations of Briddon and Jones [219] (LDF in clusters), Jones [220] (LDF in clusters) and Adams et al. [217] (HF in clusters) are reasonably close to each other as concerns H^0 , with both the BC and the T_{Ga} configurations within a few tenths of an electronvolt from each other. These calculations show qualitative differences with the results of Pavesi and coworkers [28,221,222]. A possible reason is the use in the latter calculation of a zero-relaxation or a complete instantaneous relaxation scheme. The ab initio calculations of Adams et al. [217] regarding H^+ and H^- are in good qualitative agreement with the μ SR results, but those of Pavesi and coworkers are not.

Maric et al. [230] performed large basis set ab-initio HF calculations for H_{BC}^0 in a cluster containing 8 host atoms. This cluster allows only the first NN relaxations to be included and does not contain T sites. The Ga-As bond relaxation needed to accommodate H_{BC}^0 is calculated to be 34.5%, and H forms a slightly stronger bond with its Ga than with its As NN. The calculated Ga-H and As-H bond lengths are 1.68 \AA (vs. 1.67 \AA in GaH) and 1.62 \AA (vs. 1.52 \AA in AsH₃), and the degrees of bonding [231] are $Ga-H=0.24$ and $H-As=0.46$ for GaAs. The spin density along the $\langle 111 \rangle$ direction, shown in Fig. 16, is in good qualitative agreement with the μ SR results. The calculated contact Fermi density translates into a hf frequency of 20 MHz (see Table 9).

Note that both μ SR and theory agree that it is the Ga atom that dominates the interactions. The hf parameters of Mu_T^0 and Mu_{BC}^0 are virtually identical in GaP and GaAs, the T_{Ga} site (or a site near it) is energetically favored over the T_{As} site and, in the BC configuration, hydrogen is calculated to be more strongly bound to Ga than to As. However, Stein [232] reported evidence from IR absorption that in proton-implanted GaAs, at low temperatures, a new IR band corresponding to an As-H bond occurs. This band disappears while the expected Ga-H band appears after annealing at 200 K. While the effects of implantation damage cannot be ruled out as the reason for the observation of the As-H bond, a convincing explanation for the annealing behavior has yet to be proposed.

Van de Walle and Blöchl [64] have calculated hf parameters for μ SR centers in several semiconductors at the spin LDF level in 32-atom supercells. The hf parameters in GaAs were calculated with the geometries obtained by Pavesi and coworkers [28,221,222] except that H_T^0 is fixed at the T_{Ga} site. The results, shown in Table 9 are impressively close to the experimental numbers. The shf frequencies for the NNs and second NNs to the muon

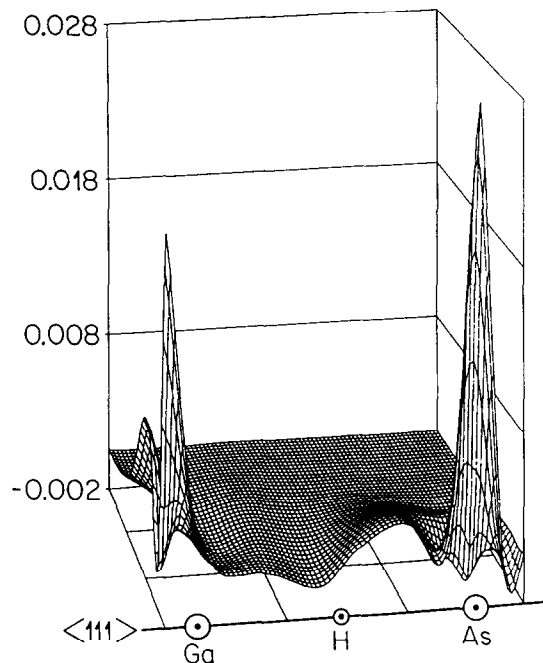


Fig. 16. Calculated [230] spin density (in atomic units) along the trigonal axis for Mu_{BC}^0 in GaAs.

Table 9
Theoretical and experimental hf frequencies (in MHz) for Mu_T^0 and Mu_{BC}^0 in GaAs

Author [Ref.]	Mu_{BC}^0		$\text{Mu}_{\text{T}_{\text{Ga}}}^0$		$\text{Mu}_{\text{T}_{\text{As}}}^0$	
	ν_c	ν_{dip}	ν_c	ν_c	ν_c	ν_c
Van de Walle et al. [64,233] ^a	106	33	2646	2497		
Maric et al. [234] ^b	20	55				
Experiment [213]	131.1	43.4	2884			

^a Spin LDF in 32-atom supercells.

^b Ab-initio HF in an 8 host-atom cluster (this cluster contains no T-sites).

can be found in the references listed. Note that the frequency for $\text{Mu}_{\text{T}_{\text{Ga}}}^0$ is much closer to the experimental value than that for the $\text{Mu}_{\text{T}_{\text{As}}}^0$ site.

2.2.2.3. H in III-V compounds other than GaAs

Less theoretical work has been published on interstitial H in compounds other than GaAs. Pavesi [235] has published a study of H in AlAs, extended to AlGaAs [236]. These are LDF calculations in 16- and 32-atom supercells. Pavesi finds H to exhibit negative-U behavior in AlAs, with a deep donor level in p-type material and a deep acceptor level in n-type material. However, as noted by Pavesi [235], the band width associated with the (periodic) H interstitial is large (of the order of 0.7 eV) while the calculated bandgap is small (1.36 vs. 2.16 eV experimentally). Therefore, the error bar on the negative-U prediction is substantial. H^0 in AlAs is calculated to be stable at the H site. Relative to this, the other interstitial sites have energies of 0.10 eV (AB_{Al}), 0.26 eV (T_{Al}), 0.31 eV (AB_{As}), 0.44 eV (T_{As}), and 0.55 eV (BC).

In addition to GaAs, Maric et al. [234] have studied H^0 at the BC site in GaP and InP at the ab-initio HF level in 8 host-atom clusters, which do not include a T site. The relaxation of the host-atom bond needed to insert H^0 at the BC site varies from 34% (InP) to 37% (GaP). In each case, hydrogen forms a stronger bond with the group III atom than with the group V atom. The calculated degrees of bonding [231] are $Ga-H=0.15$ and $H-P=0.58$ for GaP, and $In-H=0.15$ and $H-P=0.63$ for InP. Although these numbers agree with the trends obtained in compounds with the method of PRDDO (see below) and with experiment in the case of GaAs, recent μ LCR experiments [214] in GaP suggest the opposite-bonding configuration in GaP. The calculations also show that the (Koopmans'-theorem) ionization potential for H_{BC}^0 in InP is small and negative, in contrast to GaAs and GaP where it is much larger and positive. This indicates that H_{BC}^0 in InP should spontaneously ionize even at low temperatures. This prediction would explain the absence of an observed Mu_{BC}^0 signal in InP [78].

Finally, the method of PRDDO has been used [117,205] to investigate systematically the properties of H^0 in cubic BN, BP, AlP, and SiC as a function of the ionic character of the host. The calculations were performed in molecular clusters containing 44 host atoms. The first and second NN shells around the BC site were allowed to relax (within the constraints of C_{3v} symmetry), and no relaxation was included at the T sites. Three minima of the potential energy surface have been found for H^0 in compound semiconductors with the zinc-blende structure, the BC and the two T sites, one surrounded by the four le of the two host atoms, the other by the four me ones.

The total energy difference between H_{Tle}^0 and the H_{Tme}^0 sites increases linearly with the difference in the (Pauling) ionic character [237] of the host atoms, as shown in Fig. 17. This agrees qualitatively with the interpretation of μ SR data in GaAs, but disagrees with the assignment of H^0 to the C_{As} or AB_{As} sites in GaAs predicted by the LDF method in periodic supercells [28,221,222]. The calculated barrier heights [205] and energy differences between the T sites imply that H^0 becomes more strongly trapped at the T_{le} site as the

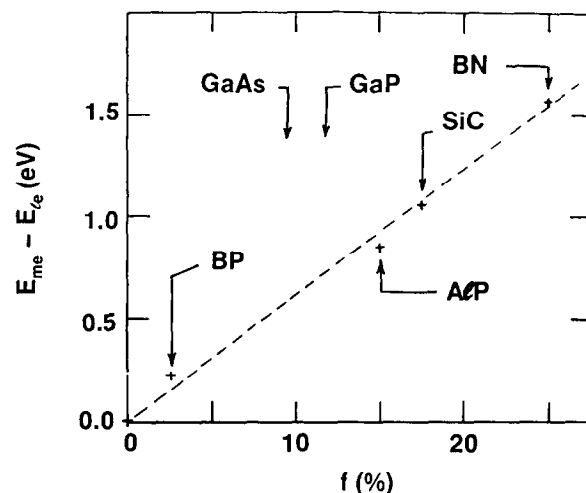


Fig. 17. Energy difference (in eV) between H^0 at the T sites with the four most electronegative (me) NNs and the least electronegative (le) NNs (H_{Tme}^0 and H_{Tle}^0) in BP, AlP, SiC, and BN, vs. the Pauling ionic character f of the host. Arrows show the location of GaAs and GaP on this scale. The energies are calculated at the PRDDO level. The T_{le} site (surrounded by four B, Si, or Al NNs) is always more stable.

ionic character of the host increases. The effective positive charge on the four NNs to H_T^0 allows the 1s-type electron to overlap with the crystal at the T_{le} site, while the effective negative charge on the four NNs to the T_{me} site repels this electron, resulting in a higher energy. The second electron on H^- is likely to render the T_{le} site even more stable and the T_{me} site much more unstable, as is found for H^- in Ref. [217].

H_{BC}^0 forms a stronger bond with the le atom than with the me one. This allows the unpaired electron to be primarily localized on the me atom, where it is more stable. The details depend on the balance between the gain in energy realized by localizing the unpaired electron on the me vs. the le atom and the relative bond strength of the two host atom-H bonds. These trends are confirmed in the case of GaAs, GaP, and InP by ab-initio HF calculations [230,234]. They are also consistent with μ LCR data in GaAs [213], but not in GaP [214] where slightly more of the odd electron is found to reside on the Ga atom.

The potential energy barrier separating the T_{le} and the BC sites is lower in compounds than in elemental semiconductors. The PRDDO calculations predict that the BC site is lower than the T_{le} site in AlP (by 0.36 eV) and 3C-SiC (by 0.09 eV), but higher than the T_{le} site in BP (by 0.45 eV) and BN (by 1.24 eV). Finally, H^+ is in all cases H_{BC}^+ , with a geometrical configuration similar to that of H_{BC}^0 .

2.2.2.4. Hydrogen dimers

Pavesi and Gianozzi [222] have considered the H_2^T and H_2^* pairs in GaAs. They find that H_2^T is stable at the T_{Ga} site, but the T_{As} site is only some 0.12 eV higher in energy. It is oriented along the $\langle 111 \rangle$ axis, with a H-H bond length somewhat longer than that of the free H_2 molecule (0.81 vs. 0.75 Å). Very little energy is required to rotate the molecule. The barrier for diffusion is rather high (about 1 eV). Finally, H_2^T is more stable than two H_{BC}^0 by 3.6 eV. The stable configuration for H_2^* has H_{BC} bound to the As and H_{AB} bound to the Ga atom. It is 0.21 eV more stable than the other possible H_2^* configuration, but is 0.93 eV higher than H_2^T .

2.2.3. II-VI compounds

Compounds such as ZnSe are attracting increasing interest for possible use as blue/green light emitters. High quality ZnSe films are grown by solid-source or gas-phase molecular beam epitaxy (MBE), or metal-organic chemical vapor deposition. In the gas-phase MBE method, H is incorporated from the H_2Se selenium source [238,239]. Little is known about isolated H interstitials.

2.2.3.1. μ SR in ZnS and ZnSe [78]

Little systematic work has been performed, but Mu_{BC}^0 has not been detected (see Table 1). Only one paramagnetic center is seen at 10 K, most likely owing to $Mu_{T_{Zn}}^0$. The non-paramagnetic μ^+ center has not been identified. In both hosts, the missing fraction is large.

2.2.3.2. Theory of H in ZnSe

A spin LDF calculation of H^0 in 8–32-atom supercells of ZnSe has been published [240]. A mixed basis set (plane waves and gaussians) was used to account for the d-valence states of Zn. The BC site is found to be energetically unfavorable. H^0 is predicted to diffuse rapidly between the T_{Zn} and T_{Se} sites, and the energy is only slightly lower at T_{Zn} . The calculated hf frequencies for $Mu_{T_{Zn}}^0$ and $Mu_{T_{Se}}^0$ are 3333 and 3248 MHz, respectively, as

compared with the measured value [78] at 3457 MHz. This again points toward T_{Zn} being the more stable site. Van de Walle and Laks [240] suggest that for a rapidly-diffusing muon, the 85 MHz difference in hf frequencies between the T_{Zn} and T_{Se} sites may not be resolved experimentally. However, the μ SR data in ZnSe [212] were taken at high fields with a high-resolution spectrometer, and differences of a few MHz are very well resolved (see, for example, Fig. 15). However, if Mu_T^0 diffuses fast enough between the two T sites, a single line would indeed be observed. The necessary hop rate $1/\tau$ should then be larger than $2\pi\nu_{12}$ or $2\pi\nu_{34}$, i.e. larger than about $12\ 500\ (\mu s)^{-1}$, which is possible if the activation energy for diffusion is very small.

2.2.4. I-VII compounds

The only semiconductors in this group for which there is any information on hydrogen-like interstitials are the copper halides [241–243]. In CuCl and CuBr, two Mu_T^0 signals have been observed, labeled Mu^I and Mu^{II} . A thermally-induced transition from Mu^I to Mu^{II} at 60 K (for CuCl) and 153 K (for CuBr) is observed. These centers are unusual for two reasons. First, the Fermi contact density at the muon is very low (only some 30% of the free-atom value) indicating a very delocalized wavefunction. In all other semiconductors, the contact density is at least 50% larger than this. Second, μ LCR data [242,243] unambiguously show that both Mu^I and Mu^{II} originate from muonium localized at the same T site, the one surrounded by four Cu NNs (T_{Cu}). At low temperatures, Mu^I tunnels locally around T_{Cu} while Mu^{II} is quasistationary, on site.

A model based on chemical arguments has been developed [91,92] to explain the low contact density at the muon in these hosts. It proposes the formation of a one-electron bond between muonium and a Cu^+ ion, and uses an umbrella site argument to explain the T_d symmetry. In this model, the muon would rapidly oscillate between equivalent AB_{Cu} sites and form a weak bond at each such site. The bond formation would be responsible for the low spin density. The authors proposed the same model to explain the low Fermi contact density reported for Mu_T^0 in Si. A theoretical study [164] concluded that this model is possible, though quite complicated for Si. In the case of copper halides, the unusual metastability observed implies that very accurate potential surfaces and spin distributions will need to be calculated.

3. Interactions with impurities and defects

The truth is the one thing that nobody will believe.

G.B. Shaw

Hydrogen reacts chemically with its environment. A diffusing H^0 interstitial is attracted to strained regions of the crystal where it can become trapped, often in a bound state. Or, an H^+ or H^- ion experiences the Coulomb field of an ionized dopant, perhaps even a dipolar field, such as that of interstitial O forming a puckered bridged bond in Si. Strain is created by extended or localized defects (from dislocations to monovacancies) or by the presence of impurities. A substitutional impurity may be too large or too small to fit comfortably at a lattice site, prefer a coordination different from that imposed on it by the host crystal, and relax or distort its environment. A distortion can spontaneously occur to remove an orbital degeneracy. The same holds for impurities that are primarily interstitial, such as O or a 3d TM.

In any case, H likes to interact with weak or stretched bonds. This allows the complex to relax toward a more favorable conformation than is possible without H. The local

rearrangement shifts the energy levels associated with the defect, sometimes from the gap to a band (passivation), from a band to the gap (activation), or simply move an energy level deeper (or shallower) within the gap.

In the majority of cases, the interaction between H and a substitutional impurity X results in the formation of a {X, H} pair with trigonal symmetry, although more than one H is trapped in some cases. The most often encountered configurations have H at the AB site of X (AB_X) or at a NN host atom to X, and a BC configuration with H more strongly bound to X (BC_X) or to a host atom. Note that this is not a true bridged bond, since H is off-center either along the $\langle 111 \rangle$ axis, or even slightly off the axis (puckered) with a very small activation energy for rotation around the axis. Typical configurations are shown in Fig. 18. The notation introduced in the figure will be used to characterize the various calculated configurations.

Experimental evidence for these phenomena sometimes comes from the direct observation of IR or Raman lines, which show an isotope shift when D is used instead of H. In a few cases, EPR evidence exists. For example, for some of the complexes involving H and a substitutional TM (see below). However, the experimental information is more often indirect. SIMS profiles of deuterated samples may show a one-to-one correspondence between the D concentration and that of a particular dopant for some depths. But typical profiles have an extremely high concentration of D near the surface, and this initial peak drops through one or more shoulders before stabilizing at the dopant concentration. The details of such profiles are not understood. Then, electrical measurements provide the concentration of charge carriers vs. depth, or capacitance transients may show the presence of a level in the gap in the depletion region. The results of such experiments always have to be interpreted, and the interpretation is based on a set of assumptions. For example, it may be assumed that under some specified condition, a hydrogen–impurity pair {X, H} breaks up, resulting in the appearance of a charge carrier or of a charged interstitial H species. However, the same electrical signal may result from the conversion of the $\{X, H\}^0$ pair to a bistable $\{X, H\}^+$ state, which also results in a new charge carrier and a positively-charged defect. Thus, the interpretation of electrical data is rarely unique, and one does not really know the

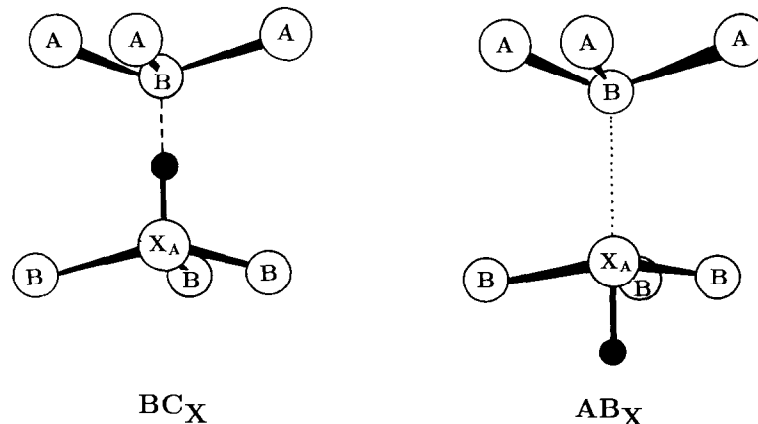


Fig. 18. Typical configurations of impurity–hydrogen pairs in semiconductors. In elemental hosts, the atoms marked A and B are of course identical. H is the full circle and X_A is an impurity substituting for atom A. In the BC configuration, H may be bound more strongly to the impurity (as illustrated) or to a host atom. Hydrogen may also be at the AB site to the impurity (as illustrated) or to a host atom. When needed, the subscript specifies the atom involved in each case. In some instances, several (metastable) configurations have been predicted to occur.

microscopic details involved, except when it is possible to combine electrical and/or SIMS data with microscopic information, e.g. from IR absorption spectroscopy, to identify the defect present. Theoretical studies play an important role when it comes to assessing which processes are likely to occur and, more importantly, which ones are not.

Bound configurations involving H are rather well described at the HF and LDF levels. Ab-initio and first-principles theorists agree on a number of qualitative features of hydrogen-impurity pairs. Disagreement exists on many finer points, such as the precise geometry of a complex, the existence, configuration, and relative energy of a metastable or bistable state, or even on general features of large complexes, those containing more than two centers (multiple vacancies, multiple hydrogen interstitials, etc.). In many cases, the basic assumption that the complex can be described using a (necessarily) small cluster or supercell should be continuously questioned. Given the known cluster- or supercell-size effects observed for isolated H, it is almost certain that such effects become larger as the relative volumes of the defect center (H, the impurity, and the displaced host atoms) and cluster or supercell increases. Systematic studies of these issues have been limited [29,30], and theorists must continue to be very careful when dealing with larger complexes.

The vast majority of the theoretical work involves hydrogen-impurity pairs, especially the cases when passivation (or activation) occurs. By now, the static (0 K) configurations of most hydrogen-dopant pairs in Si and GaAs are agreed upon, and the issues that generate discussion and controversy include the kinetics of reactivation of the pairs. Again, much more work has been carried out in Si and GaAs than in other semiconductors. In Si, theoretical studies also exist for hydrogen-vacancy complexes, and a variety of models of platelets have been proposed as well. A few studies have considered more exotic complexes such as those containing a TM atom. Finally, a couple of papers deal with one of the most unexpected of all hydrogen-impurity interactions, the catalyzed diffusion of interstitial O in Si.

This section is organized following the same scheme as the previous one, first discussing the elemental, then the compound semiconductors. Parts of the latter subsection is similar to my recent chapter in Ref. [5]. The longest subsection, by far, is that dealing with Si. Note that the discussion of the experimental work is reduced to general statements, to the specific results that are directly relevant to theoretical work, and to the most recent papers, not included in the latest reviews [4,5].

3.1. Elemental semiconductors

Even though Ge was the first semiconductor in which H-impurity interactions were detected [7–9], the vast majority of experimental and theoretical studies have been carried out in Si. Of course, silicon is the most important semiconductor, if judging by the shear volume of Si-based electronics produced vs. all the other materials combined. It turns out that silicon is also the elemental semiconductor in which H probably has the most varied interactions. As was discussed in Section 2, four states of hydrogen are energetically rather close (H_{BC}^+ , H_{BC}^0 , H_T^0 , and H_T^-), and small variations in temperature, Fermi level, or impurity content may result in wide variations in the way H diffuses and interacts. In diamond, the energy differences between the various sites are large (see Fig. 10), resulting in fewer configurations being realized. In ultra-pure Ge, the as-grown H concentration is of the order of 10^{14} cm^{-3} and, except for implantation, additional hydrogenation appears

difficult (see Section 2.1.3). Further, if theory is correct [203], the BC species are not energetically favored, which reduces the number of likely configurations.

3.1.1. Diamond

Hydrogenation has been shown [244,245] to reduce the resistivity of natural and synthetic diamond by orders of magnitude. Natural diamond has a very high resistivity ($\sim 10^{16} \Omega \text{ cm}$) while as-grown CVD films have $\rho \sim 10^6 \Omega \text{ cm}$, because of the high concentration of H present during the growth. However, anneals in the 400–800 °C range expel hydrogen from the film, and the resistivity increases dramatically to values much closer to those of natural diamond. Note that such anneals may affect other (H-unrelated) defects in the crystal. Hydrogen is believed to passivate deep traps such as grain boundaries or dangling bonds at vacancies, which increases the lifetime of charge carriers. The nature of the complexes in which H is involved has yet to be determined experimentally.

Three such complexes have been studied theoretically: the {B, H} pair [119,246], the {N, H} pair [119], and the vacancy–hydrogen complexes {V, H_n} with $n=1, \dots, 4$ [118]. Substitutional boron is the acceptor of choice in diamond, while N, the most common impurity in natural diamond, is a deep donor. The calculations were made with the semiempirical ASED-MO method [118,119] and with first-principles LDF [246] in molecular clusters containing 35 and 70 C atoms.

The {B, H} pair was studied by both groups, who agree that the pair forms and does not have trigonal symmetry, in contrast to all(?) hydrogen–impurity pairs in Si and GaAs. However, the two authors disagree on most details. The ASED-MO method [119] predicts that H forms a puckered bridged bond between B and one of its four C NNs, with B–H = 1.21 Å, H–C = 1.09 Å, and a B–H–C bond angle of 113°. Both bond lengths are very close to the ones realized in molecules such as diborane and methane, respectively, indicating that H forms a rather strong bond with both B and C. The binding energy, relative to free atomic H is 1.54 eV. Hydrogen is also found to be highly mobile near substitutional B, with an activation energy for migration between adjacent puckered BC configurations of only 0.13 eV, a value comparable with that calculated at the same level of theory for H_{BC}⁺. The formation of the {B, H} pair results in the passivation of the electrical activity of substitutional B.

On the other hand, the LDF calculations of Breuer and Briddon [246] predict a very different configuration. These authors find that H binds only to the B atom, with the B–H bond pointing along the <100> direction in the {110} plane, with B–H = 1.1 Å. The absolute minimum of the total energy actually occurs for H somewhat off the tetragonal axis, toward [011] and [0̄1̄1], a pair of configurations that are only 0.02 eV below the symmetric one. As noted by the authors, such a small energy difference may be an artifact of the calculation. However, it makes it difficult to calculate vibrational frequencies because of the strong anharmonicity this implies. The B–H stretching mode is estimated to be in the 2540–2655 cm⁻¹ range, with an anomalously low wagging mode.

The two calculated configurations of the {B, H} pair in diamond are compared in Fig. 19. Note that the vibrational stretch mode of H and the symmetry should be observable by IR spectroscopy, and should be very distinct for both configurations. The {N, H} pair in diamond is predicted at the ASED-MO level [119] to have C_{3v} symmetry, with H bridging one of the N–C bonds. The calculated bond lengths are N–H = 1.20 Å and H–C = 1.09 Å, indicating a very compressed bridged bond. The binding energy relative to free atomic hydrogen is 1.49 eV. The activation energy for BC-to-BC motion via the C site is very

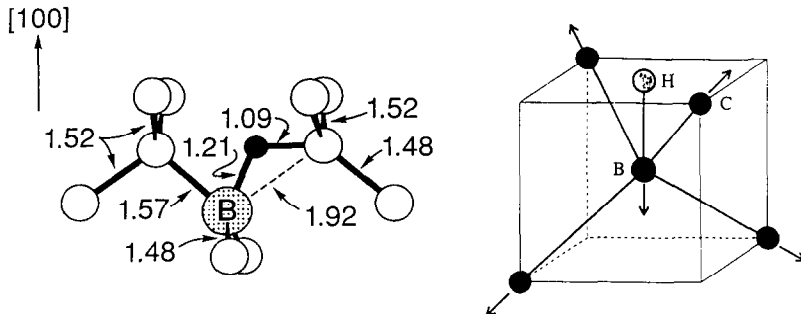


Fig. 19. Comparison of the two calculated configurations of the $\{B, H\}$ pair in diamond. The ASED-MO method [119] predicts a puckered bridged bond with H bonds to both C and B (left, the bond lengths in Å are shown), while the first-principles DFT method [246] has H along a $\langle 100 \rangle$ direction with no C-H bonding (right).

high, 2.54 eV. Finally, $\{N, H\}$ is found to have a deeper gap level than substitutional N alone.

The semiempirical ASED-MO method has also been used to investigate the configurations and binding energies of vacancy–hydrogen complexes. As from one up to four H interstitials are inserted into a vacancy, the binding energies become smaller and C–H bond lengths shorter: 5.3 eV and 1.08 Å for $\{V, H_1\}$, 4.4 eV and 1.05 Å for $\{V, H_2\}$, 3.6 eV and 1.03 Å for $\{V, H_3\}$, and 2.5 eV and 1.00 Å for $\{V, H_4\}$. All the C–H bonds have H pointing toward the center of the vacancy. Even in $\{V, H_4\}$, the nearest H atoms are 1.18 Å apart, a distance much larger than the equilibrium H–H bond length in H_2 (0.75 Å). The activation energy for $\{V, H_1\}$ diffusion is calculated to be 5.1 eV vs. 4.3 eV for the neutral vacancy alone. Note that these predictions are in qualitative agreement with the trends obtained for $\{V, H_n\}$ complexes in silicon.

3.1.2. Silicon

Many hydrogen–impurity and hydrogen–defect interactions in Si have been studied experimentally and theoretically (a review of some of the theoretical work has been published [247]). The first ones to be discussed below are the passivation or activation reactions involving shallow-level centers. This includes the passivation of shallow dopants (acceptors and donors), the re-activation of the passivated centers, and the activation of substitutional C. The interactions with oxygen are reviewed next. This includes not only the passivation of O-related thermal donors, but also the exotic issue of hydrogen-catalyzed diffusion of O. Then, the interactions with deep-level centers, such as dangling bonds (vacancies, in particular) and TM impurities are discussed. The section ends with the issues of multiple trapping of H at dopants, hydrogen-induced platelets, and a summary of calculated relative stabilities of H at various traps.

In all cases, the optical and electrical changes are caused by the formation of a covalent bond involving H. Hydrogen generally binds to a weak or dangling Si bond and is therefore not directly attached to the impurity. The changes induced upon hydrogenation are reversible by annealing at temperatures of up to a few hundred degrees Celsius. A number of the complexes are also affected by the exposure to bandgap light, i.e. the concentration of minority charge carriers. For a given complex this may mean enhanced debonding or the existence of a bistable state. Note that rapid thermal anneals involve high-intensity, above-bandgap illumination which may cause a redistribution of the bound H in the sample. The low thermal stability and the possible sensitivity to light has prevented the use of H in the

processing of Si devices, with a few exceptions dealing with the passivation of dangling bond-like defects. There, H forms strong two-electron bonds which are thermally quite stable. For example, the last step in the processing of some polycrystalline Si solar cells is hydrogenation, which substantially increases the efficiency of the cell by passivating deep traps at dislocations. Note that the thermal stability of H-complexes is higher in wide-bandgap materials such as GaN (see the end of Section 3.2.2), where annealing at 900 °C or so is required to undo the effects of hydrogenation.

3.1.2.1. Passivation of shallow acceptors

The key experimental features of the interactions between H and shallow acceptors can be summarized as follows.

- (i) The passivation of shallow single acceptors is highly efficient. Substitutional B, Al, Ga, In, and Tl are all passivated by exposure to atomic hydrogen [4].
- (ii) The passivation is caused by one (or both) of the reactions $A^- + H^+ \rightarrow \{A, H\}^0$ or $A^- + h^+ + H^0 \rightarrow \{A, H\}^0$, where h^+ is a hole. The end result is the formation of the neutral $\{A, H\}$ pair, in which H forms a covalent bond with a Si atom adjacent to the acceptor. Compensation alone cannot explain a number of key experimental observations [248]. The passivation depth can be increased by the application of an electric field.
- (iii) The lowest-energy configuration is BC_{Si} , illustrated qualitatively in Fig. 18. The acceptor is essentially three-fold coordinated, but overlaps with the H-Si bond.
- (iv) The IR- and Raman-active modes of this complex, including many isotope substitutions, have been measured, and uniaxial stress studies performed. In the case of the boron-deuterium pair, an unusual Fermi resonance between the second harmonic of the transverse B mode and the fundamental longitudinal D mode has been identified [249].

The interactions between single acceptors and hydrogen in Si are possibly the best understood of any interactions involving H in semiconductors. However, a few issues remain elusive. For example, are there metastable or even bistable states, and do they play a role in the re-activation of the acceptor? The debonding of H from the $\{B, H\}$ pair has been shown to be quite sensitive to the exposure to bandgap light [250–252]. Is H exactly on the trigonal axis or is it rotating around it [253,254]? What is the reason for the low-frequency mode (56 cm^{-1} for $\{Ga, H\}$ and 78 cm^{-1} for $\{Al, H\}$) reported [255,256] to exhibit a $\sqrt{2}$ shift when D substitutes for H? Such a low frequency is unusual for a species as light as H.

Many theorists have calculated properties of acceptor-H pairs (mostly B). DeLeo and Fowler [257,258] were the first to perform total-energy calculations on these pairs. They used the scattered-wave Xα and the MNDO methods in 16 host-atom clusters to confirm the prediction of Pankove et al. [259] that the hydrogen-acceptor pair has H near a BC position between the acceptor and one of its NNs. They studied the $\{B, H\}$ and $\{Al, H\}$ pairs. Assali and Leite [260] proposed an alternative model with H near the T_B site (1.75 Å away from the B atom) on the basis of multiple-scattering Xα calculations. They later showed [261] that a set of carefully chosen spring constants in this configuration provides vibrational frequencies in close agreement with those observed by IR absorption. However, this configuration is a saddle point of the energy [262].

Amore Bonapasta et al. [263,264] performed ab-initio HF calculations with minimal basis sets in 8 host-atom clusters. They find a tendency for H to move off the trigonal axis for acceptors larger than B. They also performed LDF calculations in 8 and 16 host-atom cells for Al, Ga, and In [265,266]. They find that H moves off the trigonal axis by some

30°, and attribute the low frequency modes reported in the cases of {Al, H} and {Ga, H} (see above) to the off-center configuration.

Chang and Chadi [146,267] studied the {B, H} pair at the LDF level with 8 atom cells. Similar calculations, but using up to 32 atom cells, were conducted by Denteneer et al. [202,268] who obtained a barrier for reorientation of H between equivalent BC configurations of 0.2 eV, remarkably close to the experimentally measured activation energies of 0.19 eV [269] and 0.22 eV [270]. However, in this calculation, the host atoms are allowed to adjust instantaneously to the motion of H. Calculations which take into account the large mass difference between H and Si should be performed to confirm this result.

Estreicher et al. [271] did approximate ab-initio HF (PRDDO) and ab-initio HF calculations (with large basis sets) in small and large molecular clusters for the B, Al, and Ga acceptors. They also found a slight tendency for H to move off the trigonal axis, by less than 0.02 Å (B), 0.05 Å (Al), and 0.10 Å (Ga). They investigated the effects of uniaxial stress on the equilibrium geometry of the various pairs. Artacho and Ynduráin [272] performed ab-initio ROHF calculations with minimal basis sets in small clusters, while Maric et al. [273,274] did closed-shell ab-initio HF calculations with split-valence polarized basis sets, also in clusters.

Finally, Zhou et al. [30] studied cell size and basis-set size effects for {B, H} at the LDF level. Their biggest calculations were made in a 64-atom cell with a 22 Ry cutoff for the plane-wave basis set. These values are larger than those used by other authors. They found rather large size effects, indicating that some of the results obtained with smaller cells or basis sets have not fully converged.

There is qualitative agreement among theorists about the ground-state configuration, even though details vary from one author to the next. LDF calculations report longer Si–H bond lengths than HF calculations. As a result, LDF predicts something closer to a three-center bond (Si–H–B), while the HF picture is an essentially three-fold coordinated B atom, overlapping only weakly with a strong Si–H bond (Si–H···B). The exact displacements of the Si and B atoms also vary from author to author, as one would expect from the large variations in cell or cluster size, basis set, and other approximations involved. There is also disagreement regarding the lowest metastable configuration. HF calculations tend to favor the H–Si···B structure, while LDF calculations predict a Si–B–H geometry.

A number of authors calculated the IR-active frequencies of H and found values quite close to the experimental ones, despite the differences in the equilibrium geometries. No wagging modes in the 600–800 cm⁻¹ range have been observed. This could be related to the tendency of H to move off the trigonal axis, as found in several calculations. The results are summarized in Table 10. Note the rather large change in frequency reported by Zhou et al. [30] for the {B, H} pair when going from the 8- to the 64-atom cell (even though both values are within 5% or so of the experimental value).

The calculated dissociation energies of H from the {B, H} pair are 2.5 eV [146] and 2.14 eV [188]. Both numbers are larger than the experimental estimates of 1.28 eV [277] and 0.87 eV [278]. The measured dissociation energies for {Al, H}, {Ga, H}, and {In, H} are 1.44 eV, 1.40 eV, and 1.42 eV, respectively. Note that the discrepancy between theory and experiment may be related to the nature of the dissociated species (location and charge state of the dissociated H) rather than theoretical error.

The interactions of H with the oxygen-vacancy pair (A-center) have also been studied theoretically. In the isolated defect, O moves off-center, bridges one of the reconstructed

Table 10
Theoretical and experimental vibrational frequencies (cm^{-1}) of H for H-acceptor pairs in Si

Pair	Author [Ref.]	Stretch	Experiment
{B, H}	DeLeo et al. 3257,258]	1880	1906
	DeLeo et al. [275]	1815	
	Chang et al. [267]	1820	
	Denteneer et al. [268]	1830	
	Bonapasta et al. [265,266]	1830	
	Zhou et al. [30] ^a	1817, 2013	
{Al, H}	DeLeo et al. [257,258]	2220	2201
	Bonapasta et al. [265,266]	1830	
{Ga, H}	Bonapasta et al. [265,266]	1880	2171
{In, H}	Bonapasta et al. [265,266]	1720	

DeLeo et al. [275] reported a wag mode at 810 cm^{-1} and Zhou et al. [30] at 232 cm^{-1} (in the 64-atom cell). The experimental values, obtained at liquid He temperature, are from Ref. [276]. No wag mode was observed.

^a The first number was obtained in the 8-atom cell, the second in the 64-atom cell.

Si–Si bonds in the vacancy, leaving the second reconstructed bond mostly unaffected. The A-center behaves as an acceptor [279,280]. The interactions of this center with H has been examined by two groups.

Gutsev et al. [281] used the semiempirical HF method of MNDO in small clusters. They found that {O, H, H} has the two Hs saturating the remaining dangling bonds in the vacancy, away from O, as one would expect. However, for {O, H}, they find that the reconstructed Si–Si bond remains while H attaches to O. This contrasts with the result of Artacho and Ynduráin [272] who find the H does bind to a Si dangling bond instead of O. They used the ab-initio ROHF technique with a minimal basis set.

Hydrogen also interacts with double acceptors, and this has been reported for Cd [282], but the case of Be is much better documented both experimentally and theoretically. Muro and Sievers [283,284] established that {Be, H} is a tunneling system in which H appears to have minima along the four $\langle 111 \rangle$ directions [285].

Denteneer et al. [202] performed LDF studies of the {Be, H} complex in 16- and 32-atom supercells. They find that H is at the C site of a Si atom adjacent to Be, with C_{2v} symmetry. The barrier for reorientation of the complex is only 0.1 eV if the atoms are allowed to adjust instantaneously to any displacement of H. A second reorientation path involving little Si participation has an activation energy of 0.4 eV.

These results disagree with those of Artacho and Ynduráin [272] who investigated this problem at the ab-initio ROHF level (minimal basis set) in molecular clusters. They found that {Be, H} is similar to the {H, A-center} problem, with Be two-fold coordinated in the vacancy (off-center) and H saturating a Si dangling bond. Their activation energy for reorientation is much higher (1.8 eV).

DeLeo et al. [286] performed MNDO calculations in a small molecular cluster, and found that {Be, H} looks more like the {B, H} pair, with Si–H almost along a $\langle 111 \rangle$ axis, and a reorientation barrier of 0.8 eV. They also studied the charge states of the complex. Finally, the {Be, H} and {Be, D} pairs have also been examined within the framework of a hindered rigid rotor model [287].

Thus, the issue of the {Be, H} complex is not resolved to everyone's satisfaction. Perhaps MD simulation will provide a key contribution, even though they are not equipped to include quantum tunneling.

3.1.2.2. Passivation of shallow donors

The shallow single donors P, As and Sb are passivated by atomic hydrogen but the reaction is less efficient than in the case of single acceptors, unless the donor concentration is very high. The passivation is owing to the formation of a covalent bond between H and a host Si atom, but the thermal stability of the pair is lower than in the case of acceptors. There is ample experimental and theoretical evidence that the complex has C_{3v} symmetry and has hydrogen at the AB site of a Si adjacent to the donor (the AB_{Si} configuration shown in Fig. 18) [4]. The re-activation is greatly enhanced by the exposure to bandgap light (see below).

The AB_{Si} configuration for the {P, H} pair was first proposed by Johnson et al. [170] a result later confirmed by a number of groups. LDF calculations in supercells with plane wave basis sets were performed by Chang and Chadi [267], Zhang and Chadi [288], Denteneer et al. [289], Amore Bonapasta et al. [265] and Zhou et al. [30]. Semiempirical HF calculations (MNDO) in 5 and 8 host-atom clusters were conducted by DeLeo et al. [290] while Estreicher et al. [271] performed approximate ab-initio HF (PRDDO) and ab-initio HF (with large basis sets) calculations in small (8 host-atom) and large (44 host-atom) clusters. Amore Bonapasta et al. [291] also performed ab-initio HF calculations (with a minimal basis set) in small clusters. Finally, LDF calculations in a 44 host-atom molecular cluster and Gaussian basis sets have also been used to calculate the IR-active modes of {P, H} by Estreicher and Jones [131]. All works found the same general configuration ($H-Si\cdots P$). However, there are differences between LDF and HF predictions regarding many details. LDF calculations predict longer Si-H bonds than HF ones (the longest one, 2.33 Å, was proposed by Chang and Chadi [267]) and report that the P atom moves toward its Si NN along the trigonal axis, while all HF calculations report it moving away from Si toward a more planar configuration with its three NNs. However, the geometries vary substantially with cell size [30], and possibly cluster size as well, although systematic cluster-size calculations have not been made for this complex. The configurational differences imply widely different Si-H bond strengths and stretching frequencies. The predicted stretching and wagging modes are compared with the experimental ones in Table 11. The lowest-lying metastable state is

Table 11

Theoretical and experimental vibrational frequencies (cm^{-1}) for H donor-H pairs in Si. The experimental values, obtained at liquid He temperature, are from Ref. [175]

Pair	Author [Ref.]	Theory		Experiment	
		Stretch	Wag	Stretch	Wag
{P, H}	Johnson et al. [170]	2145		1555	809
	Chang et al. [267]	400			
	Amore Bonapasta et al. [291]	2149	908		
	Zhang et al. [288]	1290	715		
	Denteneer et al. [289]	1460	740		
	Amore Bonapasta et al. [265]	1450	720		
	DeLeo et al. [290]	2140	630		
	Estreicher et al. [131] ^a	1856/1571	988		
	Zhou et al. [30]	1534	847		
{As, H}	Zhang et al. [288]	1260		1561	810
{Sb, H}				1562	810

^a The low frequency was calculated with Si at the lowest-energy configuration, the high one with Si displaced by 0.08 Å. This strong dependence on small displacements is indicative of large anharmonic effects.

generally found to be the Si \cdots P–H configuration [170,271,288–290] although the Si–H \cdots P one has also been proposed [291].

Note that a second stretch mode at 1647 cm $^{-1}$, 1661 cm $^{-1}$, and 1671 cm $^{-1}$ (corresponding to {P, H}, {As, H}, and {Sb, H}, respectively) has also been observed. The intensity of these lines is small (about 20–60% of the main stretch frequency), but they anneal out at the same temperature as the main lines. This second stretch mode is associated with an unidentified donor–hydrogen complex. The calculated binding energies of the {P, H} pair, 2.0 eV in Refs. [146,267] and 2.04 eV in Ref. [188], are larger than the experimental estimates of 1.2 eV [178] and 0.35–0.65 eV [278].

An area of controversy involves the re-activation kinetics of donor–hydrogen pairs. While the thermal debonding of {D, H} pairs (where D is a donor, primarily P) occurs around 100 °C in the dark, electrical measurements show that the reactivation of the passivated donors already occurs at room temperature when the sample is exposed to light [177,178]. While the debonding of {P, H} has been used to demonstrate the existence of H $^-$ in silicon [172,173], light-induced reactivation has also been assumed to result from the break-up of the {P, H} pair into P $^+$ and H $^-$. Sophisticated capacitance measurements [179,180] have used this assumption to extract the diffusivity of H $^-$ and the position of the acceptor level of interstitial H in the gap.

However, the uniqueness of the interpretation of the latter data has recently been challenged [181]. The key issue is the observed reversibility of the light-induced reactivation. Hydrogen-passivated samples are reactivated by exposure to light at room temperature and a bias left on for long periods of time to make sure that any H $^-$ is swept away. However, when the samples are left in the dark (for a day or so) at room temperature at zero bias, 30–80% of the reactivated donors return to a passivated state, without additional exposure to hydrogen [132]. This implies that either the {P, H} pair broke up and that H was not swept away by the field but trapped at an unknown site near P $^+$, or that a substantial fraction of the passivated {P, H} 0 converted to a bistable (donor) state {P, H} $^+$ upon capture of a minority charge carrier [130,182].

The reactions {P, H} 0 + h $^+$ \rightarrow {P, H} $^+$ and {P, H} $^+$ + e $^-$ \rightarrow {P, H} 0 have been studied theoretically at the approximate ab-initio and ab-initio HF level in molecular clusters and with LDF theory, also in clusters [131,183]. The results show that a bistable state indeed exists, and that the neutral (H–Si \cdots P) 0 configuration readily converts to the positively-charged (Si–H \cdots P) $^+$ configuration upon capture of a hole. Hydrogen simply rotates in the {110} plane around the Si atom to which it is attached. On the other hand, the reverse reaction is not spontaneous. It involves a large activation energy, estimated at about 2 eV at the ab-initio HF level, which is consistent with a slow recovery, even in the presence of free electrons. In a study related to the multiple trapping of H at dopants, Amore Bonapasta [292] also predicts the bistability of {P, H}, with a similar configuration.

While it is clear from the reversibility data that the concentration of minority charge carriers affects more than just the break-up rate of donor–hydrogen pairs, many details of the processes involved are as yet unclear.

Hydrogen also interacts with double donors in Si. The reversible passivation of substitutional S, Se, and Te has been reported by Roos et al. [293] (the interactions of H with oxygen-related thermal donors are discussed in a separate section below). The two donor levels recover simultaneously after isothermal annealing. The binding energies of hydrogen to the donors are around 1.4–1.6 eV. It appears that a single H is capable of

passivating the electrical activity of both donor levels, suggesting that some configurational reconstruction occurs after the capture of one H by the donor.

The structure of hydrogen–sulfur complexes has been calculated by Yapsir et al. [294] at the semiempirical HF level (MINDO/3) in cyclic clusters. When two Hs are present, they saturate two Si dangling bonds, leaving S two-fold coordinated, in a configuration similar to that found for {O, H, H} or {Be, H, H} (see above). The authors also find that a single H will also form a bond with a Si atom, near S, and is able to remove both donor levels in the gap, in agreement with the experimental observation.

3.1.2.3. Interaction with substitutional C

Although hydrogen probably interacts with interstitial as well as substitutional C, only the complexes formed with the latter have been studied so far and are considered below. A comprehensive review of the properties of carbon in silicon has recently been published [295].

Substitutional C is an iso-electronic impurity which is not electrically active in Si. However, typical C–Si bond lengths realized in free molecules are of the order of 1.85 Å, far shorter than the bond length imposed upon C by the Si crystal (2.35 Å). As a result, C pulls its four NNs inward, generating lattice strain, which attracts interstitial H. One could guess that H relieves some of the strain. For example, H could form a bond with C, allowing it to relax, and get closer to its three remaining Si NNs, leaving a three-fold coordinated Si atom with an odd electron in a non-bonding orbital. One can think of four similar scenarios (H at the AB_C, BC_C, BC_{Si}, and AB_{Si} sites), each of which leaves a neutral complex with an unpaired electron in a non-bonding orbital on C or Si. Any one of these configurations could be electrically active, depending on how much energy is needed for the unpaired electron to capture a second electron or jump to the CB. Both reactions would result in some change in the configuration of the defect. In fact, the {C, H} pair is a shallow acceptor in Ge (see below) and a deep donor in Si. The reasons why the behavior of the same pair is different in both hosts is unclear at this point.

DLTS studies in n-type (P-doped) Si [296–298] have shown that {C, H} has a deep donor level near $E_c - 0.16$ eV. The donor anneals at 300 K by the capture of an electron. The H–C dissociation kinetics yields an activation energy of 0.73 eV [298]. The closeness of this level to the that of the E3' center (H_{BC}) [129] led to some questions at first. However, double-correlation DLTS data [299] have pinpointed the zero-field level at $E_c - 0.185$ eV, leaving no doubt that both centers are indeed distinct. However, the unusually strong electric-field dependence has yet to be explained. A complicating factor is the presence of the P donor in all the samples used which, if near the {C, H} pair, could affect the field-dependence. The same could be said of the {P, H} pair, which may also acts as a donor [131,182,292]. Repeating some experiments with As instead of P may show if the dopant is involved or not.

The passivation of the P donor and the activation of C has also been reported by Kamiura and coworkers [133,300–302]. They find that the pair is stable up to 80 °C in the dark, but dissociates below room temperature under illumination. They propose a model which has H bridging one of the four C–Si bonds, and is more strongly bound to Si than to C (the electronegativity of which is larger). A relaxation would accompany a change of charge state. A carbon–hydrogen complex has also been identified by photoluminescence [303].

The equilibrium configuration and electronic structure of the neutral $\{C, H\}$ pair in Si (and Ge) has been calculated by Maric et al. [273,274] at the ab-initio HF level in 8 and 14 host-atom clusters. Two trigonal configurations of $\{C, H\}^0$ are found with virtually the same energy and structures in both hosts (a figure is in the Ge section). The lowest-energy configuration coincides with that proposed by Kamiura et al. [133]. Hydrogen is at a BC_{Si} site, C is almost sp^2 hybridized, near the plane of its three Si NNs, with 95% of the odd electron in a non-bonding orbital. An almost degenerate configuration (only 0.05 eV higher) has hydrogen at the AB_C site, with the Si atom along the trigonal axis three-fold coordinated and carrying the odd electron. The competing factors are the greater strength of the C-H vs. the Si-H bond and the greater stability of the odd electron on C vs. Si. The two possible compromises lead to different yet almost degenerate structures. The configurations of $\{C, H\}^+$ have yet to be studied at this level of theory.

A DFT calculation in periodic supercells by Kaneta and Katayama-Yoshida [304], finds qualitatively similar structures. The stable configuration has H between C and Si, and the metastable one has H at the AB_C . However, they find that, in the BC configuration, H forms a three-center bond instead of forming a two-electron bond with the Si atom. Their calculation is consistent with H_{BC} being only slightly perturbed by the presence of C. This result is consistent with the prediction of Denteneer et al. [202] (for the $\{Si, H\}$ in Ge) that the electrical activity of the pair is the same as that of H at the same location without the impurity present. However, it conflicts with the much stronger perturbation described by Maric et al. [273,274].

3.1.2.4. Interactions with oxygen

Interstitial oxygen (O_i) is found in concentrations of the order of 10^{16} cm^{-3} in CZ-grown Si. It forms a puckered bridged bond and its activation energy for diffusion [305–307] is about 2.5 eV. Interstitial O has been studied theoretically by a number of groups (see, for example, Ref. [40] and references cited therein). O-related thermal donors (TDs) are double donors appearing in CZ-Si after 400–450 °C anneals. These centers were first observed several decades ago [19–21].

It is known that over a dozen TDs evolve into each other with annealing time, becoming gradually shallower, until their donor levels disappear into the CB. They are denoted TD1, TD2, etc., and the evolution is believed to be caused by more and more O_i s clustering around an unidentified core. However, the evolution from TD_n to $TD(n+1)$ involves an activation energy of only 1.7 eV or so [308,309], a number much smaller than the known activation energy for O_i diffusion. This has led to theoretical studies [310] suggesting that oxygen dimers (not molecules, but rather pairs of adjacent interstitials) diffuse with a lower activation energy than isolated O_i . A wide variety of possible O_i aggregates has been calculated by various groups, with and without the presence of self-interstitials [311–318].

Although some of the models are quite sophisticated and have many of the desired features (see, for example, Ref. [318]), the structure of the various TDs has not been resolved to everyone's satisfaction. However, their electrical activity is passivated [319–322] by exposure to atomic hydrogen below 200 °C. This passivation reaction is reversible by anneals at higher temperatures.

In a recent paper [323] the formation of six H-related shallow (thermal) donors in H-doped CZ-Si is reported. It is not clear how or if these donors are related to the usual (oxygen-related) TDs.

In addition to passivating TDs, hydrogen was observed to play an unexpected role with O_i in the 350–450 °C range. CZ-Si samples annealed in a hydrogen plasma show a tremendous increase in the rate of TD formation over samples annealed in an identical manner in an H₂ (or any inert) gas [324,325]. This enhancement is illustrated in Fig. 20. The enhancement factors are about 5, 30, and 300 at 450 °C, 400 °C, and 350 °C, respectively, leading to an activation energy in the 1.8–2.0 eV range. In studies unrelated to TDs, it was shown that hydrogen also increases the reorientation rate of O_i among adjacent puckered BC sites, without altering its 1136 cm⁻¹ stretch mode [326].

It is now accepted that the underlying reason for this enhancement is the catalyzed diffusion of O_i by atomic H [327], although it is not clear if this affects directly or indirectly TD formation. This topic has recently been reviewed [328]. Many questions remain unanswered. For example, H appears to be (or become) incorporated in the TDs [323,329], although no formation of an O–H bond has been detected by IR spectroscopy [330].

Stein and coworkers [331–333] performed systematic studies to unravel the effects of the many unknown parameters in this process. His work includes D substitutions, SIMS profiling after various annealing times, and variations in the plasma exposure and temperature. These studies raised further questions. For example, the very abrupt profiles of TD

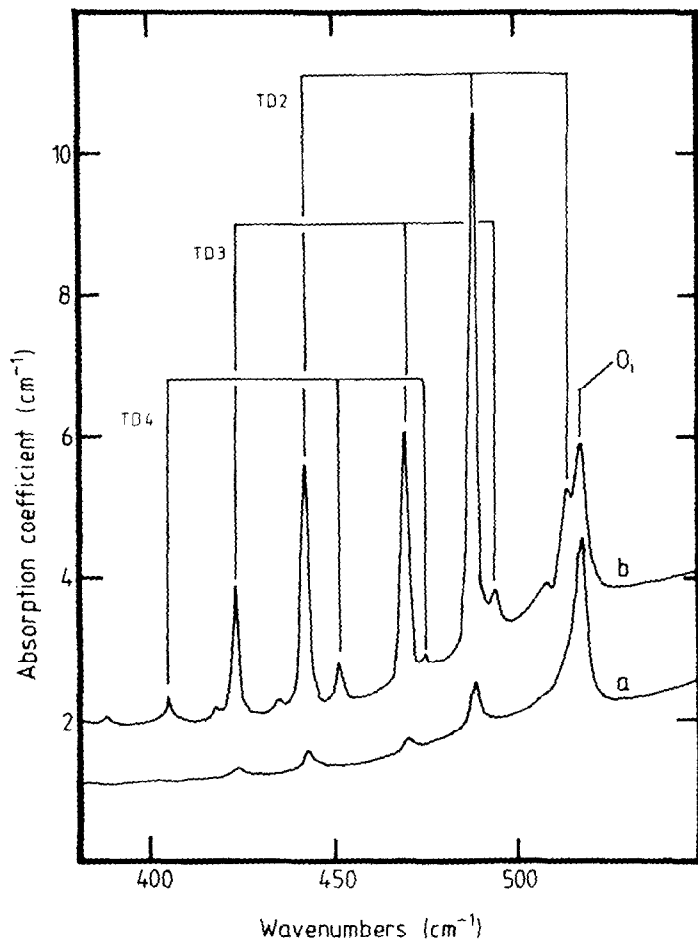


Fig. 20. Comparison of the absorption lines of the TD2, TD3, and TD4 centers in samples annealed for two hours in (a) an H₂ gas and (b) an H plasma. The figure is from Ref. [324] with permission.

concentration after annealing in a H plasma have a surprising shape (Fig. 21). One would expect a much softer shoulder on the bulk side and a rapid convergence toward the maximum TD concentration closer to the surface than are observed. The profiles could be explained if the diffusivities of H and O_i converge under high doses of H exposure.

A related piece of experimental information was provided by μ SR [77] and positron channeling (from muon decay) [334] spectra obtained under identical conditions in FZ- and CZ-Si. μ SR in the FZ material gives the usual normal (Mu_T^0), anomalous (Mu_{BC}^0), and diamagnetic (μ^+) signals. In CZ-Si, however, only Mu_{BC}^0 is seen, and the other two signals totally disappear (see Figs. 45 and 72 in Ref. [77]). The channeling experiments indicate the presence of an oxygen-trapped muonium state at a tetrahedral site. These experiments have not been systematically pursued but indicate that qualitative differences in the behavior of positive muons are apparent in O-rich and O-poor material.

This problem is both fascinating and excessively difficult to model theoretically. It is a dynamic process which involves high activation energies, and no experimental clues as to the microscopic processes involved are available. The unknowns abound, and the full problem has a large number of degrees of freedom. The first step in the series of processes taking place is the interaction between an isolated H and one O_i. The reaction has been studied by two groups. Estreicher [335] has used the method of PRDDO in 5–35 host-atom clusters while Jones et al. [336] performed first-principles LDF calculations in 35 and 44 host-atom clusters.

Estreicher and Jones et al. agree that the effect of H is purely catalytic (no O–H bond is formed). The role of H is to stabilize the transition-point configuration in the O_i diffusion path by saturating a Si bond that would otherwise be a dangling bond. This lowers the activation energy for the diffusion of O_i, resulting in enhanced diffusion. However, the two authors differ on the quantitative aspects of this problem.

The first model [335] uses the HF results that H⁰ in Si is stable at the BC site and metastable at the T site, with H_T⁰ being a rapidly diffusing species (at low and intermediate temperatures). It also uses the μ SR result that Mu_T⁰ is not seen in CZ-Si, while the Mu_{BC}⁰ signal is the same in CZ- and FZ-Si. The assumption is that H_T⁰ is the species attracted

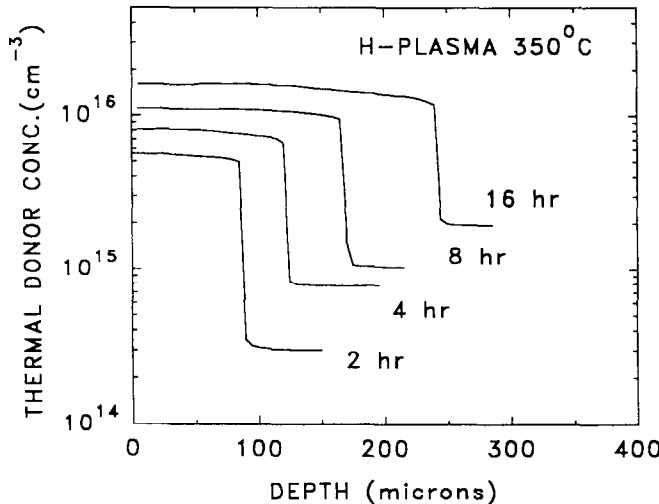


Fig. 21. Depth profiles for TDs formed at times from 2 to 16 h under H r.f. plasma exposure at 350 °C. The figure is from Ref. [333] with permission (a similar figure was also published in Ref. [332]).

to the strained region of the crystal near O_i . The calculations begin with H_T^0 at the T site immediately adjacent to O_i . Then, O_i is moved from one puckered BC site to the next in the $\{110\}$ plane, and the coordinates of H^0 and of the three Si NNs to O_i and H are optimized for each intermediate position of O_i . The initial, saddle point, and final configurations resulting from this calculation are shown in Fig. 22.

The activation energy for O_i diffusion, calculated at the PRDDO level, drops from 4.1 eV when no H is present to 1.25 eV when H is present. The final configuration has a puckered O_i at a Si-Si bond adjacent to the initial one, near an almost bond-centered H, a configuration 0.66 eV lower in energy than the initial one. It is assumed that at the temperatures at which H-activated diffusion occurs, the H jumps out of the BC site and pushes O_i toward a further BC site, etc. In this model, a single H could induce several jumps of O_i at temperatures at which isolated O_i is not mobile. A comparison of the calculated transition-point configurations for O_i diffusion with and without H is shown in Fig. 23.

The model proposed by Jones et al. [336] starts with H at the AB site to one of the two Si to which O_i is bound, with an Si-H bond length of 1.5 Å. The energy with O_i in its saddle-point configuration between adjacent puckered BC sites is found to be only 1.4 eV above the initial one. This is much lower than the calculated activation energy of isolated O_i , 2.8–2.9 eV at the same theoretical level. The saddle point for the diffusion of O_i with

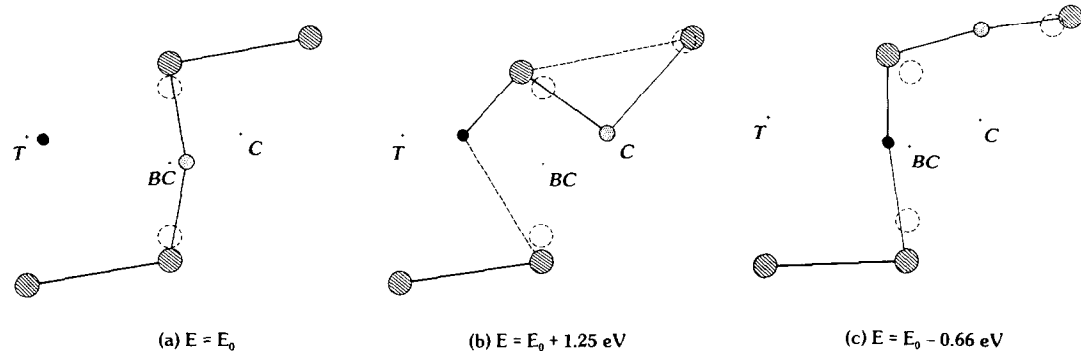


Fig. 22. Initial configuration (a), transition point (b), and final configuration (c) of the model for H-assisted diffusion of O_i . The full circle is H, the dotted circle is O, and the shaded circles are Si atoms. The figure is from Ref. [335] with permission.

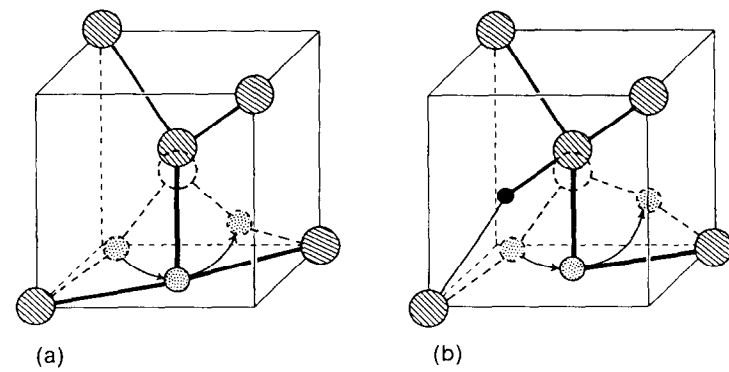


Fig. 23. Qualitative comparison between the transition-point configurations for O_i diffusion in Si without (a) and with (b) the help of H. Except for the central host atom, the relaxation of the host atoms is not shown for simplicity. Dashed lines show the initial and final configurations. The full circle is H, the dotted circle is O, and the shaded circles are Si atoms. The figure is from Ref. [335] with permission.

H is not the same as the one without H. The reason for the lowering of the activation energy for diffusion of O_i is again that H saturates a Si bond which would be a dangling bond without the presence of H. However, H remains at the AB_{Si} site throughout the displacement of O_i, in contrast to the situation described above where H moved from the T to a BC site. After the jump of O_i, H is assumed to jump to another AB site and activate another step in the diffusion of O_i.

There is no microscopic experimental evidence of the processes taking place. Both models are based on static potential surface calculations, and are limited in their scope. It is clear that a dynamic study, if feasible for such large activation energies, is highly desirable. However, both studies predict a catalytic role of H, the first such effect ever observed for H in a semiconductor.

3.1.2.5. H and TM impurities

TM impurities can be deliberately introduced into a semiconductor to control the lifetime of charge carriers (for example gold in Si [337]). More often, they are undesired contaminants. Third-row TMs tend to be interstitial impurities, fourth-row TMs are found both interstitial and substitutional, and fifth-row TMs are almost exclusively substitutional. Their behavior is very varied and few features are common to all TM impurities. Copper diffuses faster than any other impurity (as Cu⁺), while Ti hardly moves below the melting point of Si. Isolated interstitial Cu does not affect the electrical properties of the material, while Ti and V have enormous electron and hole-capture cross-sections. Even in concentrations as low as 10¹² cm⁻³, the latter impurities reduce the efficiency of solar cells by as much as 20% [338,339]. Other TMs easily pair up with dopants. A well-known example is the {Fe, B} pair [340]. Further, many TM impurities introduce more than one level in the gap. Electrical measurements [341] show that the electrical activity of the slow diffusers Ti and V is not affected by hydrogenation.

It was observed as early as 1982 that the electrical activity of some TM impurities such as Au or Fe is reduced or removed by hydrogenation [342,343]. The DLTS spectra or spreading resistance profiles (see, for example, Figs. 3.1 and 3.2 in Ref. [4]) show the change in electrical activity, but provide no information on the microscopic interactions taking place. Hydrogen has been credited with passivating all or some of the deep levels associated with Au, Ag, Cr, Fe, Mn, Pt, Pd, Zn, as well as those of complexes involving Cu and Ni (for details and references, see Ref. [4]). However, several authors have reported new deep levels arising from the formation of H-TM complexes [344–347]. More recently, microscopic techniques such as EPR or local vibrational-mode spectroscopy have provided detailed, microscopic, information on several charge states of {Pt, H, H} complexes [348–350].

Theoretical studies lag in this area. The electronic structure of isolated, light-TM impurities have been studied (see Ref. [351] and references cited therein), but only one publication so far reports the potential energy surface and electronic structure calculations for TM-hydrogen interactions [36]. Theoretical difficulties abound. First, most TM impurities have high spin multiplicities. This makes spin-averaged calculations questionable and, in open-shell calculations, often causes convergence difficulties. Second, TM impurities may a priori be found in a variety of spin and charge states with different configurations. Third, many TM elements are orbitally degenerate at high-symmetry sites in most charge and/or spin states, distort the crystal and/or move off the high-symmetry axis, and must be treated in low symmetry, which increases the computational requirements.

The study of Woon et al. [36] focused on interstitial Ti^0 (spin triplet), Ti^+ (spin quartet), Cu^0 (spin doublet), and Cu^+ (spin singlet), and their interactions with H^0 . These calculations were performed in small and large molecular clusters at the PRDDO level and in small clusters with ab-initio UHF.

The calculated activation energy for diffusion of Cu^+ is 0.24 eV, a number consistent with the experimental estimates (0.43 eV in Ref. [352] and 0.15 eV in Ref. [353]). The calculated activation energy for interstitial Ti^+ (3.3 eV) is larger than that for Ti^0 (2.3 eV) because the way the d orbitals are populated changes the impurity wavefunction from cigar-shaped (Ti^0) to mostly spherical (Ti^+).

Substitutional Ti^0 is found to be a trap for H^0 , with a binding energy of 1.8 eV (relative to free atomic H^0). Hydrogen renders Ti_s^0 electrically active. The lowest-energy configuration has H bridging a Ti–Si bond, with a roughly equal degree of bonding to both atoms.

Interstitial Ti^+ at the T site has a t_2 level in the gap with spin 3/2. It is also found to form a strong bond with H (with Ti–H along a $\langle 111 \rangle$ axis). The binding energy relative to H_T^0 is about 2 eV. However, hydrogen removes only one of the three levels from the gap, leaving the electrical activity of $\{\text{Ti}^+, \text{H}\}$ virtually unchanged. The authors speculate that up to three H interstitials might be needed to passivate this center, making the prospect of H passivation of Ti unlikely.

Isolated interstitial Cu^+ repels H^0 . On the other hand, Cu^0 does form a bond with H^0 , but only a weak one (about two-thirds of a two-electron covalent bond).

Finally, LDF calculations of the $\{\text{Ni}, \text{H}, \text{H}\}$ complex in clusters [354] have recently been completed in the case of substitutional Ni^+ . The calculations show that the two H atoms are at AB sites of two Si atom NNs to the Ni atom. The main features of the calculated complex are in agreement with some experimental data obtained for $\{\text{Pt}, \text{H}, \text{H}\}$ [355].

3.1.2.6. Hydrogen–vacancy interactions

Vacancies and vacancy aggregates are common intrinsic defects in Si. Their properties have been reviewed by Watkins [356]. Vacancies can be created by implantation damage as well as treatments which affect the surface: exposure to a H plasma, etching, or various chemical treatments which may remove Si atoms from the surface, leaving a vacancy that could propagate into the bulk. Further, the strain caused by high concentrations of O_i such as those occurring in CZ-Si also result in higher concentrations of vacancies relative to FZ material. Vacancies are more abundant in p- than in n-type material because self-interstitials are easily trapped at group-III dopants, leaving an excess of vacancies.

EPR studies [356,357] have shown that vacancies are more stable in the charge states in which the electrons are paired, that is V^{2+} , V^0 , and V^{2-} , which are all spin singlets. On the basis of Green's function calculations [358], Baraff et al. have shown that the vacancy is a negative-U defect. This result was confirmed in a MD study [359]. All the charge states except V^{2+} are orbital triplets in T_d symmetry. As a result, the vacancy distorts to a lower symmetry (tetragonal) configuration in which the four dangling bonds reconstruct and form two pairs of long bonds which show a substantial amount of covalent overlap (see below). The ground-state configuration of V^0 has been calculated by a number of authors (see Ref. [41] and references cited therein).

The vacancy is very mobile in Si and forms pairs or larger complexes with many impurities as well as with itself. In particular, it is a strong trap for interstitial hydrogen. A great number of Si–H IR absorption bands have been reported in hydrogenated samples. In proton-implanted ones, the number of bands increases with the ion energy (see Refs.

[1,4] and Refs. [360–367]). It is difficult to determine which line corresponds to which defect. However, a few of the lines have now been identified with some degree of certainty. The current situation is as follows. It is very likely that a strong line near 2210 cm^{-1} , which corresponds to a defect complex with T_d symmetry, should be assigned to $\{\text{V}, \text{H}_4\}$. Recently, the IR modes associated with the H_2^* pair have been unambiguously identified [155]. At 77 K, the stretch modes are at 2061.5 cm^{-1} (H_{BC}) and 1838.3 cm^{-1} (H_{AB}), with one wag mode at 817.2 cm^{-1} (H_{AB}). These modes had previously been observed, but (incorrectly) assigned to some of the $\{\text{V}, \text{H}_n\}$ complexes. Further, Stein [361] has reported that a line near 1990 cm^{-1} anneals around room temperature into two lines at 1835 and 2065 cm^{-1} . The latter are probably the H_2^* pair, which suggests that the 1990 cm^{-1} line could well correspond to H_{BC}^0 , and the anneal to the capture by H_{BC}^0 of another interstitial H. The 1990 cm^{-1} line is indeed very close to the 1945 cm^{-1} frequency proposed by Van de Walle et al. [27] for H_{BC}^0 . Recent MD simulations [149] which include H_{BC}^0 are consistent with this value. However, since other authors did report lower frequencies for H_{BC} [142,145], some uncertainty remains as to the correct interpretation of the 1990 cm^{-1} line. Finally, a line at 1946 cm^{-1} has been proposed [366] for $\{\text{V}, \text{H}_1\}$ and one at 1980 cm^{-1} for $\{\text{V}, \text{H}_2\}$ [367]. However, the most recent work [128] suggests the assignment 2060 cm^{-1} , 2120 cm^{-1} , 2160 cm^{-1} , and 2220 cm^{-1} for $\{\text{V}, \text{H}_n\}$ with $n=1, 2, 3$, and 4 , respectively. Low-temperature implants and low-temperature electron irradiation experiments are under way [128] to obtain a definite identification of the IR signature of the various $\{\text{V}, \text{H}_n\}$ complexes. Note that there is agreement that the H-stretching frequency of $\{\text{V}, \text{H}_n\}$ increases with n due to the crowding effect of more H having to squeeze inside a vacancy.

The various states of the vacancy have deep levels in the gap which can be passivated by exposure to atomic hydrogen. Only $\{\text{V}, \text{H}_4\}$ is electrically inactive. This role of hydrogen has been recognized early (for a review, see Ref. [1]). A number of authors have calculated the configurations and/or electronic structures and vibrational modes of the $\{\text{V}, \text{H}_n\}$ complexes at various levels of theory [41,161,368–377]. The calculations, methods used, and key results have recently been reviewed in the introduction section in Ref. [41]. The key areas of agreement among the various authors are as follows.

- (i) Hydrogen–vacancy interactions lead to the formation of strong Si–H bonds, with the H atoms pointing toward the center of the vacancy approximately along trigonal axes. Only one study, which uses a tight-binding method, finds H to lie at AB sites outside the vacancy [378].
- (ii) Only the $\{\text{V}, \text{H}_n\}$ complexes with $n < 4$ have electrically active levels in this gap.
- (iii) The Si–H bonds become shorter and the stretching frequencies higher as the number of H atoms in the vacancy increases.
- (vi) The dissociation energies are of the order of 2.2–3.5 eV (see, for example, Refs. [41,377]). These fall between the Si–H bond strength at internal surfaces [379–381] (2.5 ± 0.2 eV) and that of SiH_4 (~ 4 eV).

The energy-optimized configurations [41] of V^0 , $\{\text{V}, \text{H}_1\}^0$, $\{\text{V}, \text{H}_1\}^+$, $\{\text{V}, \text{H}_2\}^0$, $\{\text{V}, \text{H}_3\}^0$, and $\{\text{V}, \text{H}_4\}^0$, are shown in Fig. 24. Similar configurations were obtained (or assumed) by other authors. The Si–H stretching frequencies corresponding to the four $\{\text{V}, \text{H}_n\}$ complexes have been calculated by Deák and coworkers [375,376] with the MINDO/3 method in periodic clusters, and by Park et al. [161] using the MD ab-initio tight-binding package developed by Sankey and Niklewski [71]. Typical error bars on calculated frequencies are at least of the order of 5% (about 100 cm^{-1} for the frequencies considered here), which makes them of limited use to positively identify a specific IR mode. The predicted frequencies

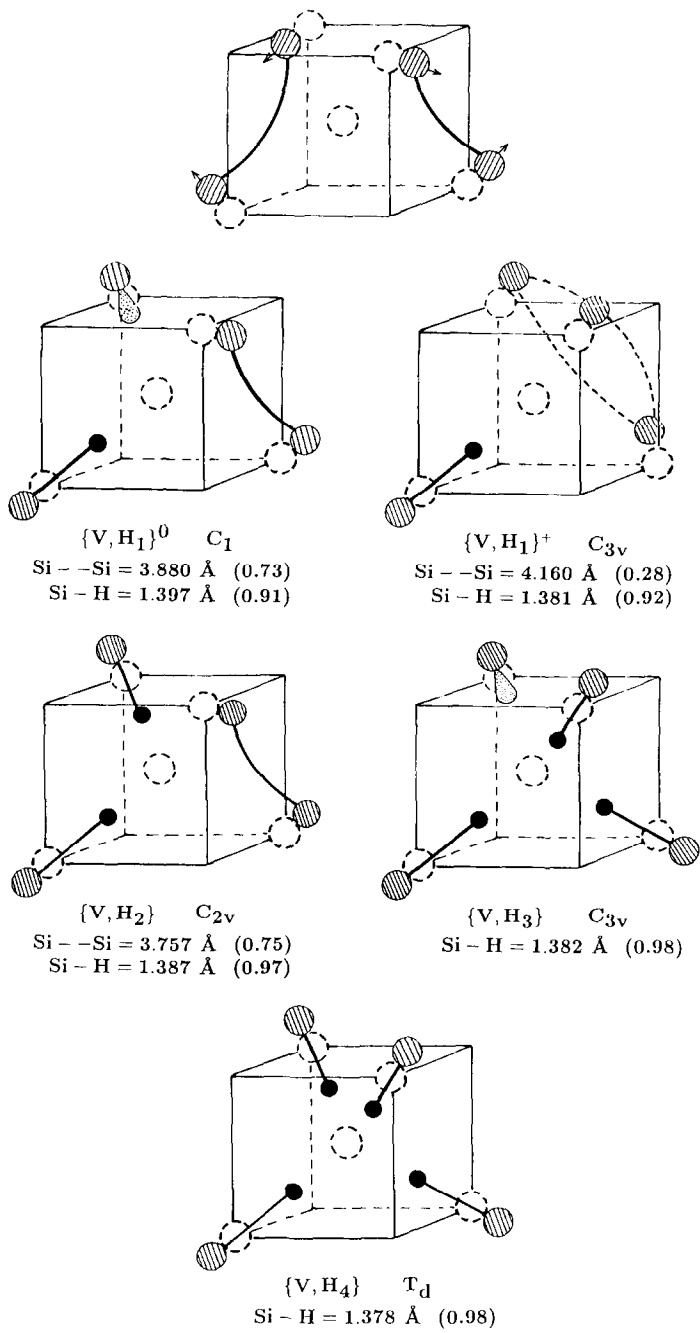


Fig. 24. Structure of the neutral vacancy and various vacancy–hydrogen complexes in Si calculated at the ab-initio HF level in Ref. [41]. In the case of V^0 , the pairs of host atoms are 3.759 Å (within the pair) and 3.929 Å (between pairs) apart. The amount of covalent bonding in the reconstructed bonds amounts to 73% of a two-electron bond (the bond strength is much less). The symmetry is D_{2d} . For each complex shown, the symmetry, relevant bond lengths, and degrees of bonding (in parentheses) are given.

(in cm^{-1}) of Deák (scaled) and of Park (at room temperature) are 2057 and 2168 for $\{V, H_1\}$, 2080 and 2268 for $\{V, H_2\}$, 2106 and 2301 for $\{V, H_3\}$, and 2109 and 2334 for $\{V, H_4\}$.

Corbett et al. [382] were the first to suggest that hydrogen-decorated vacancies are mobile in Si. The need for this assumption arose when trying to explain the shape of SIMS profiles of samples exposed to a H plasma. The idea is that the plasma etches off Si atoms from the surface, leaving a vacancy, into which a host atom from the second layer beneath the surface jumps, etc. This results in vacancies being pumped in from the surface into the bulk. This implies that vacancies are found in above-equilibrium concentrations in the sub-surface region, which contains large amounts of atomic hydrogen as well. There is no direct experimental evidence for this. The mobility of $\{V, H_n\}$ complexes was later also assumed by Sopori and coworkers [157–160] to explain the increased diffusivity of H in vacancy-rich (poly-Si) vs. vacancy-poor (CZ-, FZ-Si) material.

Roberson and Estreicher have calculated at the PRDDO and ab-initio HF levels in molecular clusters a diffusion path for $\{V, H_1\}$, and concluded that the $\{V, H_{n>1}\}$ complexes are not mobile [41]. The static potential energy calculations predict that the rate-limiting step is the break-up of the Si–H bond and formation of the new Si–H bond with the host atom moving into the vacancy. The diffusion of this species, even if it is slower than that of isolated H^0 , would involve the motion of an already-trapped hydrogen, and thus would not be trap-limited in the temperature range at which enhanced diffusion was reported.

Theoretical proof (for example, MD simulations) and experimental evidence for this mechanism is lacking. Ongoing MD studies [161] have so far failed to prove the diffusion of the pair for simulation times of 1 ps at 1500 K. Longer simulation times in larger supercells may be required. It is also possible that the capture of an electron or hole enhances the diffusion, or that an alternative mechanism exists.

3.1.2.7. Multiple trapping

SIMS profiles of Si samples exposed to a H (or deuterium) plasma show several features (see, for example, Fig. 1 in Ref. [383]): (i) the H concentration is very high at the surface, perhaps as large as 10^{21} cm^{-3} , but within the first few hundred angströms, it drops precipitously to about 10 times the concentration of dopants in the sample; (ii) in the next $0.5 \mu\text{m}$ or so, the concentration of H continues to drop toward the dopant concentration, but does so slowly, and the profiles show a ‘shoulder’, which is more pronounced in p- than in n-type material; (iii) finally, the H concentration stabilizes at the dopant concentration for depths of several micrometers. The interpretation of SIMS profiles in terms of the diffusion of hydrogen (or deuterium) has been discussed by Kalejs and Rajendran [384].

The latter part of the profile is easily understood since the passivation of dopants (formation of H-dopant pairs) can be confirmed by electrical measurements. The shoulders occurring closer to the surface are not understood. However, the excess H in that region scales with the concentration of the dopant [382]. Real-time hydrogenation studies by Seager et al. [169] show a logarithmic time-dependence of the penetration of the diffusion front as a result of the loss of mobile hydrogen. The lifetime of untrapped (mobile) H is inversely proportional to the doping level, indicating trapping associated with the dopant. They proposed that already-passivated donors and acceptors act as traps for more H interstitials. Marwick et al. [385,386] reported very high concentrations of H in buried p⁺-type Ga- or B-doped layers after treatment in a H (or D) plasma at 200 °C. They find a linear correlation between the H and the dopant concentration, with about 5–8 times more H than dopants. Stutzmann et al. [387] observed new Si–H (and Si–D) stretching frequencies in heavily-hydrogenated (deuterated) samples containing high concentrations of B acceptors. Further, recent Mössbauer spectroscopy studies [388] in Sb-doped silicon show several components

which can be explained if $\{Sb, H_n\}$ complexes, with $n > 1$, are formed. Finally, the modeling of SIMS profiles [389] results in very good agreement with the observed data if multiple trapping of H at dopants is assumed.

Although some of these data may be caused by other (unrelated) phenomena, the collection of these experimental results points toward a mechanism by which a single dopant attracts and traps more than one H interstitial. In the case of acceptors, it is believed that a long-ranged Coulomb attraction is responsible for the passivation of the negatively charged acceptor by H^+ . In the sub-surface region of plasma-exposed samples, where SIMS profiles show a very high concentration of H, it is reasonable to assume that a charged acceptor will attract all the H^+ in its vicinity prior to being passivated by the nearest one. This would result in an uneven H distribution in the sample, higher near the dopants than elsewhere. Two theoretical models have been developed to investigate this issue.

Korpás et al. [390,391] systematically studied all the possible configurations of {B, H, H} and {P, H, H} complexes, with the H atoms at T, BC, AB sites as well as various locations for H_2^T , but did not include the possibility of bistability of some of the complexes in their analysis. They find that {B, H} and {P, H} are traps for H. The lowest-energy configuration of {B, H, H} has the two H at BC sites but bridging two B-Si bonds, i.e. it has two $B \cdots H$ -Si bonds, along two different trigonal axes, but involving the same B atom, which carries the odd electron. When a third H binds to this complex, it forms a bond with the B atom at the AB_B site [392].

In the case of donors, they find that in {P, H, H}, both H atoms are bound to a host atom, one in a BC configuration $Si-H \cdots P$, the second AB to another Si-atom NN to P. The second-lowest configuration has trigonal symmetry $P-H-Si-H$. The third H atom [392] gives in a trigonal center with a five-fold coordinated donor: $H-P-H \cdots Si-H$.

Amore Bonapasta [292] performed LDF calculations in 8–32-atom supercells. He found a bistable configuration $\{P, H\}^+$ of the phosphorus-hydrogen pair which has H at the BC site, $(Si-H \cdots P)^+$, similar to that obtained by Estreicher and coworkers [130,131,182,183] to explain the reversibility of light-induced re-activation of the donors (see above). Amore Bonapasta found that this species is a donor which traps a second H to form the trigonal $Si-H \cdots P-H$ complex, which ionizes, traps a third H and becomes $H-Si-H-P-H$. The latter breaks up into the {H, P} pair plus an H_2^T molecule, and the cycle can continue. The reasons for the existence of the two successive bistable states are the two unbound electrons (lone pair) on the P atom in the passivated {P, H} complex. Note that the $Si-H \cdots P-H$ structure is different from that obtained by Korpás et al. ($P-H-Si-H$).

In the case of acceptors, Amore Bonapasta found that the $H-Si-H-B$ complex is lower in energy than substitutional B and an H_2^T molecule. The capture of a third H results in the formation of $H-Si-H-B-H$, which breaks up into the {B, H} pair and a nearby H_2^T . Note that the stable configuration for {B, H, H} is different from that proposed by Korpás et al. who found that the $H-Si-H-B$ structure is over 2 eV higher in energy.

Thus, there is experimental and theoretical support for the concept of multiple trapping of H at dopants, even though theorists disagree on the lowest-energy configurations. As the amount of H at a dopant site grows, so does the number of degrees of freedom. Static potential surface calculations become increasingly clumsy at treating this issue. However, this seems to be a nice problem to be addressed at the MD level.

3.1.2.8. Hydrogen platelets

Very large two-dimensional defect structures appear in the sub-surface region of Si samples exposed to a H or D plasma. These defects, known as platelets [383], are disk-

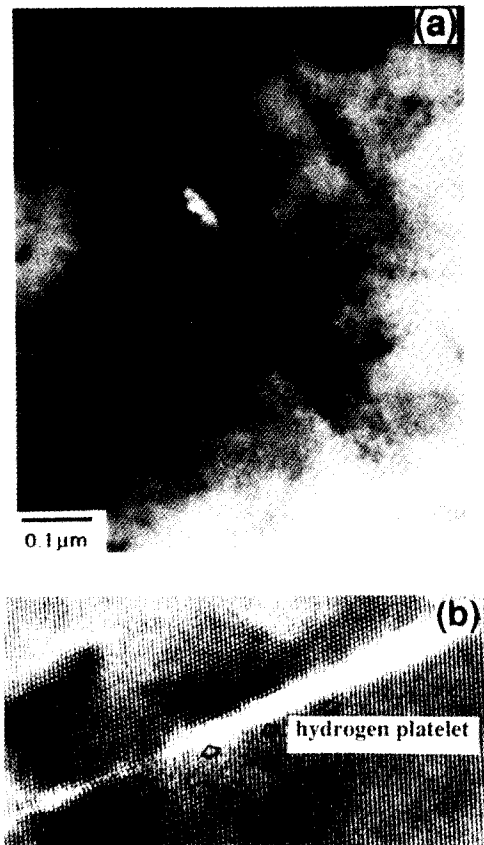


Fig. 25. TEM micrograph showing (a) a view of a platelet in the [011] plane (note the core surrounded by a disk-like structure) and (b) a lattice image of the platelet. The figure is from Ref. [158] with permission.

like features in {111} planes, with radii as large as a thousand angströms. They are believed to contain very large amount of H atoms in their core as well as in the disk itself. A micrograph of a platelet is shown in Fig. 25.

The platelets have optimal nucleation (150 °C) and growth (275 °C) temperatures [393]. Plasma treatments which include both temperatures in succession generate vastly more platelets than treatments at 275 °C throughout. The platelets begin to dissociate around 500 °C.

In addition to preventing the penetration of H into the bulk, platelets may act as an uncontrolled source of H during rapid thermal anneals [394]. However, they are also tremendous gettering centers [395]. It is quite conceivable that platelets could be deliberately grown in the sub-surface region of contaminated samples to provide gettering centers for unwanted impurities such as transition metals. After the gettering anneals, etches would remove both the platelets and the gettered contaminants. Raman spectra [393] of the platelet-rich region show a dominant feature around 2140 cm^{-1} (at room temperature), which shifts to 1570 cm^{-1} when D is used instead of H. These frequencies suggest that strong Si–H bonds are present, such as H saturating isolated dangling bonds. More weakly bound structures, such as H_2^* complexes, have IR modes at lower frequencies (see Table 6).

IR and Raman studies [396] have shown that four or more bands overlap in the 2000–2200 cm⁻¹ region. The relative intensities of the bands depend on the history of the sample and can be varied by annealing. The experimental results are consistent with at least three distinct structures, one of which corresponds to a H-saturated dangling bond. NMR studies [397] of D platelets indicate the presence of D₂ molecules as well. Positron annihilation spectroscopy [398] demonstrates the presence of void-like structures such as those visible in Fig. 25.

A number of theorists have studied the relative energies of a variety of structures involving many H interstitials in Si in order to establish which structures, if any, are energetically favorable over isolated H_{BC}, H₂^{*}, or H₂^T. Such calculations involve studying large defect structures in rather small clusters or cells, with many (sometimes most) host atoms in distorted configurations. As a result, these calculations are less accurate than calculations performed at the same level for highly-localized defects.

Van de Walle et al. [26,27] performed LDF calculations in 32-atom supercells. They found that a small amount of energy is gained (relative to isolated H_{BC}⁰) by aligning bond-centered hydrogen centers in an adjacent Si–Si bond in a {111} plane. Putting two H atoms per Si–Si bond also results in a small gain in energy. However, both configurations are unstable against H₂^T formation. They proposed a mechanism for hydrogen-assisted Frenkel pair (vacancy–self-interstitial) formation. The energy needed to form a Frenkel pair has been estimated at about 8 eV [399,400], while one gains about 2.2 eV by forming a Si–H bond in a vacancy. Thus, forming four Si–H bonds in a vacancy results in a net gain of 0.2 eV per H atom.

Deák and coworkers [187,376] used the semiempirical MINDO/3 approximation to ab initio HF in 32-atom cyclic clusters. They proposed five possible configurations for platelets: (a) sets of H₂^{*}s arranged parallel to each other in a {111} plane; (b) pairs of H bridging the same Si–Si bond (similar to the configuration proposed by Van de Walle); (c) H_{BC}⁰s at adjacent Si–Si bonds in a {111} plane, with parallel spins; (d) aligned H₂^Ts; and (e) Hs saturating dangling bonds after the removal of two layers of Si atoms. A modest gain in total energy (relative to isolated H_{BC}⁰s) is found for models (b), (c), and (e), the largest gain occurring for model (e), 0.33 eV per H atom.

Zhang and Jackson [401] examined a variety of structures similar to those mentioned above and, in addition, a combination of H₂^{*}s arranged anti-parallel to each other with or without a half-stacking fault. The two latter possibilities lead to a gain in energy, but of at most 0.33 eV. Note that H₂^{*}s can be made to alternate only in one dimension.

Roberson and Estreicher [41] proposed a mechanism which includes the assumption by Corbett et al. [382] that vacancies are pumped from the surface into the bulk by the exposure to a H plasma. The model is based on the static potential surface calculations which suggest that {V, H} pairs are mobile, albeit slower than H or V alone. The model implies different behaviors at different temperatures.

At low temperatures, {V, H} pairs form but diffuse too slowly to form larger defects before trapping additional H interstitials and becoming inactive {V, H₄} complexes. At high temperatures, {V, H} pairs dissociate, leaving isolated Vs and Hs which rapidly diffuse out of the region of interest. However, at intermediate temperatures, the {V, H} pairs have a chance to migrate, trap each other or trap a vacancy before being saturated by Hs. A complex such as {V, V, H} is likely to be attracted to further vacancies or {V, H} pairs, as well as Hs.

The attractive features of this model include the much larger gains in energy than the models that do not include dangling bonds. Since vacancies are created at the surface (using the energy of the plasma) and diffuse into the bulk with a small activation energy, the dangling bonds do not have to be created by H. Further, the model predicts different behaviors for different ranges of temperatures. However, MD simulations [161] do not show the break-up of {V, H} even at 1500 K, leaving unexplained the observation that platelets are not nucleated above 250 °C or so [393]. Finally, the planar nature of the platelet is not implied by this model.

The processes involved in the nucleation of platelets and the various configurations of H in them are not known. However, the following is very likely: (i) H alone is not sufficient. All the structures involving combinations of H in {111} planes lead to a gain in energy far too small to produce huge platelets; (ii) H_2^* is not involved. The dominant vibrational frequencies observed for platelets are higher than those measured for H_2^* centers [155] which, in addition, break up around 200 °C, a temperature much lower than the 275 °C at which platelets grow best [393]; finally (iii), vacancies play a role. They provide traps for H with gains in energy of about 2.5–3.0 eV per H atom. If vacancies are indeed present in above-equilibrium concentrations, they are the strongest trap for H and therefore cannot be ignored.

The low nucleation temperature of platelets (150 °C) suggests that an initial and necessary reaction occurs below (but not above) that temperature. The strong Si–H bonds formed at dangling bonds are stable up to much higher temperatures. However, some vacancy–dopant pairs are stable above room temperature [402,403], and may even be mobile [402]. Dopants are also present in the subsurface region. The trapping of H at a vacancy–dopant pair could substantially increase its dissociation energy [404], leading to the creation of a possible nucleation site. Careful and systematic measurements of minimal platelet nucleation temperatures in samples doped with a variety of donors (or acceptors) could clarify this point.

3.1.2.9. Calculated relative stabilities

The energies of a variety of configurations of H in Si relative to free atomic hydrogen have been calculated at the LDF [188] and HF [41] levels. Fig. 26 compares the series of predictions.

The two sets of relative stabilities agree on a number of points. First, the most stable trap for H is the dangling bond. The value in Ref. [188] for the isolated (pre-existing) dangling bond is close to that obtained in Ref. [41] for {V, H}. Further, the two calculations agree that H traps at substitutional impurities with binding energies (relative to free atomic H) of the order of 1.5–2.5 eV. Direct comparison of specific traps cannot be made, because different centers were considered by the two authors.

The biggest area of disagreement involves the stability of H_{BC}^0 , which is found to be a substantial 1.05 eV at the LDF level, while HF calculations find that it costs some 0.8 eV to form H_{BC}^0 starting with H_{free}^0 . Solubility data [405–407] indicate that H is found in Si in concentrations in excess of that of the dopant(s). However, the hidden hydrogen could be for example in the form of H_2^T dimers or multiple H trapped at dopants, which both bind with a substantial gain in energy relative to free atomic hydrogen.

3.1.3. Germanium

In the mid-1970s, large ultra-pure Ge single crystals were used to produce gamma-ray detectors. These crystals, grown in an H_2 ambient, contained in the order of 10^{14} H atoms

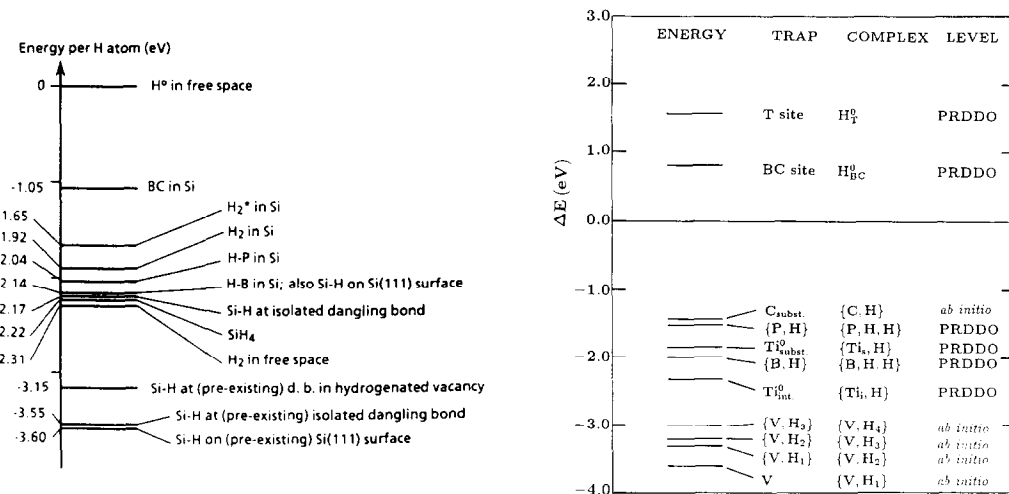


Fig. 26. Stability of hydrogen at various traps in Si calculated relative to free atomic hydrogen. The figure on the left, from Ref. [188] with permission, was obtained from LDf calculations in periodic supercells. The one on the right, from Ref. [41] with permission, is the result of various approximate ab-initio (PRDDO) and ab-initio HF calculations in molecular clusters.

per cm³, a concentration at least 100 times larger than that of shallow dopants. Except for H, the dominant impurities are substitutional C, with some Si, O, and a few TM. The highly sensitive photothermal ionization spectroscopy (PTIS) technique, as well as DLTS in some cases, found that H interacts with these impurities and changes their electrical activity (for a recent review of the experimental work, see the section by Haller in Ref. [3]).

The normally inactive substitutional C and Si forms the shallow acceptors [7–9] A(C, H) and A(Si, H), which dissociate at 200 °C and room temperature, respectively, and have trigonal symmetry [408]. Interstitial O forms the shallow donor [7,8,409] D(O, H), the behavior of which is more complicated [410]. Note that H–O interactions have been observed to give rise to deep levels as well [411]. Partial passivation by hydrogen of the double acceptors Be and Zn was also observed [412]. The shallow acceptors A(Be, H) and A(Zn, H) also have trigonal symmetry [408]. Substitutional Cu interacts with H and forms the semi-shallow A(Cu, H₂) complex [413]. Complexes involving H and other TM impurities are also believed to exist [1]. Hydrogen also interacts with dangling bonds forming, for example, divacancy–hydrogen complexes [414].

Two reports of (partial) shallow-acceptor passivation have been published [1,199]. The {B, H} complex thermally dissociates around 120 °C, a temperature lower than that of the same pair in Si, but still appreciable. The passivation of shallow donors has not been reported, either because of an unexpectedly low thermal stability of the pair, or because of a small capture cross-section of H by shallow donors (see the discussion in Section 2.1.3).

Theoretical studies of the {C, H}, {Si, H}, and {O, H} pairs in Ge have been carried out. The interpretation of the earliest optical spectra was consistent with H being at a site with T_d symmetry. This led to a tunneling model [9,415] which explained some of the features of the data. The subsequent empirical calculations [416,417] of the electronic structures of A(C, H) and D(O, H) did not include total energy calculations, and the equilibrium site of H was not determined. A static model for D(O, H) with C_{3v} symmetry

was also proposed [418,419] which explained qualitatively all the features of the experimental data better than the tunneling model.

The first total energy calculation for the {Si, H} pair in Ge was carried out at the LDF level in 16- and 32-atom supercells [202]. This study found that the pair is weakly bound. The binding energy relative to interstitial H in the perfect crystal is less than 0.05 eV for all charge states. In n-type Ge, the {Si, H}⁻ pair has H at the AB site of Si (0.2 Å of the T_{Si} site toward Si). In intrinsic and p-type Ge, the {Si, H}^{0/+} pair has H in a BC configuration between Si and one of its NNs. It is proposed that the energy level of a H-impurity pair is virtually identical to the level of H at the same site in the perfect crystal (no impurity present), i.e. that the electrical activity of the {X, H} pair depends only on the site of H, and not on the nature of the impurity X, the strengths of the bonds involved, or the amount of relaxation of the crystal caused by the trapping of H. This conclusion is much more likely to hold in situations such as the present one where H is very weakly bound than in those where H forms stronger covalent bonds. In the {Si, H} case, this would make the pair a shallow acceptor in intrinsic and p-type Ge and a donor in n-type Ge.

Maric et al. [273,274] studied the neutral {B, H}, {C, H}, and {Si, H} pairs in Ge in 8 and 14 host-atom clusters of Ge at the ab-initio HF level with split-valence polarized basis sets and pseudopotentials corrected for relativistic effects. In the case of {Si, H}, the results agree with the previous study in that the pair is weakly bound. However, in the neutral charge state, the equilibrium configuration has H AB to Si instead of at the BC site (see Fig. 18). The AB_{Si} configuration is only 0.08 eV more stable than the unbound configuration with interstitial H_{T_{Si}}⁰ near the Si atom. Charged states were not considered. The bond lengths and degrees of bonding in the lowest-energy configuration are shown in Fig. 27(a). Note that the odd electron is primarily localized on a Ge atom.

The same calculation predicts that the {C, H} pair is much more strongly bound, in qualitative agreement with the higher thermal stability observed experimentally for {C, H} (~200 °C) than for {Si, H} (~room temperature). The calculated {C, H} pair in Ge is found to have two nearly degenerate configurations, at the BC_{Ge} and AB_C (+0.07 eV) sites, as shown in Figs. 27(b) and 27(c). In the former case, the odd electron resides primarily on the three-fold coordinate C atom. In the latter case, it is on a three-fold coordinated Ge atom. Note that a very similar set of configurations was found for the {C, H} pair in Si by the same authors [273,274].

The binding energies of the {Si, H}, {C, H}, and of H⁰_{BC} relative to free atomic hydrogen (far outside the cluster) were also calculated. The result are shown in Fig. 28. The low (high) stability of the {Si, H} ({C, H}) pairs in Ge can be understood in the following way. In unrelaxed Ge, substitutional C forms four C–Ge bonds which are 25% longer than the corresponding bond in free radicals (2.45 vs. 1.94 Å). In the case of Si in Ge, the initial bond length mismatch is considerably smaller (2.40 vs. 2.45 Å). This implies that C will distort the crystal much more than Si. As a result, much more energy can be gained when H relaxes the strained configuration in the case of C than in the case if Si. Note that HF calculations always find that it costs energy to insert free atomic H into the BC site in C, Si, and Ge. This conflicts with DFT calculations which find a gain in energy.

Finally, the {B, H} pair [273,274] is found to be virtually identical in Ge and Si. The potential energy surface for H near B⁻ is a bit more flat in Ge than in Si (a result qualitatively consistent with a lower thermal stability), but is otherwise very similar. This suggests that the low efficiency of acceptor passivation in Ge is not caused by an unusually

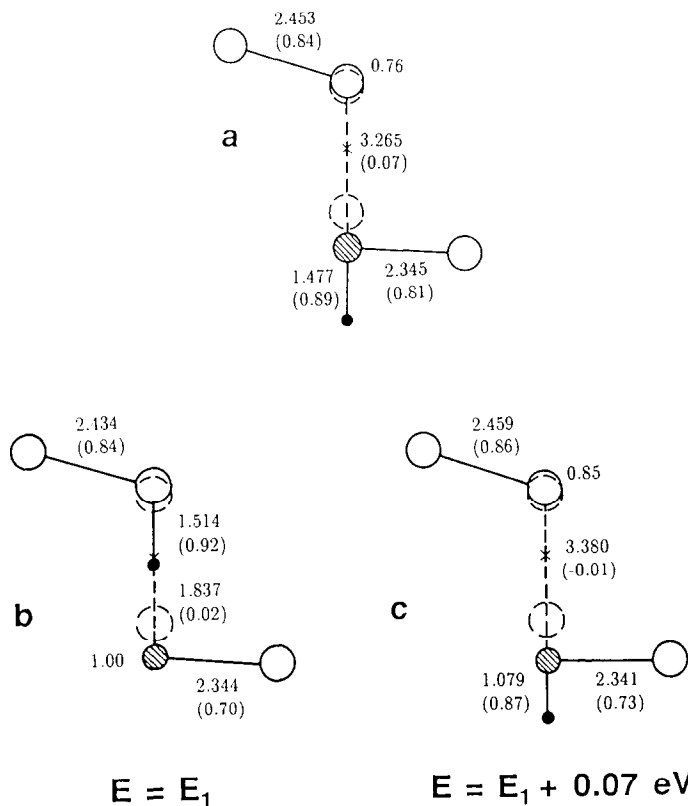


Fig. 27. Lowest-energy configurations of the neutral {Si, H} (a) and {C, H} ((b), (c)) pairs in Ge calculated at the ab-initio HF level [273,274]. The {Si, H} configuration does not agree with the BC configuration found in Ref. [202], although both authors find small binding energies for H. The bond lengths and bond indices (in parentheses) are given. A large fraction of the odd electron always resides on the three-fold coordinated atom (shown near the atom). The full circle is H, the shaded circle is Si (a) or C ((b), (c)), and the open circles are Ge host atoms. The dashed circles represent the lattice sites. The configuration (c) is calculated to be only 0.07 eV higher than (b).

unstable pair but by other reasons. In Section 2.1.3, it was suggested that the BC site is less stable than the T site in Ge, in contrast to Si. This implies a low concentration of H_{BC}^0 and H_{BC}^+ species and an increased probability of H_2^T formation. The low concentration of H^+ reduces the capture radius of hydrogen by ionized acceptors, and molecule formation in samples containing a high concentration of H would impede the diffusion of H.

The interactions involving H and interstitial O (O_i) in Ge have also been studied [420] at the semiempirical HF level (MNDO) in large clusters. The calculated equilibrium configuration of O_i is an electrically inactive puckered bridged bond. The interstitial diffuses via a y-lid or split- $\langle 110 \rangle$ configuration shown in Fig. 29(a). The lowest-energy and transition-point configurations are similar to those found in Si. It was found (Section 3.1.2.4) that H stabilizes the transition-point configuration for O_i in Si, thus lowering its activation energy for diffusion and enhancing its diffusivity. In the case of Ge, however, the calculations predict that the transition-point configuration is lowered to the point that it becomes a minimum of the energy. The stable configuration of the $\{O_i, H\}^+$ pair in Ge, shown in Fig. 29(b), is found to be more stable for H than H_{BC}^+ by 0.36 eV. This pair is predicted to be a single donor, in agreement with the experimental observation. These results have yet to be confirmed by other theorists or by experiment. A di-oxygen-hydrogen complex is also found to be a single donor.

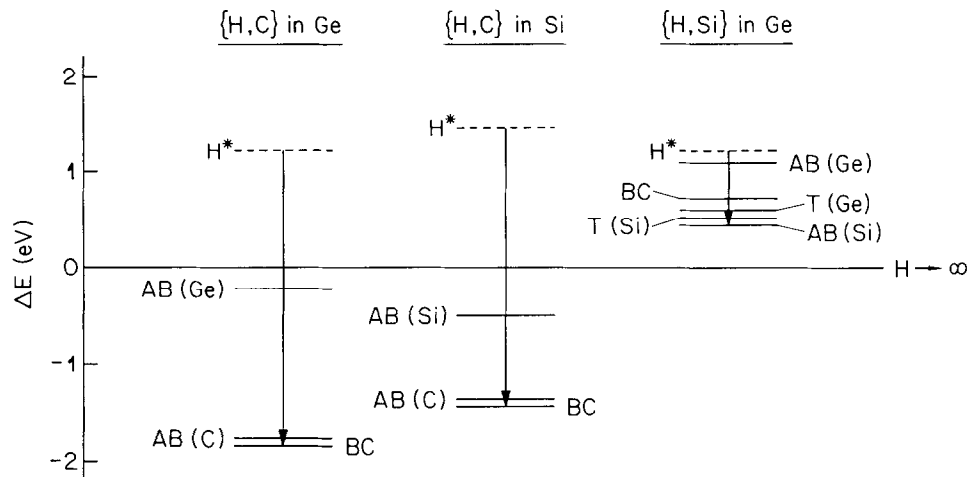


Fig. 28. Energy differences between free atomic H far outside the cluster and H in the H_{BC}^0 , {Si, H} and {C, H} configurations in Ge. For comparison, the relative energy of the {C, H} pair in Si is also shown. The {Si, H} pair is only marginally more stable than H_{BC}^0 , while the {C, H} pair is much more stable in both Si and Ge. Note that the figure includes the energies of several metastable states (not discussed here). The notation used is H^* for H_{BC}^0 , AB(C) for H^0 at the AB_C site of the {C, H} complexes, etc. This figure is from Ref. [274] with permission.

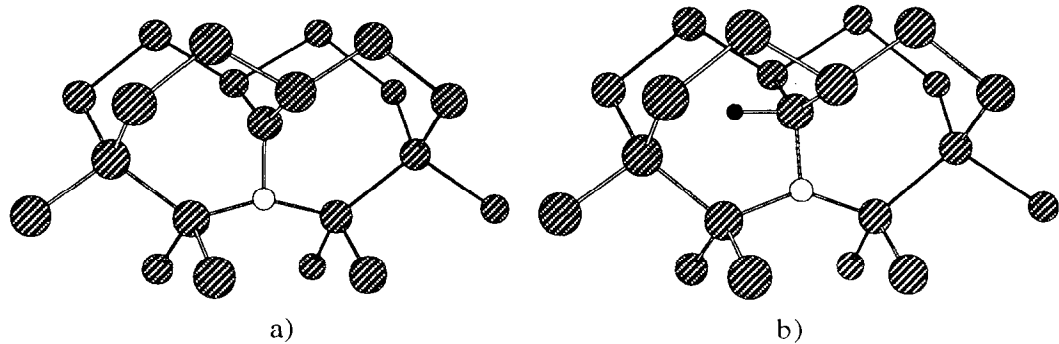


Fig. 29. Comparison of the transition-point configuration for O_i diffusion (a) with the calculated [420] equilibrium configuration of the {O_i, H} pair (b) in Ge (see text). The open circle is O_i, the full circle is H, and the shaded circles are some of the Ge atoms in the cluster.

3.2. Compound semiconductors

Theoretical studies of hydrogen-containing complexes in compound semiconductors are more involved than in elemental hosts for several reasons. First, the host crystal is partly ionic, and the long-ranged interactions (the Madelung energy depends on the site of the impurity) are not properly included in clusters or supercells, despite the screening that occurs. This implies an additional uncertainty in the theoretical predictions, especially when dealing with charged defect centers. The ionic character ranges from a fraction of one percent (BP) to some 75% in copper halides (see the discussion in Chapter 2 of Ref. [421]).

Second, the number of possible configurations is much greater in a compound than in elemental materials, because there are two inequivalent T, BC, and AB sites. Further, in some compounds, the host atoms themselves prefer to be three- or five-fold coordinated rather than four-fold, which is imposed upon them by the crystalline structure. The presence of H may allow one atom to realize locally a more favorable coordination, resulting in

structures which are not commonly realized in elemental materials. Thus, the potential energy surface has many stationary points and this increases the computational requirements.

Third, some compound semiconductors favor the wurtzite structure to the zinc-blende structure (in particular the nitrides), while SiC can be found in thousands of polytypes. GaN may be grown in the cubic (zinc-blende) or hexagonal (wurtzite) phases depending on the substrate. While all the host atoms are four-fold coordinated and make perfect or nearly perfect tetrahedral angles at equilibrium, the zinc-blende and wurtzite crystals have very different interstitial sites, potential surfaces, and diffusion paths (see Section 2.2.1). This again increases the required theoretical effort and demands new experience.

This section is divided into four subsections corresponding to the IV–IV, III–V, II–VI, and I–VII compounds. Most of the theoretical work has been performed on GaAs, which has its own sub-subsection. Otherwise, isolated studies have been conducted in a variety of compounds, and they are mentioned in the appropriate location. In some cases, no theoretical work has been published and this is mentioned as well.

3.2.1. IV–IV compounds

At this time, no theoretical work has been published on complexes involving H in hosts such as a polytype of SiC, SiGe alloys or superlattices, or SiGeC alloys (these typically contain less than 2 at.% C). The importance of these materials is growing, and there is little doubt that hydrogen will be found to play some roles in them, presumably passivating and activating similar centers as in elemental semiconductors. The passivation of dangling or strained bonds near interfaces is likely to be of particular importance in the case of superlattices (see, for example, Refs. [422,423]).

3.2.2. III–V compounds

3.2.2.1. Gallium arsenide

In GaAs, just as in Si, both acceptors and donors are easily passivated by hydrogen. Passivation results from the formation of bound pairs, just as in Si, and numerous experimental studies have provided microscopic information of the nature of these complexes (for a detailed review, see Ref. [5]). A number of theoretical investigations have been carried out and their results are reviewed below.

The formation of H-dopant complexes in GaAs has been studied by several authors, and there is general agreement about the ground-state properties of the pairs. The vibrational modes associated with hydrogen have been calculated and are often close to the experimentally measured ones. Disagreements deal mostly with the finer details, in particular the metastable states. However, it is fair to say that the ground-state chemistry of acceptor–H and donor–H pairs is generally understood, and that the results in compounds are consistent with the intuition gained from extensive studies previously done in Si. The debate has now shifted to the possible bistability of some pairs, the kinetics of passivation and reactivation, the possibility that H has negative-U properties in GaAs, and other more complex issues.

Several groups have calculated the equilibrium structure and vibrational properties of H–acceptor and H–donor pairs in GaAs. All have used LDF with ab-initio pseudopotentials in supercells or clusters. The following authors used 26, 44, and 52 host-atom clusters and Gaussian basis sets with s and p symmetry (some of the papers cited below contain theoretical and experimental results). Briddon et al. [424–426] studied the interactions of H with the Be_{Ga} acceptor and the Si_{Ga} donor, Jones and coworkers [427–429] focused on {C, H} pairs,

including the C_{As} acceptor and C_{Ga} donor, and Rahbi et al. [430] investigated the $\{S_{As}, H\}$ pair.

The following authors have used supercells and plane-wave basis sets with various cutoff energies. Pavesi and Gianozzi [431] (16- and 32-atom cells, 12 Ry cutoff) studied the $\{Si_{As}, H\}$ and $\{Si_{Ga}, H\}$ pairs, Chang [432] (18-atom cells, 9 Ry cutoff) the $\{Be_{Ga}, H\}$ and $\{Si_{Ga}, H\}$ pairs, and Amore Bonapasta (16- and 32-atom cells, 12–16 Ry cutoff) the $\{C_{As}, H\}$ and $\{C_{Ga}, H\}$ pairs [433] as well as the interactions between H interstitials and the As_{Ga} antisite and interstitial As [434].

In all but one case (the $\{C_{Ga}, H\}$ pair), these authors agree on the equilibrium configuration of the various H-shallow dopant pairs. For acceptors, they find that H is near a BC site. For donors, H is almost always found to be AB to the donor. The finer details (exact bond lengths and vibrational frequencies, metastable configurations and their energy relative to the ground state, etc.) vary from author to author.

The calculated vibrational modes associated with hydrogen for H-acceptor pairs are compared with the experimental values in Table 12. Note that the general agreement between theory and experiment is very good. In a BC configuration, H is strongly bound, the minimum of the potential energy is well defined, and, except in the case of C (see below) the local vibrational modes are harmonic to a good approximation.

In the lowest-energy configuration of the $\{Be, H\}$ pair, $Be \cdots H-As$, hydrogen forms a much weaker bond with Be than with As. The calculated Be-H distance is 1.77 Å in Refs. [424–426] and 1.86 Å in Ref. [432]. Both distances are much longer than the equilibrium Be-H bond length (it is ≈ 1.3 Å in BeH_2). The calculated H-As bond lengths are 1.54 Å [424–426] and 1.55 Å [432], much closer to the equilibrium H-As bond length, e.g. in AsH_3 (1.52 Å). A metastable state, some 0.3 eV higher in energy, is found at the AB_{As} [424–426] or the C_{Be} site [432]. The former configuration corresponds to a bound H and the latter one to atomic-like H.

The calculated [431] bond lengths for the $\{Si, H\}$ complex are $Si-H=1.55$ Å and $H-Ga=1.70$ Å, indicating a larger overlap between H and Si than between H and Ga. The predicted dissociation energy (relative to H at the BC site) is 1.75 eV. A metastable state is found with H at the AB_{Si} site ($+0.36$ eV), very near the atomic-like state $H_{T_{Si}}^0$ ($+0.40$ eV).

In the ground state of the $\{C, H\}$ pair, Jones and Öberg [427] found H to be much more strongly bound to C ($C-H=1.13$ Å) than to Ga ($H-Ga=2.20$ Å). The Ga atom is almost three-fold coordinated. The wag mode at 720 cm^{-1} is predicted to have a very small

Table 12
Theoretical and experimental vibrational frequencies (cm^{-1}) of H for H-acceptor pairs in GaAs

Pair	Theory			Experiment		
	Stretch	Wag	Ref.	Stretch	Wag	Ref.
$Be \cdots H-As$	2018	301	[424–426]	2037	–	[436]
	2080		[432]			
$Si-H \cdots Ga$	2100	260	[431]	2095	–	[437]
$C-H \cdots Ga$	2605	718	[431]	2635	739 ^a	[226,438–440]
	2781	724	[433]			

If several numbers were published by an author, the results in the Table correspond to the value obtained at the highest level of theory and/or in the largest cluster or cell. The theoretical level is discussed in the text.

^a The wag mode has also been seen in deuterated samples at 647.2 cm^{-1} , [435].

IR intensity, which would explain why it has not been observed. The calculated activation energy of reorientation is 0.67 eV, close to the experimental value [441] of 0.5 eV. A metastable state with H at the AB_C site is 0.5 eV above the ground state. Amore Bonapasta finds a similar configuration [433]. The passivation of the C_{As} acceptor in GaAs and AlAs has been the subject of intense studies in the past couple of years. The Raman-active [429] and IR-active [435] modes have been measured and calculated. The peculiar features resulting from the anharmonicity of this vibration have recently been discussed in detail [428,429,442]. The same pair has also been studied in AlAs (see below).

The calculated vibrational modes associated with hydrogen for H-donor pairs are compared with experimental values in Table 13. Note that the AB_D (D is the donor) configuration is predicted by most authors, except in the case of the $\{\text{C}_{\text{Ga}}, \text{H}\}$ pair for which two predictions contradict each other (both are LDF calculations, the first in clusters, the second in supercells). Note also that the various calculated vibrational frequencies are much further from each other (and from experiment) than in the case of acceptors, where H was at a BC site. In the AB configuration, H is bound to an atom which is roughly sp^2 hybridized, leading to a longer and softer bond, for which vibrational amplitudes tend to be larger and anharmonic effects more pronounced.

The AB_Si configuration for the $\{\text{Si}_{\text{Ga}}, \text{H}\}$ pair with a five-fold coordinated Si atom was first proposed by Pajot et al. [443]. Theory [424–426] finds H at the proposed site, but with the Si atom only four-fold coordinated, after breaking the Si-As bond along the H-Si axis. The Si-As distance is calculated to be 3.10 Å in Refs. [424–426] and 2.67 Å in Ref. [431]. The Si atom moves back toward the plane of three of its As NNs, where it is sp^2 hybridized. Hydrogen then attaches to the dangling p orbital along the AB direction, with bond length H-Si=1.59 Å [424–426], 1.63 Å [431], or 1.66 Å [432].

In Refs. [424–426], the BC_Si configuration ($\text{Si}-\text{H}\cdots\text{As}$) is 0.4 eV higher in energy, and the AB_As configuration for H is 0.8 eV above the ground state. In Ref. [431], the two lowest metastable states correspond to atomic-like hydrogen at the T_{Si} (0.36 eV) and the T_{As} (0.81 eV) sites. Finally, in Ref. [432], the AB_As site is the lowest metastable state (0.7 eV above the ground state) and the BC_Si configuration is another 0.4 eV higher.

Although the $\{\text{C}_{\text{Ga}}, \text{H}\}$ pair Ga has not been observed, Jones and Öberg [427] have predicted its equilibrium geometry and vibrational modes. The lowest-energy configuration is similar to that found for the $\{\text{Si}, \text{H}\}$ pair by the same group (see above), with $\text{H-C}=1.08$ Å (an almost perfect two-electron covalent C-H bond) and $\text{C}\cdots\text{As}=3.16$ Å. The high stretch frequency predicted (Table 13) is consistent with a strong C-H bond. On the other

Table 13
Theoretical and experimental vibrational frequencies (cm^{-1}) of H for H-donor pairs in GaAs

Pair	Theory			Experiment		
	Stretch	Wag	Ref.	Stretch	Wag	Ref.
$\text{H-Si}\cdots\text{As}$	1813	982	[424–426]	1717	896	[443]
	1460	850	[431]			
	1350	840	[432]			
$\text{H-C}\cdots\text{As}$	3246	1115	[427]	–	–	–
$\text{C-H}\cdots\text{As}$	2760	930	[433]	–	–	–

If several numbers were published by an author, the results in the Table correspond to the values obtained at the highest level of theory and/or in the largest cluster or cell. Note that there is disagreement about the lowest-energy configuration of the $\{\text{C}_{\text{Ga}}, \text{H}\}$ pair. The theoretical level is discussed in the text.

hand, Amore Bonapasta [433] finds a BC_C configuration for this pair with substantially different vibrational frequencies.

The passivation of the S_{As} donor has been studied by Chang [432]. The lowest-energy configuration has H at the AB_{Ga} site with $\text{Ga}-\text{H}=1.63 \text{ \AA}$, while the S atom moves away and becomes three-fold coordinated. The BC site is 0.7 eV higher in energy, and the AB_{S} configuration is 1.6 eV above the ground state.

In the context of the passivation by hydrogen of the EL2 center in GaAs, Amore Bonapasta [434] has investigated the interactions of the arsenic antisite (As_{Ga}) and arsenic interstitial (As_i) with one or more H atoms. While As_i is found to bind rather weakly with up to three H atoms, the structures obtained in the case of As_{Ga} are more stable and have C_{3v} symmetry. The antisite can bind one or two Hs, the latter configuration is found to be electrically inactive, with a dissociation energy of 2.3 eV. The first H binds to As_{Ga} at the AB site, with $\text{H}-\text{As}_{\text{Ga}}=1.63 \text{ \AA}$. The second H attaches to an As NN to As_{Ga} on the same trigonal axis, forming an H_2^* -like complex: $\text{H}-\text{As}_{\text{Ga}} \cdots \text{H}-\text{As}$. The three bond lengths are 1.56 \AA , 1.80 \AA , and 1.61 \AA , respectively.

The reactivation of hydrogen–shallow dopant pairs in GaAs has received a lot of attention in recent years as a means of measuring the mobility of H^+ and H^- , in a manner similar to that proposed in Si. The reactivation of H-passivated dopants is enhanced by an external electric field. The interpretation of the experiments generally assumes that the pair breaks up, leading to a free, charged, hydrogen species drifting in the applied field. Such experiments have been used to demonstrate the existence (and measure the diffusivity) of H^+ (see, for example, Refs. [444,445]) and H^- (see, for example, Refs. [446–448]) in GaAs. This would imply the existence of both a donor and an acceptor level of H in the gap.

The uniqueness of the interpretation of these data has recently been challenged by Morrow [227] who suggests that the conversion to a bistable state of the pairs may explain just as well the measured concentration depth profiles. These two conflicting interpretations of the same data is reminiscent of a similar debate in silicon (see above), where light-induced reactivation of donor–hydrogen pairs could result from a light-enhanced debonding (leaving free H^-), a transition of $\{\text{P}, \text{H}\}$ from a neutral to a charged state (leaving a bound H), or a combination of the two. The observation of the reversibility of the reactivation reaction in Si strongly suggests that the bistable state is created at least some of the time. In the case of GaAs, the reversibility has not been investigated (in Si, it occurs over some 24 h, at zero bias, in the dark). In any case, a careful re-evaluation of some of the experimental data may lead to unexpected new twists. Note that Chevallier and Pajot [229] argue that the acceptor level of H in GaAs is in the CB.

3.2.2.2. III–V compounds other than GaAs

The passivation by hydrogen of the Si_{Al} donor [449] in AlAs has been studied at the LDF level with ab-initio pseudopotentials in 16- and 32-atom supercells and a plane-wave basis set (12 Ry cutoff). The equilibrium configuration is very similar to that found by the same group for the $\{\text{Si}_{\text{Ga}}, \text{H}\}$ pair in GaAs [431]. Hydrogen is at the AB_{Si} site, $\text{H}-\text{Si}=1.68 \text{ \AA}$ and $\text{Si}-\text{As}=2.70 \text{ \AA}$. Two metastable states are predicted, the first at the AB_{As} site (+0.49 eV) and the second at the BC_{Si} site (+0.81 eV). The calculated H-stretch frequencies in the ground state are close to the experimental value in the 16-atom cell but not in the 32-atom cell: the stretch (wag) frequencies are 1684 (758) cm^{-1} in the 16-atom cell, and 1323 (814) cm^{-1} in the 32-atom cell, and the measured values are 1610 (891) cm^{-1} [449].

The calculated dissociation energy is 1.85 eV, in agreement with the measured value (2 eV).

The passivation of the C_{As} acceptor in AlAs [450] (and $Al_xGa_{1-x}As$ [451]) has also been investigated experimentally and theoretically, and compared with the same defect in GaAs (see above). Again, H is at the BC_C site (preferentially bridging a C–Ga bond in the alloy). The H-stretch frequencies are calculated to be 2558 cm^{-1} , some 300 wavenumbers lower than the experimental number (2885 cm^{-1}).

3.2.2.3. Additional issues

A number of centers have been observed or are suspected to exist in III–V compounds but have not (yet) been studied theoretically. The following list is not exhaustive, but illustrates the types of issues that need additional investigation.

Stein [232] reported IR evidence of an As–H bond at low temperature in proton-implanted GaAs. At 200 K, the As–H IR line disappears while the (expected) Ga–H one appears. The defect involved at low temperature has not been identified (the Ga–H bond is possibly H_{BC}).

{N, H} complexes have been detected [452] in GaP and GaAs. They consist of two H atoms bound to N, and exist in several (metastable or bistable) states.

A larger complex consisting of two C_{As} and one H, has been observed in as-grown GaAs epitaxial layers [453]. The structure of this center has not been established.

IR-active local vibrational modes at 2379.9 cm^{-1} (1729.4 cm^{-1}) have been seen in hydrogenated (deuterated) GaP. They are assigned to P–H (P–D) bonds near a Zn acceptor [454]. The passivation of the Zn acceptor by H in InP has been reported [455,456] to be much more efficient than the passivation of shallow donors [455] such as S or Sn. A number of other hydrogen-related complexes in InP have also been detected [457]. The consequences of hydrogenation in InGaAlP and InGaP heterostructures have recently been discussed [458].

Finally, a number of new materials are becoming increasingly important. One example is GaN. This (direct) wide-bandgap semiconductor has many potential applications, such as a UV emitting laser (a review of the history, properties, and promises of GaN has been written by Pankove [459]). It normally crystallizes in the wurtzite structure, but cubic (or β -) GaN can also be grown, e.g. on cubic SiC substrates. Nitrogen vacancies make the as-grown material n-type. GaN is easily hydrogenated [460,461], and H remains trapped in the material [462] up to some $900\text{ }^{\circ}\text{C}$. Hydrogen could be used to passivate the compensating defects [463], but is likely to affect the electrical and optical properties of other centers as well.

Another example is SiGe (alloys, epitaxial layers, and strained superlattices). Hydrogen could be used to passivate lattice damage [464]. Judging by the substantial differences observed in the behavior of H in Si and Ge, its properties in superlattices are tough to estimate, as they may be dominated by Si, Ge, or the details of the interfaces, for example. Clearly, a lot of systematic work remains to be done, both for theorists and experimentalists.

3.2.3. II–VI compounds

Wide-bandgap semiconductors such as ZnSe are of great interest for applications involving short wavelengths such as blue diodes or lasers. Like many wide-bandgap materials, one type of doping is much easier to realize than the other. In the case of ZnSe, p-type

doping is difficult (Cl is an efficient donor). It is believed that some compensation of the acceptor is responsible for the problem.

Li-doped ZnSe has been successfully used as a p-type material to make a blue LED [465] but, more recently, N has emerged as the acceptor of choice [466]. Gas-source MBE-grown ZnSe, using elemental Zn and H₂Se as sources, produced a high-quality ZnSe material containing some H [467]. Rather high concentrations of N have been introduced ($\sim 5 \times 10^{18} \text{ cm}^{-3}$), leading to a net acceptor concentration $N_A - N_D$ of the order of 10^{17} cm^{-3} .

SIMS and electrical measurements [238,239,468] indicate that H does not affect the conductivity of the donor (Cl), but efficiently passivates the N acceptor. The passivation persists for long anneals (450 °C for 1 h), rapid thermal anneals (500 °C for 2 min), and survives the injection of minority charge carriers, a process known to facilitate the debonding of acceptor-H and especially donor-H pairs in Si. It is possible that H also reacts with some native defects and thus impedes a compensation mechanism. At this time, precious little microscopic evidence is available, either from theory or from experiment. In particular, background noise in IR absorption experiments has so far prevented the observation of N-H or Se-H bonds [469].

Finally, the IR-active modes of H have been measured [470–473] in heavily H⁺- and D⁺-implanted CdS, CdTe, ZnTe, and ZnSe. Hydrogen is found to form stronger bonds with the non-metal atom (S, Te, Se) and only weak lines have been associated with the metal-H bond. The latter result is not surprising since H forms very weak bonds with both Cd and Zn (0.72 and 0.89 eV in diatomics, respectively).

3.2.4. I-VII compounds

I am not aware of any theoretical or experimental work related to H-containing complexes in I-VII semiconductor compounds. Muon spin-rotation studies in copper halides (see Section 2.2.4) show two Mu_{TCu}^0 species, with a weak non-paramagnetic component which has not been identified and could be either Mu^- or Mu^+ (or even originate from muons stopping in the cryostat). Because of the weak covalent character of these crystals, I see no reason to speculate that the chemistry of hydrogen would be similar to that in Si or GaAs. However, H has surprised me in the past...

4. Concluding remarks

Hydrogen started as the simplest possible impurity that could be introduced into a semiconductor. It turns out that it is probably the most diverse of any impurity in any crystal. It interacts with virtually everything in its path, changing the electrical and optical properties of the material, catalyzing the diffusion of some species, or creating its own defect centers.

It was thought at first that H could be used in device processing, for example to control the electrical activity of specific centers. Then, it was realized that the thermal stability of the complexes is too low for most practical purposes (polycrystalline Si solar cells are a counter-example). Now, hydrogen seems to be coming back. Among the properties that are of potential importance in Si are the use of hydrogen platelets as powerful gettering centers. In heterostructures, hydrogen may allow the formation of sharp interfaces, reduce their strain, or even selectively passivate their electrical activity. In the nitrides, H forms complexes

which survive up to 900 °C or so, temperatures high enough for use in most processing steps.

A lot of what has been learned so far will be useful when trying to understand these other roles of hydrogen. So far, theory and experiment have worked hand in hand, thanks in part to the sometimes heated debates about areas of disagreement. Theoretical work involves a lot of computer time, experience, know-how, and perhaps a touch of magic. Several of these ingredients are part of the experimental work as well. It is most useful, in my view, to have a choice of techniques that can be used to study the same problem: tight-binding methods with total energy capabilities, semiempirical HF, approximate ab-initio HF, ab-initio HF using RHF, UHF, and ROHF wavefunctions with a variety of basis sets, perhaps complemented by limited correlation treatments, first-principles LDF with a range of pseudopotentials, localized or plane-wave basis sets and, last but not least, simulations.

In many situations, the various methods agree at least qualitatively. In other cases, the disagreements force theorists to think a little deeper, to defend their point of view, to strengthen their case. But in the end, it is the experimentalist who holds the pieces of the Truth, while the theorist only tries to approximate it. I believe that many of these pieces are now in full view.

Let me conclude with a brief (incomplete) list of comments and issues that deserve further thought and effort. Some are unsolved problems, others are simple observations.

- (i) Muon spin-rotation data are available in seventeen elemental and compound semiconductors. μ_{BC}^0 has been observed only in five: the elemental semiconductors c-C, Si, Ge, and the two compounds GaP and GaAs. There is no neutral bond-centered species in the more ionic hosts, even in SiC. Many complexes formed by H involve a BC site, for example H_2^* and many hydrogen-impurity pairs. Are hydrogen interactions much simpler in hosts in which no H_{BC}^0 exists? Further, if H_{BC}^0 does not form, does it imply that H_{BC}^+ does not form either? And what about alloys, superlattices, or heterostructures? I suggest that μ SR studies could be a most useful tool to obtain an idea of the behavior of isolated H in new materials.
- (ii) The role of MD simulations is becoming more important. So far, all of the simulations related to hydrogen have been performed in Si, and deal with the diffusion of H or H-vacancy complexes. Many other issues would be clarified by MD treatments. Oxygen-hydrogen interactions, the {Be, H} pair, the formation, break-up, and/or diffusion of species such as H_2^* , the nucleation of platelets, just to name a few. This list involves only Si. Many problems will be identified in other hosts. One must also recognize the limitations of these simulations. In particular, the electrons remain at 0 K even for high temperatures of the nuclei. This approximation must break down at some point, and electronic excited states become critical.
- (iii) Is the H-catalyzed diffusion of O_i in Si limited to O_i in Si? There are other bond-centered interstitials (B_i in Si for example) the diffusivity of which may also be boosted by exposure to atomic hydrogen. Perhaps a similar mechanism occurs in other hosts? Rapid rather than slow formation of TDs may not be of crucial technical importance, but the gettering of other species is. It is clearly relevant to understand the details of what is happening in the case of O_i in Si, then to look for chemically similar situations (in Si or other hosts) and pursue systematic studies in these cases.
- (iv) The microscopic processes occurring when a Si surface is exposed to a H plasma or an H_2 gas are not understood. There have been reports of substantial passivation after the exposure of Si to low-temperature forming gas, if specific conditions are realized

[474]. It seems as if free H₂ easily breaks up into atomic species on some Si surfaces but not on others. Theoretical studies of the interactions between various surfaces and an H₂ gas are needed.

- (v) Is bistability a widespread phenomenon? A number of hydrogen-related defects in Si and GaAs have been shown or suggested to exist in more than one charge state. For example, H_{BC} (0 and +), H_T (0 and -), several H-acceptor pairs (0 and -), several H-donor pairs (0 and +), {C, H} (0 and + in Si, 0 and - in Ge), some of the vacancy-hydrogen complexes, etc. Any closed-shell defect center capturing H⁰ will have an unpaired electron, often in a non-bonding orbital. When free charge carriers are available, electron or hole capture may result in the transition to a bistable state, dissociation, or perhaps enhanced diffusion. These possibilities should be explored by repeating the same experiment, when possible, under illumination and in the dark, in and out of a depletion region.

The literature search for this article includes work up to roughly December, 1994. I have tried to be fair and complete when discussing the (microscopic) theoretical work performed in the field of hydrogen in crystalline semiconductors. If I have forgotten some contributions or misrepresented someone's work, please accept my apologies.

Acknowledgements

Many thanks to Bob Jones and Steve Pearson for carefully reading the manuscript and making numerous enlightening comments and suggestions. Thanks also to Roger Lichteni, who always found the time to discuss, proof-read, and comment, especially on the sections containing μ SR results. This work was supported in part by the grant D-1126 from the R.A. Welch Foundation and the contract RAI-4-14195 from the National Renewable Energy Laboratory.

Appendix: Nomenclature

Lattice sites (see Figs. 1 and 2)

AB _A	anti-bonding site (A refers to the nearest host atom. The subscript is needed in compounds)
BC	bond-centered (or near bond-centered) site
C	the C-site is midway between adjacent second NNs
H	hexagonal interstitial site
I _A	self-interstitial (A refers to the interstitial atom. The subscript is needed in compounds)
M	the M-site is midway between two adjacent C sites
R	one of the most important interstitial sites in the wurtzite lattice
T _A	tetrahedral interstitial site (A refers to the four NNs. The subscript is needed in compounds)
V _A	vacancy (atom A is missing. The subscript is only needed in compounds)

Hydrogen and muonium species

H_T^0 or H_T^-	hydrogen at (or near) the T site in the 0 or -1 charge state
H_{BC}^0 or H_{BC}^+	hydrogen at (or near) the BC site in the 0 or +1 charge state
H^*	old notation for H_{BC}^0
H_2^T	molecular hydrogen at (or near) the T site
H_2^*	bond-centered/anti-bonding hydrogen dimer
Mu_T^0 or Mu_T^-	muonium at (or near) the T site in the 0 or -1 charge state
Mu_{BC}^0 or Mu_{BC}^+	muonium at (or near) the BC site in the 0 or +1 charge state
Mu^*	old notation for Mu_{BC}^0
μ^+	non-paramagnetic μ SR species (it is Mu_T^- , Mu_{BC}^+ , or a muonium bound state)

References

- [1] S.J. Pearton, J.W. Corbett and T.S. Shi, *Appl. Phys. A*, **43** (1987) 153.
- [2] J.I. Pankove and N.M. Johnson (eds.), *Semiconductors and Semimetals*, Vol. 34, 1991.
- [3] S.M. Myers, M.I. Baskes, H.K. Birnbaum, J.W. Corbett, G.G. DeLeo, S.K. Estreicher, E.E. Haller, P. Jena, N.M. Jonhson, R. Kirchheim, S.J. Pearton and M. Stavola, *Rev. Mod. Phys.*, **64** (1992) 559.
- [4] S.J. Pearton, J.W. Corbett and M.J. Stavola, *Hydrogen in Crystalline Semiconductors*, Springer-Verlag, Berlin, 1992.
- [5] S.J. Pearton, Hydrogen in compound semiconductors, *Mater. Sci. Forum*, **148-149** (1994).
- [6] R.A. Street, *Hydrogenated Amorphous Silicon*, Cambridge University Press, New York, 1991.
- [7] R.N. Hall, *IEEE Trans. Nucl. Sci.*, **NS-21** (1974) 260.
- [8] R.N. Hall, *IOP Conf. Ser.*, **23** (1975) 190.
- [9] E.E. Haller, B. Joós and L.M. Falicov, *Phys. Rev. B*, **21** (1980) 4729.
- [10] C.T. Sah, J.Y.C. Sun and J.J.T. Tzou, *Appl. Phys. Lett.*, **43** (1983) 204.
- [11] C.T. Sah, J.Y.C. Sun and J.J.T. Tzou, *J. Appl. Phys.*, **54** (1983) 4378.
- [12] C.T. Sah, J.Y.C. Sun, J.J.T. Tzou and S.C.S. Pan, *Appl. Phys. Lett.*, **43** (1983) 962.
- [13] J.I. Pankove, D.E. Carlson, J.E. Berkeyheiser and R.O. Vance, *Phys. Rev. Lett.*, **53** (1983) 2224.
- [14] J.H. Brewer, K.M. Crowe, F.N. Gygax, R.F. Johnson, B.D. Patterson, D.G. Fleming and A. Schenck, *Phys. Rev. Lett.*, **31** (1973), 143.
- [15] S.T. Pantelides, *Hyp. Int.*, **6** (1979) 145.
- [16] J.S.Y. Wang and C. Kittel, *Phys. Rev. B*, **7** (1973) 713.
- [17] V.A. Singh, C. Weigel, J.W. Corbett and L.M. Roth, *Phys. Status Solidi, (b)*, **81** (1977) 637.
- [18] V.A. Singh, J.W. Corbett, C. Weigel and L.M. Roth, *Phys. Lett. A*, **65** (1978) 261.
- [19] W. Kaiser, H.L. Frisch and H. Reiss, *Phys. Rev.*, **112** (1958) 1546.
- [20] U. Gösele and T.Y. Tan, *Appl. Phys. A*, **28** (1982) 79.
- [21] R.C. Newman, *J. Phys. C*, **18** (1985) L967.
- [22] S.K. Estreicher, *MRS Proc.*, **240** (1992) 643.
- [23] S.K. Estreicher, A.K. Ray, J.L. Fry and D.S. Marynick, *Phys. Rev. Lett.*, **55** (1985) 1976.
- [24] S.K. Estreicher, *Phys. Rev. B*, **37** (1988) 858.
- [25] D.S. Marynick, A. Derecskei-Kovacs, S.K. Estreicher, M.A. Roberson and Dj.M. Maric, *Cross Cuts*, **3** (1994) 1.
- [26] C.G. Van de Walle, Y. Bar-Yam and S.T. Pantelides, *Phys. Rev. Lett.*, **60** (1988) 2761.
- [27] C.G. Van de Walle, P.J.H. Denteneer, Y. Bar-Yam and S.T. Pantelides, *Phys. Rev. B*, **39** (1989) 10791.
- [28] L. Pavesi, P. Giannozzi and F.K. Reinhart, *Phys. Rev. B*, **42** (1990) 1864.
- [29] R. Luchsinger, Y. Zhou and P.F. Meier, in R. Gruber and M. Tomassini (eds.), *Proc. 6th Joint EPS-APS Int. Conf. on Physics Computing*, EPS, Geneva, Switzerland, 1994, p. 17.
- [30] Y. Zhou, R. Luchsinger and P.F. Meier, *Phys. Rev. B*, **51** (1995) 4166.
- [31] E. Clementi and C. Roetti, *Atomic Data Nucl. Data Tables*, **14** (1974) 177.
- [32] C.C.J. Roothaan, *Rev. Mod. Phys.*, **23** (1951) 69; **32** (1960) 179.
- [33] J.P. Lowe, *Quantum Chemistry*, Academic Press, Orlando, FL, 1978.
- [34] W.R. Wadt and P.J. Hay, *J. Chem. Phys.*, **82** (1985) 284.
- [35] L.R. Kahn, P. Baybutt and D.G. Truhlar, *J. Chem. Phys.*, **65** (1976) 3826.

- [36] D.E. Woon, D.S. Marynick and S.K. Estreicher, *Phys. Rev. B*, **45** (1992) 13383.
- [37] H.F. Schaeffer III (ed.), *Methods of Electronic Structure Theory*, Plenum, New York, 1977.
- [38] P.A. Schultz and R.P. Messmer, *Phys. Rev. B*, **34** (1986) 2532.
- [39] Chr. Møller and M.S. Plesset, *Phys. Rev.* **46** (1934) 618.
- [40] M.A. Roberson, S.K. Estreicher and C.H. Chu, *J. Phys.: Condens. Matter*, **5** (1993) 8943.
- [41] M.A. Roberson and S.K. Estreicher, *Phys. Rev. B*, **49** (1994) 17040.
- [42] J.J.P. Stewart, *J. Comp. Chem.*, **10** (1989) 209, 221; **12** (1991) 320.
- [43] J.A. Pople and D.L. Beveridge, *Approximate Molecular Orbital Theory*, McGraw-Hill, New York, 1970.
- [44] R.C. Bongham, M.J.S. Dewar and D.H. Lo, *J. Am. Chem. Soc.*, **97** (1975) 1285.
- [45] M.J.S. Dewar and W. Thiel, *J. Am. Chem. Soc.*, **99** (1977) 4899, 4907.
- [46] M.J.S. Dewar, M.C. McKee and H.S. Rzepa, *J. Am. Chem. Soc.*, **100** (1978) 3607.
- [47] T.A. Halgren and W.N. Lipscomb, *J. Comp. Chem.*, **58** (1973) 1569.
- [48] D.S. Marynick and W.N. Lipscomb, *Proc. Nat. Acad. Sci. (USA)*, **79** (1982) 1341.
- [49] L. Throckmorton and D.S. Marynick, *J. Comp. Chem.*, **6** (1985) 652.
- [50] A. Derecskei-Kovacs, D. Woon and D.S. Marynick, to be published.
- [51] P. Hohenberg and W. Kohn, *Phys. Rev., B*, **136** (1964) 864.
- [52] W. Kohn and L.J. Sham, *Phys. Rev., A*, **140** (1965) 1133.
- [53] L.J. Sham and W. Kohn, *Phys. Rev.*, **145** (1966) 561.
- [54] E. Wigner, *Phys. Rev.*, **46** (1934) 1002.
- [55] L. Hedin and B.I. Lundqvist, *J. Phys. C*, **4** (1971) 2064.
- [56] D.M. Ceperley and B.J. Adler, *Phys. Rev. Lett.*, **45** (1980) 566.
- [57] S. Perdew and A. Zunger, *Phys. Rev. B*, **23** (1981) 5048.
- [58] P. Ordejón and F. Ynduráin, *Phys. Rev. B*, **44** (1991) 12794.
- [59] C.G. Van de Walle, *Phys. Rev. Lett.*, **64** (1990) 669.
- [60] R. Jones and A. Sayyash, *J. Phys. C*, **19** (1986) L653; R. Jones, *J. Phys. C*, **21** (1988) 5735.
- [61] R. Jones, *Molec. Simul.*, **4** (1989) 669.
- [62] D.R. Hamann, M. Schlüter and C. Chiang, *Phys. Rev. Lett.*, **43** (1979) 1494.
- [63] G.B. Bachelet, D.R. Hamann and M. Schlüter, *Phys. Rev. B*, **26** (1982) 4199.
- [64] C.G. Van de Walle and P.E. Blöchl, *Phys. Rev. B*, **47** (1993) 4244.
- [65] M.S. Hybertsen and S.G. Louie, *Phys. Rev. B*, **34** (1986) 5390.
- [66] Z.H. Levine and S.G. Louie, *Phys. Rev. B*, **25** (1982) 6310.
- [67] C.S. Wang and W.E. Pickett, *Phys. Rev. Lett.*, **51** (1983) 597.
- [68] R. Wang, *Phys. Rev. B*, **44** (1991) 1057.
- [69] R. Car and M. Parrinello, *Phys. Rev. Lett.*, **55** (1985) 2471.
- [70] R. Stumpf and M. Scheffler, *Comp. Phys. Commun.*, **79** (1994) 441.
- [71] O.F. Sankey and D.J. Niklewski, *Phys. Rev. B*, **40** (1989) 3979.
- [72] J. Harris, *Phys. Rev. B*, **31** (1985) 1770.
- [73] D.E. Boucher and G.G. DeLeo, *Phys. Rev. B*, **50** (1994) 5247.
- [74] C.Z. Wang, C.T. Chan and K.M. Ho, *Phys. Rev. B*, **39** (1989) 8586.
- [75] Y.K. Park and C.W. Myles, *Phys. Rev. B*, **48** (1993) 17086.
- [76] I.I. Gurevich, I.G. Ivanter, E.A. Meleshko, B.A. Nikol'skii, V.S. Roganov, V.I. Selivanov, V.P. Smilga, B.V. Sokolov and V.D. Shestakov, *Zh. Eksp. Teor. Fiz.*, **60** (1971) 471; *Sov. Phys. JETP*, **33** (1971) 253.
- [77] B.D. Patterson, *Rev. Mod. Phys.*, **60** (1988) 69.
- [78] J.W. Schneider, Hp. Baumelere, H. Keller, R.F. Kiefl, W. Kündig, W. Odermatt, B.D. Patterson, T.L. Estle, S.L. Rudaz, K.W. Blazey and C. Schwab, *Hyp. Int.*, **32** (1986) 607.
- [79] T.L. Estle, R.F. Kiefl, J.W. Schneider and C. Schwab, *MRS Proc.*, **163** (1990) 407.
- [80] T.L. Estle and R.F. Kiefl, Ref. [2].
- [81] A. Abragam, *Comptes Rendus Acad. Sci. (Paris) Ser. 2*, **29** (1984) 95.
- [82] S.R. Kreitzman, J.H. Brewer, D.R. Harschman, R. Keitel, D.L. Williams, K.M. Crowe and E.J. Ansaldo, *Phys. Rev. Lett.*, **56** (1986) 181.
- [83] R.F. Kiefl, S.R. Kreitzman, M. Celio, R. Keitel, G.M. Luke, J.H. Brewer, D.R. Noakes, P.W. Percival, T. Matsuzaki and K. Nishiyama, *Phys. Rev. A*, **34** (1986) 681.
- [84] R.L. Lichti, C.D. Lamp, S.R. Kreitzman, R.F. Kiefl, J.W. Schneider, Ch. Niedermayer, K. Chow, T. Pfitz, T.L. Estle, S.A. Dodds, B. Hitti and R.C. DuVarney, *Mater. Sci. Forum*, **83-87** (1992) 1115.
- [85] S.R. Kreitzman, *Hyp. Int.*, **63-65** (1990) 1055.
- [86] Yu.V. Gorelkinsky and N.N. Nevinnyi, *Pisma Zh. Tekh. Nauk.*, **13** (1987) 105 (*Sov. Tech. Phys. Lett.*, **13** (1987) 45).
- [87] Yu.V. Gorelkinsky and N.N. Nevinnyi, *Physica B*, **170** (1991) 155.
- [88] R.F. Kiefl, M. Celio, T.L. Estle, S.R. Kreitzman, G.M. Luke, T.M. Riseman and E.J. Ansaldo, *Phys. Rev. Lett.*, **60** (1988) 224.
- [89] Hp. Baumeler, R.F. Kiefl, H. Keller, W. Kündig, W. Odermatt, B.D. Patterson, J.W. Schneider, T.L. Estle, S.L. Rudaz, D.P. Spencer, K.W. Blazey and I.M. Savic, *Hyp. Int.*, **32** (1986) 659.

- [90] M.C.R. Symons, *Hyp. Int.*, 17–19 (1984) 771.
- [91] S.F.J. Cox and M.C.R. Symons, *Chem. Phys. Lett.*, 126 (1986) 516.
- [92] S.F.J. Cox, *J. Phys. C*, 20 (1987) 3187.
- [93] T.A. Claxton, A. Evans and M.C.R. Symons, *J. Chem. Soc. Faraday Trans. 2*, 82 (1986) 2031.
- [94] T.L. Estle, S.K. Estreicher and D.S. Marynick, *Hyp. Int.*, 32 (1986) 637.
- [95] T.L. Estle, S.K. Estreicher and D.S. Marynick, *Phys. Rev. Lett.*, 58 (1987) 1547.
- [96] S.K. Estreicher, *Phys. Rev. B*, 36 (1987) 9122.
- [97] R.F. Kiefl, J.W. Schneider, H. Keller, W. Kündig, W. Odermatt, B.D. Patterson, K.W. Blazey, T.L. Estle and S.L. Rudaz, *Phys. Rev. B*, 32 (1985) 530.
- [98] Preliminary results were published in R.L. Lichti, K.H. Chow, T.L. Estle, B. Hitti, R.F. Kiefl, S.R. Kreitzman and J.W. Schneider, *Mater. Sci. Forum*, 143–147 (1994) 915.
- [99] S.R. Kreitzman, B. Hitti, R.L. Lichti, T.L. Estle and K.H. Chow, *Phys. Rev. B*, in press.
- [100] H. Simmler, P. Eschle, H. Keller, W. Kündig, W. Odermatt, B.D. Patterson, B. Pümpin, I.M. Savic, J.W. Schneider, U. Straumann and P. Truöl, *Hyp. Int.*, 64 (1990) 535.
- [101] J.W. Schneider, Hp. Baumeler, H. Keller, R.F. Kiefl, W. Kündig, W. Odermatt, B.D. Patterson, T.L. Estle, S.L. Rudaz, K.W. Blazey and C. Schwab, *Hyp. Int.*, 32 607 (1986).
- [102] B.D. Patterson, Hp. Baumeler, H. Keller, R.F. Kiefl, W. Kündig, W. Odermatt, J.W. Schneider, W.J. Choyke, T.L. Estle, D.P. Spencer, K.W. Blazey and I.M. Savic, *Hyp. Int.*, 32 625 (1986).
- [103] M. Rivot, *Comptes Rendus Acad. Sci. (Paris)*, 28 (1849) 317.
- [104] E. Holzschuh, H. Graf, E. Recknagel, A. Weidinger, Th. Wichert and P.F. Meier, *Phys. Rev. B*, 20 (1979) 4391.
- [105] E. Holzschuh, W. Kündig, P.F. Meier, B.D. Patterson, J.P.F. Sellschop, M.C. Stemmet and H. Appel, *Phys. Rev. A*, 25 (1982) 1272.
- [106] B.D. Patterson, *Hyp. Int.*, 17–19 (1984) 517.
- [107] N. Sahoo, K.C. Mishra and T.P. Das, *Phys. Rev. Lett.*, 55 (1985) 1506.
- [108] S.K. Estreicher and D.S. Marynick, *Phys. Rev. Lett.*, 56 (1986) 1511; N. Sahoo, K.C. Mishra and T.P. Das, *Phys. Rev. Lett.*, 56 (1986) 1512.
- [109] Dj.M. Maric, M.A. Roberson and S.K. Estreicher, *Mater. Sci. Forum*, 143–147 (1994) 1245.
- [110] S.K. Estreicher, M.A. Roberson and Dj.M. Maric, *Phys. Rev. B*, 50 (1994) 17018.
- [111] D.R. Lide (ed.), *CRC Handbook of Chemistry and Physics*, 75th edn., CRC Press, Boca Raton, FL, 1994, pp. 9–64, 5.
- [112] S.F.J. Cox, P.R. Briddon and R. Jones, *Hyp. Int.*, 64 (1990) 603.
- [113] N. Sahoo, S.K. Mishra, K.C. Mishra, A. Coker, T.P. Das, C.K. Mitra, L.C. Snyder and A. Glodeanu, *Phys. Rev. Lett.*, 50 (1983) 913.
- [114] A. Mainwood and A.M. Stoneham, *J. Phys. C*, 17 (1984) 2513.
- [115] S.K. Estreicher, A.K. Ray, J.L. Fry and D.S. Marynick, *Phys. Rev. B*, 34 (1986) 6071.
- [116] P. Briddon, R. Jones and G.M.S. Lister, *J. Phys. C*, 21 (1988) L1207.
- [117] C.H. Chu and S.K. Estreicher, *Phys. Rev. B*, 42 (1990) 9486.
- [118] S.P. Mehandru, A.B. Anderson and J.C. Angus, *J. Mater. Res.*, 7 (1992) 689.
- [119] S.P. Mehandru and A.B. Anderson, *J. Mater. Res.*, 9 (1994) 383.
- [120] T. Hoshino, T. Asada and K. Terakura, *Phys. Rev. B*, 39 (1989) 5468.
- [121] S. Vogel, M. Celio, Dj.M. Maric and P.F. Meier, *J. Phys.: Condens. Matter*, 1 (1989) 4729.
- [122] M. Casarin, G. Granozzi, E. Tondello and A. Vittadini, *Chem. Phys.*, 154 (1991) 385.
- [123] N. Paschedag, H.U. Suter, Dj.M. Maric and P.F. Meier, *Phys. Rev. Lett.*, 70 (1993) 154.
- [124] J.W. Schneider, R.F. Kiefl, K.H. Chow, S. Johnston, J. Sonier, T.L. Estle, B. Hitti, R.L. Lichti, S.H. Connell, J.P.F. Sellschop, C.G. Smallman, T.R. Anthony and W.F. Banholzer, *Phys. Rev. Lett.*, 71 (1993) 557.
- [125] K.J. Chang and D.J. Chadi, *Phys. Rev. Lett.*, 62 (1989) 937.
- [126] E. Westhauser, E. Albert, M. Hamma, E. Recknagel, A. Weidinger and P. Moser, *Hyp. Int.*, 32 (1986) 589.
- [127] B. Bech Nielsen, K. Bonde Nielsen and J.P. Byberg, *Mater. Sci. Forum*, 143–147 (1994) 909.
- [128] B. Bech Nielsen, private communication.
- [129] B. Holm, K. Bonde Nielsen and B. Bech Nielsen, *Phys. Rev. Lett.*, 66 (1991) 2360.
- [130] S.K. Estreicher, C.H. Seager and R.A. Anderson, *Mater. Sci. Forum*, 83–87 (1992) 63.
- [131] S.K. Estreicher and R. Jones, *Appl. Phys. Lett.*, 64 (1994) 1670.
- [132] C.H. Seager and R.A. Anderson, *Appl. Phys. Lett.*, 63 (1993) 1531.
- [133] Y. Kamiura, T. Okashita and F. Hashimoto, *Mater. Sci. Forum*, 143–147 (1994) 921.
- [134] W. Császár and A.L. Endrös, *Phys. Rev. Lett.*, 73 (1994) 312.
- [135] K.H. Chow, R.F. Kiefl, J.W. Schneider, B. Hitti, T.L. Estle, R.L. Lichti, C. Schwab, R.C. DuVarney, S.R. Kreitzman, W.A. MacFarlane and M. Senba, *Phys. Rev. B*, 47 (1993) 16004.
- [136] K.H. Chow, R.L. Lichti, R.F. Kiefl, S. Dunsiger, T.L. Estle, B. Hitti, R. Kadono, W.A. MacFarlane, J.W. Schneider, D. Schumann and M. Shelley, *Phys. Rev. B*, 50 (1994) 8918.
- [137] S.T. Picraux and F.L. Vook, *Phys. Rev. B*, 18 (1978) 2066.
- [138] B. Bech Nielsen, *Phys. Rev. B*, 37 (1988) 6353.

- [139] C.O. Rodrigues, M. Jaros and S. Brand, *Solid State Commun.*, **31** (1979) 43.
- [140] J.M. Baranowski, *Phys. Rev. B*, **39** (1989) 8616.
- [141] J.W. Corbett, S.N. Sahu, T.S. Shi and L.C. Snyder, *Phys. Lett. A*, **93** (1983) 303.
- [142] P. Deák, L.C. Snyder and J.W. Corbett, *Phys. Rev. B*, **37** (1988) 6887.
- [143] P. Deák, L.C. Snyder, J.L. Lindström, J.W. Corbett, S.J. Pearton and A.J. Tavendale, *Phys. Lett. A*, **126** (1988) 427.
- [144] P. Deák, L.C. Snyder and J.W. Corbett, *Phys. Rev. B*, **43** (1991) 4545.
- [145] G.G. DeLeo, M.J. Dorogi and W.B. Fowler, *Phys. Rev. B*, **38** (1988) 7520.
- [146] K.J. Chang and D.J. Chadi, *Phys. Rev. B*, **40** (1989) 11644.
- [147] R. Jones, *Physica B*, **170** (1991) 181.
- [148] P.R. Briddon and R. Jones, *Hyp. Int.*, **64** (1990) 593.
- [149] Y.K. Park and S.K. Estreicher, unpublished work.
- [150] F. Buda, G.L. Chiarotti, R. Car and M. Parrinello, *Phys. Rev. Lett.*, **63** (1989) 294.
- [151] G. Panzarini and L. Colombo, *Phys. Rev. Lett.*, **73** (1994) 1636.
- [152] A. Van Wieringen and N. Warmoltz, *Physica*, **22** (1956) 849.
- [153] P.E. Blöchl, C.G. Van de Walle and S.T. Pantelides, *Phys. Rev. Lett.*, **64** (1990) 1401.
- [154] N.M. Johnson and C. Herring, *Phys. Rev. B*, **38** (1988) 1581.
- [155] J.D. Holbech, B. Bech Nielsen, R. Jones, P. Sitch and S. Öberg, *Phys. Rev. Lett.*, **71** (1993) 875.
- [156] J.W. Corbett, J.L. Lindström and S.J. Pearton, *MRS Proc.*, **104** (1988) 229.
- [157] B.L. Sopori, *MRS Proc.*, **262** (1992) 407.
- [158] B.L. Sopori, K. Jones and X.J. Deng, *Appl. Phys. Lett.*, **61** (1992) 2560.
- [159] B.L. Sopori, *Mater. Sci. Forum*, **83-87** (1992) 1531.
- [160] B.L. Sopori, X. Deng, J.P. Benner, A. Rohatgi, P. Sana, S.K. Estreicher, Y.K. Park and M.A. Roberson, *Proc. First World PV Conf.*, IEEE Press, in press.
- [161] Y.K. Park, S.K. Estreicher, C.W. Myles and P.A. Fedders, *Phys. Rev. B*, in press.
- [162] H. Katayama-Yoshida and K. Shindo, *Phys. Rev. Lett.*, **51** (1983) 207.
- [163] S.A. Kuten, V.I. Rapoport, A.V. Mudry, R.B. Gelfand, A.L. Pushkarchuk and A.G. Ulyashin, *Hyp. Int.*, **39** (1988) 379.
- [164] Dj.M. Maric, S. Vogel, P.F. Meier and S.K. Estreicher, *Hyp. Int.*, **64** (1990) 573.
- [165] R. Ramirez and C.P. Herrero, *Phys. Rev. Lett.*, **73** (1994) 126.
- [166] C.S. Nichols, D.R. Clarke and C.G. Van de Walle, *Phys. Rev. Lett.*, **63** (1989) 1090.
- [167] E. Tarnow and R.A. Street, *Phys. Rev. B*, **45** (1992) 3366.
- [168] M. Capizzi and A. Mittiga, *Appl. Phys. Lett.*, **50** (1987) 918.
- [169] C.H. Seager, R.A. Anderson and D.K. Brice, *J. Appl. Phys.*, **68** (1990) 3268.
- [170] N.M. Johnson, C. Herring and D.J. Chadi, *Phys. Rev. Lett.*, **56** (1986) 769.
- [171] N.M. Johnson and S.K. Hahn, *Appl. Phys. Lett.*, **48** (1986) 709.
- [172] A.J. Tavendale, S.J. Pearton and A.A. Williams, *Appl. Phys. Lett.*, **56** (1990) 949.
- [173] J. Zhu, N.M. Johnson and C. Herring, *Phys. Rev. B*, **41** (1990) 12354.
- [174] C.H. Seager, private communication.
- [175] K. Bergman, M. Stavola, S.J. Pearton and J. Lopata, *Phys. Rev. B*, **37** (1988) 2770.
- [176] K. Bergman, M. Stavola, S.J. Pearton and T. Hayes, *Phys. Rev. B*, **38** (1988) 9643.
- [177] C.H. Seager and R.A. Anderson, *Solid State Commun.*, **76** (1990) 285.
- [178] N.M. Johnson and C. Herring, *Phys. Rev. B*, **45** (1992) 11379.
- [179] N.M. Johnson and C. Herring, *Phys. Rev. B*, **46** (1992) 15554.
- [180] N.M. Johnson, C. Herring and C.G. Van de Walle, *Phys. Rev. Lett.*, **73** (1994) 130.
- [181] C.H. Seager, R.A. Anderson and S.K. Estreicher, *Phys. Rev. Lett.*, in press (comment on Ref. [180]).
- [182] S.K. Estreicher, C.H. Seager and R.A. Anderson, *Appl. Phys. Lett.*, **59** (1991) 1773.
- [183] S.K. Estreicher and R. Jones, *Mater. Sci. Forum*, **143-147** (1994) 1215.
- [184] K.J. Chang and D.J. Chadi, *Phys. Rev. B*, **42** (1990) 7651.
- [185] S.B. Zhang, W.B. Jackson and D.J. Chadi, *Phys. Rev. Lett.*, **65** (1990) 2575.
- [186] J.W. Corbett, S.N. Sahu, T.S. Shi and L.C. Snyder, *Phys. Lett. A*, **93** (1983) 303.
- [187] P. Deák, and L.C. Snyder, *Radiation Effects Defects Solids*, **111-112** (1989) 77.
- [188] C.G. Van de Walle, *Phys. Rev. B*, **49** (1994) 4579.
- [189] J.E. Graebner, B. Golding, L.C. Allen, D.K. Biegelstein and M. Stutzmann, *Phys. Rev. Lett.*, **52** (1984) 553.
- [190] Y.J. Chabal and C.K.N. Patel, *Phys. Rev. Lett.*, **53** (1984) 210.
- [191] J.E. Graebner, L.C. Allen and B. Golding, *Phys. Rev. B*, **31** (1985) 904.
- [192] J.B. Boyce and M. Stutzmann, *Phys. Rev. Lett.*, **54** (1985) 562.
- [193] P. Stallinga, T. Gregorkiewicz, C.A.J. Ammerlaan and Yu.V. Gorelkinskii, *Phys. Rev. Lett.*, **71** (1993) 117.
- [194] K.L. Brower, *Phys. Rev. B*, **42** (1990) 3444.
- [195] K.L. Brower and S.M. Myers, *Appl. Phys. Lett.*, **57** (1990) 162.
- [196] K.L. Brower, S.M. Myers, A.H. Edwards, N.M. Johnson, C.G. Van de Walle and E.H. Poindexter, *Phys. Rev. Lett.*, **73** (1994) 1456.

- [197] P. Stallinga, T. Gregorkiewicz and C.A.J. Ammerlaan, *Phys. Rev. Lett.*, **73** (1994) 1457.
- [198] R.L. Lichti, K.H. Chow, D.W. Cooke, S.F.J. Cox, E.A. Davis, R.C. DuVarney, T.L. Estle, B. Hitti, S.R. Kreitzman, R. Macrae, C. Schwab and A. Singh, *Hyp. Int.*, **86** (1994) 711.
- [199] K. Kohler, J.W. Coburn, D.E. Horne, E. Kay and J.H. Keller, *J. Appl. Phys.*, **57** (1985) 59.
- [200] M. Stutzmann, J.-B. Chevrier, C.P. Herrero and A. Breitschwert, *Appl. Phys. A*, **53** (1991) 47.
- [201] G.S. Khoo and C.K. Ong, *J. Phys. C*, **20** (1987) 1385.
- [202] P.J.H. Denteneer, C.G. Van de Walle and S.T. Pantelides, *Phys. Rev. Lett.*, **62** (1989) 1884.
- [203] S.K. Estreicher and Dj.M. Maric, *Phys. Rev. Lett.*, **70** (1993) 3963.
- [204] N. Sahoo, S.B. Sulaiman, K.C. Mishra and T.P. Das, *Phys. Rev. B*, **39** (1989) 13389.
- [205] S.K. Estreicher, C.H. Chu and D.S. Marynick, *Phys. Rev. B*, **40** (1989) 5739.
- [206] J. Dabrowski and M. Scheffler, *Mater. Sci. Forum*, **83-87** (1992) 735.
- [207] J. Schlichting, G. Czack, E. Koch-Bienemann, P. Kuhn and F. Schröder, in G. Kirschstein (ed.), *Gmelin Handbook of Inorganic Chemistry*, suppl. Vol. B2, Springer-Verlag, Berlin, 1984.
- [208] G. Pensl and R. Helbig, *Adv. Solid St. Phys.*, **30** (1990) 133; U. Rössler (ed.), *Festkörperprobleme*, Vieweg, Braunschweig.
- [209] M.A. Roberson and S.K. Estreicher, *Phys. Rev. B*, **44** (1991) 10578.
- [210] M.A. Roberson and S.K. Estreicher, *MRS Proc.*, **242** (1992) 355.
- [211] This assignment was suggested by T.L. Estle, private communication.
- [212] J.W. Schneider, private communication.
- [213] R.F. Kiefl, M. Celio, T.L. Estle, G.M. Luke, S.R. Kreitzman, J.H. Brewer, D.R. Noakes, E.J. Ansaldi and K. Nishiyama, *Phys. Rev. Lett.*, **58** (1987) 1780.
- [214] J.W. Schneider, K. Chow, R.F. Kiefl, S.R. Kreitzman, A. MacFarlane, R.C. duVarney, T.L. Estle, R.L. Lichti and C. Schwab, *Phys. Rev. B*, **47** (1993) 10193.
- [215] R. Kadono, A. Matsushita, K. Nagamine, K. Nishiyama, K.H. Chow, R.F. Kiefl, A. MacFarlane, D. Schumann, S. Fujii and S. Tanigawa, *Phys. Rev. B*, **50** (1994) 1999.
- [216] K.H. Chow, R.F. Kiefl, D.W. Cooke, S.F.J. Cox, E.A. Davis, T.L. Estle, B. Hitti, M. Leon, R.L. Lichti, W.A. MacFarlane, A. Morrobel-Sosa, M.A. Paciotti, J.W. Schneider, C. Schwab and L. Zavieh, *Phys. Rev. B*, in press.
- [217] T.R. Adams, M.A. Roberson and R.L. Lichti, *Phil. Mag. B*, in press.
- [218] R.L. Lichti, private communication.
- [219] P. Briddon and R. Jones, in B. Monemar (ed.), *Shallow Impurities in Semiconductors*, IOP, Bristol, 1989, p. 459.
- [220] R. Jones, *Molec. Simul.*, **4** (1989) 113.
- [221] L. Pavesi and P. Giannozzi, *Physica B*, **170** (1991) 392.
- [222] L. Pavesi and P. Giannozzi, *Phys. Rev. B*, **46** (1992) 4621.
- [223] M.H. Yuan, L.P. Wang, S.X. Jin, J.J. Chen and G.G. Qin, *Appl. Phys. Lett.*, **58** (1991) 925.
- [224] G. Roos, N.M. Johnson, C. Herring and J.S. Harris, *Appl. Phys. Lett.*, **59** (1991) 461.
- [225] A.W.R. Leitch, Th. Prescha and J. Weber, *Phys. Rev. B*, **44** (1991) 1375.
- [226] B. Clerjaud, F. Gendron, M. Krause and W. Ulrich, *Phys. Rev. Lett.*, **65** (1990) 1800.
- [227] R.A. Morrow, *J. Appl. Phys.*, **74** (1993) 6174.
- [228] S.J. Pearton, W.C. Dautremont-Smith, J. Lopata, C.W. Tu and C.R. Abernathy, *Phys. Rev. B*, **36** (1987) 4260.
- [229] J. Chevallier and B. Pajot, *Mater. Sci. Forum*, **83-87** (1992) 539.
- [230] Dj.M. Maric, S. Vogel, P.F. Meier and S.K. Estreicher, *Phys. Rev. B*, **40** (1989) 8545.
- [231] D.R. Armstrong, P.G. Perkins and J.J.P. Stewart, *J. Chem. Soc. Dalton Trans.*, (1973) 838.
- [232] H.J. Stein, *Appl. Phys. Lett.*, **57** (1990) 792.
- [233] C.G. Van de Walle and L. Pavesi, *Phys. Rev. B*, **47** (1993) 4256.
- [234] Dj.M. Maric, S. Vogel, P.F. Meier, T.A. Claxton and S.F.J. Cox, *Hyp. Int.*, **64** (1990) 567.
- [235] L. Pavesi, *Solid State Commun.*, **83** (1992) 317.
- [236] L. Pavesi, in S. Adachi (ed.), *Properties of Aluminum Gallium Arsenide*, EMIS Data Review series No. 7, Inst. Elec. Eng., London, 1993, p. 303.
- [237] L. Pauling, *The Chemical Bond*, Cornell University Press, Ithaca, NY, 1967.
- [238] P.A. Fisher, E. Ho, J.L. House, G.S. Petrich and L.A. Kolodziejski, *MRS Proc.*, **340** (1994) 451.
- [239] P.A. Fisher, E. Ho, J.L. House, G.S. Petrich, L.A. Kolodziejski, J. Walker and N.M. Johnson, *J. Crystal Growth*, in press.
- [240] C.G. Van de Walle and D.B. Laks, in E.M. Anastassakis and J.D. Joannopoulos (eds.), *Proc. 20th Int. Conf. Defects Semiconductors*, World Scientific, Singapore, 1990, p. 654.
- [241] R.F. Kiefl, W. Odermatt, Hp. Baumeler, J. Felber, H. Keller, W. Küdlig, P.F. Meier, B.D. Patterson, J.W. Schneider, K.W. Blazey, T.L. Estle and C. Schwab, *Phys. Rev. B*, **34** (1986) 1474.
- [242] J.W. Schneider, M. Celio, H. Keller, W. Küdlig, W. Odermatt, B. Pümpin, I.M. Savic, H. Simmler, T.L. Estle, C. Schwab, R.F. Kiefl and D. Renker, *Phys. Rev. B*, **41** (1990) 7254.
- [243] J.W. Schneider, R.F. Kiefl, K. Chow, S.F.J. Cox, S.A. Dodds, R.C. DuVarney, T.L. Estle, R. Kadono, S.R. Kreitzman, R.L. Lichti and C. Schwab, *Phys. Rev. Lett.*, **68** (1992) 3196.
- [244] M.I. Landstrass and K.V. Ravi, *Appl. Phys. Lett.*, **55** (1989) 975, 1391.
- [245] S. Albin and L. Watkins, *Appl. Phys. Lett.*, **56** (1990) 1454.

- [246] S.J. Breuer and P.R. Briddon, *Phys. Rev. B*, **49** (1994) 10332.
- [247] G.G. DeLeo, *Physica B*, **170** (1991) 295.
- [248] See Ref. [4], p.69.
- [249] G.D. Watkins, W.B. Fowler, M. Stavola, G.G. DeLeo, D.M. Kozuch, S.J. Pearton and J. Lopata, *Phys. Rev. Lett.*, **64** (1990) 467.
- [250] C.H. Seager and R.A. Anderson, *Appl. Phys. Lett.*, **59** (1991) 585.
- [251] T. Zundel and J. Weber, *Phys. Rev. B*, **43** (1991) 4361.
- [252] T. Zundel, J. Weber and L. Tilly, *Physica B*, **170** (1991) 361.
- [253] C.P. Herrero, M. Stutzmann and A. Breitschwerdt, *Solid State Commun.*, **68** (1988) 1085.
- [254] C.P. Herrero, M. Stutzmann and A. Breitschwerdt, *Phys. Rev. B*, **43** (1991) 1555.
- [255] M. Stavola, S.J. Pearton, J. Lopata and W.C. Dautremont-Smith, *Phys. Rev. B*, **37** (1988) 8313.
- [256] M. Stavola, Y.M. Cheng and G. Davies, *Mater. Sci. Forum*, **143-147** (1994) 885.
- [257] G.G. DeLeo and W.B. Fowler, *Phys. Rev. B*, **31** (1985) 6861.
- [258] G.G. DeLeo and W.B. Fowler, *J. Electron. Mater. A*, **14** (1985) 745.
- [259] J.I. Pankove, D.J. Zanzucchi, C.W. Magee and G. Lucovsky, *Appl. Phys. Lett.*, **46** (1985) 421.
- [260] L.V.C. Assali and J.R. Leite, *Phys. Rev. Lett.*, **55** (1985) 980.
- [261] E.C.F. da Silva, L.V.C. Assali, J.R. Leite and A. Dal Pino, Jr., *Phys. Rev. B*, **37** (1988) 3113.
- [262] See the Comment by DeLeo et al. and the Response by Assali et al. in *Phys. Rev. Lett.*, **56** (1986) 402 and 403.
- [263] A. Amore Bonapasta, A. Lapicciarella, M. Tomassini and M. Capizzi, *Phys. Rev. B*, **36** (1987) 6228.
- [264] A. Amore Bonapasta, A. Lapicciarella, M. Tomassini and M. Capizzi, *Europhys. Lett.*, **7** (1988) 145.
- [265] A. Amore Bonapasta, P. Giannozzi and M. Capizzi, *Phys. Rev. B*, **44** (1991) 3399.
- [266] A. Amore Bonapasta, P. Giannozzi and M. Capizzi, *Phys. Rev. B*, **45** (1992) 11744.
- [267] K.J. Chang and D.J. Chadi, *Phys. Rev. Lett.*, **60** (1988) 1422.
- [268] P.J.H. Denteneer, C.G. Van de Walle and S.T. Pantelides, *Phys. Rev. B*, **39** (1989) 10809.
- [269] M. Stavola, K. Bergman, S.J. Pearton and J. Lopata, *Phys. Rev. Lett.*, **61** (1988) 27861.
- [270] G. Cannelli, R. Cantelli, M. Capizzi, C. Coluzza, F. Cordero, A. Frova and A. LoPresti, *Phys. Rev. B*, **44** (1991) 11486.
- [271] S.K. Estreicher, L. Throckmorton and D.S. Marynick, *Phys. Rev. B*, **39** (1989) 13241.
- [272] E. Artacho and F. Ynduráin, *Solid State Commun.*, **72** (1989) 393.
- [273] Dj.M. Maric, P.F. Meier and S.K. Estreicher, *Mater. Sci. Forum*, **83-87** (1992) 119.
- [274] Dj.M. Maric, P.F. Meier and S.K. Estreicher, *Phys. Rev. B*, **47** (1993) 3620.
- [275] G.G. DeLeo and W.B. Fowler, *Bull. APS*, **34** (1989) 834.
- [276] M. Stavola, S.J. Pearton, J. Lopata and W.C. Dautremont-Smith, *Appl. Phys. Lett.*, **50** (1987) 1086.
- [277] T. Zundel and J. Weber, *Phys. Rev. B*, **39** (1989) 13549.
- [278] N.M. Johnson, C. Doland, F. Ponce, J. Walker and G. Anderson, *Physica B*, **170** (1991) 3.
- [279] G.D. Watkins and J.W. Corbett, *Phys. Rev.*, **121** (1961) 1001.
- [280] J.W. Corbett, G.D. Watkins, R.M. Chrenko and R.S. McDonald, *Phys. Rev.*, **121** (1961) 1015.
- [281] G.L. Gutsev, G.S. Myakinkaya, V.V. Frolov and V.B. Glazman, *Phys. Status Solidi (b)*, **153** (1989) 659.
- [282] M. Gebhard, B. Vogt and W. Witthuhn, *Phys. Rev. Lett.*, **67** (1991) 847.
- [283] K. Muro and A.J. Sievers, in O. Engström (ed.), *Proc. 18th Int. Conf. Physics Semiconductors*, World Scientific, Singapore, 1986, p. 891.
- [284] K. Muro and A.J. Sievers, *Phys. Rev. Lett.*, **57** (1986) 897.
- [285] R.E. Peale, K. Muro and A.J. Sievers, *Phys. Rev. B*, **41** (1990) 5881.
- [286] G.G. DeLeo, W.B. Fowler, T.M. Sudol and V.L. Gates, unpublished.
- [287] K.R. Martin, W.B. Fowler and G.G. DeLeo, *Mater. Sci. Forum*, **83-87** (1992) 69.
- [288] S.B. Zhang and D.J. Chadi, *Phys. Rev. B*, **41** (1990) 3882.
- [289] P.J.H. Denteneer, C.G. Van de Walle and S.T. Pantelides, *Phys. Rev. B*, **41** (1990) 3885.
- [290] G.G. DeLeo, W.B. Fowler, T.M. Sudol and K.J. O'Brian, *Phys. Rev. B*, **41** (1990) 7581.
- [291] A. Amore Bonapasta, A. Lapicciarella, M. Tomassini and M. Capizzi, *Phys. Rev. B*, **39** (1989) 12630.
- [292] A. Amore Bonapasta, *Phys. Rev. B*, **46** (1992) 10119.
- [293] G. Roos, G. Pensl, N.M. Johnson and C. Holm, *Appl. Phys. Lett.*, **67** (1990) 1897.
- [294] A.S. Yapsir, P. Deák, R.K. Singh, L.C. Snyder and J.W. Corbett, *Phys. Rev. B*, **38** (1988) 9936.
- [295] G. Davies and R.C. Newmann, in T.S. Moss (ed.), *Handbook on Semiconductors*, Vol. 3, Chapt. 21, Elsevier, Amsterdam, 1994, p. 1557.
- [296] A.L. Endrös, *Phys. Rev. Lett.*, **63** (1989) 70.
- [297] A.L. Endrös, W. Krühler and J. Grabmaier, *Physica B*, **170** (1991) 365.
- [298] A.L. Endrös, W. Krühler and F. Koch, *J. Appl. Phys.*, **72** (1992) 2264.
- [299] W. Csaszár and A.L. Endrös, *Phys. Rev. Lett.*, **73** (1994) 312.
- [300] Y. Kamiura, M. Yoneta and F. Hashimoto, *Appl. Phys. Lett.*, **59** (1991) 3165.
- [301] Y. Kamiura, M. Yoneta, Y. Nishiyama and F. Hashimoto, *J. Appl. Phys.*, **72** (1992) 3394.
- [302] Y. Kamiura, F. Hashimoto and M. Yoneta, *MRS Proc.*, **262** (1992) 455.
- [303] A.N. Safonov and E.C. Lightowers, *Mater. Sci. Forum*, **143-147** (1994) 903.

- [304] C. Kaneta and H. Katayama-Yoshida, D.J. Lockwood (ed.), *Proc. 22nd Int. Conf. Physics Semiconductors*, World Scientific, Singapore, 1995, in press.
- [305] J.W. Corbett, R.S. McDonald and G.D. Watkins, *J. Phys. Chem. Solid*, 25 (1964) 873.
- [306] J.C. Mikkelsen, *Appl. Phys. Lett.*, 40 (1982) 336.
- [307] G.D. Watkins, J.W. Corbett and R.S. McDonald, *J. Appl. Phys.*, 53 (1982) 7097.
- [308] H.J. Stein, S.K. Hahn and C. Shatas, *J. Appl. Phys.*, 59 (1986) 3495.
- [309] M. Claybourn and R.C. Newman, *Appl. Phys. Lett.*, 51 (1987) 2197.
- [310] L.C. Snyder, J.W. Corbett, P. Deák; and R. Wu, *MRS Proc.*, 104 (1988) 179.
- [311] L.C. Snyder and J.W. Corbett, *MRS Proc.*, 59 (1988) 207.
- [312] M. Saito and A. Oshiyama, *Phys. Rev. B*, 38 (1988) 10711.
- [313] R. Jones, *Semicond. Sci. Technol.*, 5 (1990) 255.
- [314] R. Jones, S. Öberg and A. Umerski, *Mater. Sci. Forum*, 65–66 (1990) 287.
- [315] D.J. Chadi, *Phys. Rev. B*, 41 (1990) 10595.
- [316] M. Needels, J.D. Joannopoulos, Y. Bar-Yam and S.T. Pantelides, *Phys. Rev. B*, 43 (1991) 4208.
- [317] P. Deák, L.C. Snyder and J.W. Corbett, *Phys. Rev. Lett.*, 66 (1991) 747.
- [318] P. Deák, L.C. Snyder and J.W. Corbett, *Phys. Rev. B*, 45 (1992) 11612.
- [319] S.J. Pearton, A.M. Chantre, L.C. Kimerling and W.C. Dautremont-Smith, *MRS Proc.*, 59 (1986) 457.
- [320] A.M. Chantre, S.J. Pearton, L.C. Kimerling, K.D. Cummings and W.C. Dautremont-Smith, *Appl. Phys. Lett.*, 50 (1987) 513.
- [321] N.M. Johnson and S.K. Hahn, *Appl. Phys. Lett.*, 48 (1986) 709.
- [322] D.I. Bohne, P. Deák and J. Weber, *MRS Proc.*, 262 (1992) 395.
- [323] S.A. McQuaid, R.C. Newman and E.C. Lightowers, *Semicond. Sci. Technol.*, 9 (1994) 1736.
- [324] A.R. Brown, M. Claybourn, R. Murray, P.S. Nandhra, R.C. Newman and J.H. Tucker, *Semicond. Sci. Technol.*, 3 (1988) 591.
- [325] H.J. Stein and S.K. Hahn, *Appl. Phys. Lett.*, 56 (1990) 63.
- [326] M. Stavola, J.R. Patel, L.C. Kimerling and P.E. Freeland, *Appl. Phys. Lett.*, 42 (1983) 73.
- [327] R. Murray, *Physica B*, 170 (1991) 115.
- [328] R.C. Newman and R. Jones, Oxygen in Silicon, *Semiconductors and Semimetals*, Vol. 42, Chapt. 8, 1994, pp. 289–352 (for a more detailed review of the O–H problem).
- [329] E.C. Lightowers, R.C. Newman and J.H. Tucker, *Semicond. Sci. Technol.*, in press.
- [330] H.J. Stein, private communication.
- [331] H.J. Stein and S.K. Hahn, *Electrochem. Soc. Proc.*, 91 (1991) 461.
- [332] H.J. Stein, S.K. Hahn and P.M. Richards, *Mater. Sci. Forum*, 83–87 (1992) 105.
- [333] H.J. Stein and S.K. Hahn, *J. Appl. Phys.*, 77 (1994) 3477.
- [334] B.D. Patterson, A. Bosshard, U. Straumann, P. Truöl, A. Wüest and Th. Wichert, *Phys. Rev. Lett.*, 52 (1984) 938.
- [335] S.K. Estreicher, *Phys. Rev. B*, 41 (1990) 9886.
- [336] R. Jones, S. Öberg and A. Umerski, *Mater. Sci. Forum*, 83–87 (1992) 551.
- [337] G.D. Watkins, M. Kleverman, A. Thilderkvist and H.G. Grimmeiss, *Phys. Rev. Lett.*, 67 (1991) 1149.
- [338] J.R. Davis, Jr., A. Rohatgi, R.H. Hopkins, P.D. Blais, P. Rai-Choudhury, J.R. McCormick and H.C. Mollenkopf, *IEEE Trans. Electron. Dev.*, 27 (1980) 677.
- [339] J.T. Borenstein, J.I. Hanoka, B.R. Bathey, J.P. Kalejs and S. Mil'shtein, *Appl. Phys. Lett.*, 62 (1993) 1615.
- [340] M. Höne, U. Juda, H. Riemann, J.-M. Spaeth and S. Greulich-Weber, *Phys. Rev. B*, 49 (1994) 16999.
- [341] R. Singh, S.J. Fonash and A. Rohatgi, *Appl. Phys. Lett.*, 49 (1986) 800.
- [342] S.J. Pearton and A.J. Tavendale, *Phys. Rev. B*, 26 (1982) 7105.
- [343] S.J. Pearton, *MRS Proc.*, 59 (1986) 457.
- [344] E.Ö. Sveinbjörnsson and O. Engström, *Appl. Phys. Lett.*, 61 (1992) 2323.
- [345] E.Ö. Sveinbjörnsson and O. Engström, *Mater. Sci. Forum*, 143–147 (1994) 821.
- [346] T. Sadoh, M. Watanabe, H. Nakashima and T. Tsurushima, *Mater. Sci. Forum*, 143–147 (1994) 761.
- [347] T. Sadoh, M. Watanabe, H. Nakashima and T. Tsurushima, *J. Appl. Phys.*, 75 (1994) 3978.
- [348] P.M. Williams, G.D. Watkins, S. Uftring and M. Stavola, *Phys. Rev. Lett.*, 70 (1993) 3816.
- [349] P.M. Williams, G.D. Watkins, S. Uftring and M. Stavola, *Mater. Sci. Forum*, 143–147 (1994) 891.
- [350] M. Höne, U. Juda, Yu.V. Martynov, T. Gregorkiewicz, C.A.J. Ammerlaan and L.S. Vlasenko, *Phys. Rev. B*, 49 (1994) 13423.
- [351] F. Beeler, O.K. Anderson and M. Scheffler, *Phys. Rev. B*, 41 (1990) 1603.
- [352] R.N. Hall and J.H. Racette, *J. Appl. Phys.*, 35 (1964) 379.
- [353] R. Keller, M. Deicher, W. Pfeiffer, M. Skudlik, D. Steiner and Th. Wichert, *Phys. Rev. Lett.*, 65 (1990) 2023.
- [354] R. Jones, A. Resende, S. Öberg and P.R. Briddon, to be published.
- [355] S.J. Uftring, M. Stavola, P.M. Williams and G.D. Watkins, *Phys. Rev. B*, in press.
- [356] G.D. Watkins, in S.T. Pantelides (ed.), *Deep Centers in Semiconductors*, Gordon and Breach, New York, 1986.
- [357] G.D. Watkins, in B. Henderson and A.E. Hughes (eds.), *Defects and their Structure in Non-Metallic Solids*, Plenum, New York, 1976.

- [358] G.A. Baraff, E.O. Kane and M. Schlüter, *Phys. Rev. Lett.*, **43** (1979) 956; *Phys. Rev. B*, **21** (1980) 5662.
- [359] R. Virkkunen, M. Alatalo, M.J. Puska and R.N. Nieminen, *Comp. Mater. Sci.*, **1** (1993) 151.
- [360] H.J. Stein, *J. Electron. Mater.*, **4** (1975) 159.
- [361] H.J. Stein, *Phys. Rev. Lett.*, **43** (1979) 1030.
- [362] N.N. Gerasimenko, M. Rolle, L.J. Cheng, Y.H. Lee, J.C. Corelli and J.W. Corbett, *Phys. Status Solidi, (b)*, **90** (1978) 689.
- [363] M. Cardona, *Phys. Status Solidi, (b)*, **118** (1983) 463.
- [364] B. Bech Nielsen and H.G. Grimmeiss, *Phys. Rev. B*, **40** (1989) 12403.
- [365] T.S. Shi, S.N. Sahu, G.S. Oehrlein, A. Hiraki and J.W. Corbett, *Phys. Status Solidi (a)*, **74** (1982) 329.
- [366] G.R. Bai, M.W. Qi, L.M. Xie and T.S. Shi, *Solid State Commun.*, **56** (1985) 277.
- [367] L.M. Xie, M.W. Qi and J.M. Chen, *J. Phys. Condensed Matter*, **3** (1991) 8519.
- [368] V.A. Singh, C. Weigel, J.W. Corbett and L.M. Roth, *Phys. Status Solidi, (b)*, **81** (1977) 637.
- [369] W.E. Pickett, *Phys. Rev. B*, **23** (1981) 6603.
- [370] A.M. Grekhov, V.M. Gun'ko, G.M. Klapchenko and Y.P. Tsyashchenko, *Sov. Phys. Semicond.*, **17** (1983) 1186 (*Fiz. Tekh. Poluprovodn.*, **17** (1983) 652).
- [371] D.P. DiVincenzo, J. Bernholc and H.M. Brodsky, *Phys. Rev. B*, **28** (1983) 3246.
- [372] G.G. DeLeo, W.B. Fowler and G.D. Watkins, *Phys. Rev. B*, **29** (1984) 1819.
- [373] U.V. Frolov and B.N. Mukashev, *Phys. Status Solidi, (b)*, **148** (1988) K105.
- [374] G.R. Bai, J.K. Zhou, J.M. Chen, T.S. Shi, W.M. Qi and L.M. Xie, *Sci. Sin. A*, **31** (1988) 499, 630.
- [375] P. Deák, M. Heinrich, L.C. Snyder and J.W. Corbett, *Mater. Sci. Eng. B*, **4** (1989) 57.
- [376] P. Deák, L.C. Snyder, M. Heinrich, C.R. Ortiz and J.W. Corbett, *Physica B*, **170** (1991) 253.
- [377] C.G. Van de Walle and R.A. Street, *Phys. Rev. B*, **49** (1994) 14766.
- [378] J.M. Baranowski and J. Tatarkiewicz, *Phys. Rev. B*, **35** (1987) 7450.
- [379] S.M. Myers, D.M. Follstaedt, H.J. Stein and W.R. Wampler, *Phys. Rev. B*, **45** (1992) 3914.
- [380] H.J. Stein, S.M. Myers and D.M. Follstaedt, *J. Appl. Phys.*, **73** (1993) 2755.
- [381] S.M. Myers, D.M. Follstaedt, H.J. Stein and W.R. Wampler, *Phys. Rev. B*, **45** (1992) 3914.
- [382] J.W. Corbett, J.L. Lindström and S.J. Pearton, *MRS Proc.*, **104** (1988) 229.
- [383] N.M. Johnson, F.A. Ponce, R.A. Street and R.J. Nemanich, *Phys. Rev. B*, **35** (1987) 4166.
- [384] J.P. Kalejs and S. Rajendran, *Appl. Phys. Lett.*, **55** (1989) 2763.
- [385] A.D. Marwick, G.S. Oehrlein and M. Wittmer, *Appl. Phys. Lett.*, **59** (1991) 198.
- [386] A.D. Marwick, M. Wittmer and G.S. Oehrlein, *Mater. Sci. Forum*, **83-87** (1992) 39.
- [387] M. Stutzmann, W. Beyer, L. Tapfer and C.P. Herrero, *Physica B*, **170** (1991) 240.
- [388] Z.N. Liang, C. Haas and L. Niesen, *Phys. Rev. Lett.*, **72** (1994) 1846.
- [389] J.T. Borenstein, J.W. Corbett and S.J. Pearton, *J. Appl. Phys.*, **73** (1993) 2751.
- [390] L. Korpás, J.W. Corbett and S.K. Estreicher, *Superlatt. Microstruct.*, **10** (1991) 121.
- [391] L. Korpás, J.W. Corbett and S.K. Estreicher, *Phys. Rev. B*, **46** (1992) 12365.
- [392] L. Korpás and S.K. Estreicher, unpublished work.
- [393] N.M. Johnson, C. Herring, C. Doland, J. Walker, G. Anderson and F. Ponce, *Mater. Sci. Forum*, **83-87** (1992) 33.
- [394] K. Srikanth and S. Ashok, *J. Appl. Phys.*, **70** (1991) 4779.
- [395] B.L. Sopori, private communication.
- [396] J.N. Heyman, J.W. Ager III, E.E. Haller, N.M. Johnson, J. Walker and C.M. Doland, *Phys. Rev. B*, **45** (1992) 13363.
- [397] J.B. Boyce, N.M. Johnson, S.E. Ready, J. Walker and G.B. Anderson, *MRS Proc.*, **262** (1992) 401.
- [398] P. Asoka-Kumar, H.J. Stein and K.G. Lynn, *Appl. Phys. Lett.*, **64** (1994) 1684.
- [399] Y. Bar-Yam and J.D. Joannopoulos, *J. Electron. Mater.*, **14a** (1985) 261.
- [400] R. Car, P.J. Kelly, A. Oshiyama and S.T. Pantelides, *J. Electron. Mater.*, **14a** (1985) 269.
- [401] S.B. Zhang and W.B. Jackson, *Phys. Rev. B*, **43** (1991) 12142.
- [402] G.D. Watkins and J.W. Corbett, *Phys. Rev.*, **134** (1964) A1359.
- [403] G.A. Samara, *Phys. Rev. B*, **39** (1989) 12764.
- [404] J.L. Hastings and S.K. Estreicher, to be published.
- [405] S.A. McQuaid, M.J. Binns, R.C. Newman, E.C. Lightowers and J.B. Clegg, *Appl. Phys. Lett.*, **62** (1993) 1612.
- [406] M.J. Binns, S.A. McQuaid, R.C. Newman and E.C. Lightowers, *Semicond. Sci. Technol.*, **8** (1993) 1908.
- [407] M.J. Binns, S.A. McQuaid, R.C. Newman and E.C. Lightowers, *Mater. Sci. Forum*, **143-147** (1994) 861.
- [408] J.M. Kahn, R.E. McMurray, Jr., E.E. Haller and L.M. Falicov, *Phys. Rev. B*, **36** (1987) 8001.
- [409] B. Joós, E.E. Haller and L.M. Falicov, *Phys. Rev. B*, **22** (1980) 832.
- [410] E.E. Haller and L.M. Falicov, *Phys. Rev. Lett.*, **41** (1978) 1192.
- [411] A.J. Tavendale and S.J. Pearton, *J. Appl. Phys.*, **54** (1983) 3213.
- [412] R.E. McMurray, Jr., N.M. Haegel, J.M. Kahn and E.E. Haller, *Solid State Commun.*, **61** (1987) 27.
- [413] J.M. Kahn, L.M. Falicov and E.E. Haller, *Phys. Rev. Lett.*, **57** (1986) 2077.
- [414] E.E. Haller, G.S. Hubbard, W.L. Hansen and A. Seeger, *IOP Conf. Ser.*, **31** (1977) 309.
- [415] L.M. Falicov and E.E. Haller, *Solid State Commun.*, **53** (1985) 1211.

- [416] J. Oliva and L.M. Falicov, *Phys. Rev. B*, **28** (1983) 7366.
- [417] J. Oliva, *Phys. Rev. B*, **29** (1984) 6846.
- [418] J. Broeckx, P. Clauws and J. Vennik, *J. Phys. C*, **13** (1980) L141.
- [419] F.S. Ham, *Phys. Rev. B*, **38** (1988) 5474.
- [420] P. Deák, B. Schröder, A. Annen and A. Scholtz, *Phys. Rev. B*, **48** (1993) 1924.
- [421] J.C. Phillips, *Bonds and Bands in Semiconductors*, Academic, San Diego, CA, 1973.
- [422] V. Higgs and M. Kittler, *Appl. Phys. Lett.*, **65** (1994) 2804.
- [423] G. Ohta, S. Fukatsu, Y. Ebuchi, T. Hattori, N. Usami and Y. Shiraki, *Appl. Phys. Lett.*, **65** (1994) 2975.
- [424] P.R. Briddon and R. Jones, *Phys. Rev. Lett.*, **64** (1990) 2535.
- [425] P.R. Briddon and R. Jones, *Mater. Sci. Forum*, **65-66** (1990) 169.
- [426] P.R. Briddon and R. Jones, *Physica B*, **170** (1991) 413.
- [427] R. Jones and S. Öberg, *Phys. Rev. B*, **44** (1991) 3673.
- [428] R. Jones, J. Goss, C. Ewels and S. Öberg, *Phys. Rev. B*, in press.
- [429] J. Wagner, K.H. Bachem, R. Jones, S. Öberg, B.D. Davidson, R.C. Newman, T.J. Bullough and T.B. Joyce, unpublished work.
- [430] R. Rahbi, B. Theys, R. Jones, B. Pajot, S. Öberg, K. Sommoggi, M.L. Fille and J. Chevallier, in press.
- [431] L. Pavesi and P. Giannozzi, *Phys. Rev. B*, **43** (1991) 2446.
- [432] K.J. Chang, *Solid State Commun.*, **78** (1991) 273.
- [433] A. Amore Bonapasta, *Phys. Rev. B* (1993) 8771.
- [434] A. Amore Bonapasta, *Mater. Sci. Forum*, **143-147** (1994) 235; *Phys. Rev. B*, **51** (1995) 4172.
- [435] B.R. Davidson, R.C. Newman, T.J. Bullough and T.B. Joyce, *Phys. Rev. B*, **48** (1993) 17106.
- [436] P.S. Nandhra, R.C. Newman, R. Murray, B. Pajot, J. Chevallier, R.B. Beall and J.J. Harris, *Semicond. Sci. Technol.*, **3** (1988) 356.
- [437] J. Chevallier, B. Pajot, A. Jalil, R. Mostefaoui, R. Rahbi and M.C. Boissy, *MRS Proc.*, **104** (1988) 337.
- [438] B. Clerjaud, *Physica B*, **170** (1991) 383.
- [439] D.M. Kozuch, M. Stavola, S.J. Pearton, C.R. Abernathy and J. Lopata, *Appl. Phys. Lett.*, **57** (1990) 2561.
- [440] J. Wagner, K.H. Bachem, B.R. Davidson, R.C. Newman, T.J. Bullough and T.B. Joyce, *Phys. Rev. B*, **51** (1995) 4150.
- [441] B. Clerjaud, D. Cote, F. Gendron, W.-S. Hahn, M. Krause, C. Porte and W. Ulrici, *Mater. Sci. Forum*, **83-87** (1992) 563.
- [442] R. Jones, *Phil. Trans. Roy. Soc., London A*, **350** (1995) 189.
- [443] B. Pajot, R.C. Newman, R.C. Murray, A. Jalil, J. Chevallier and R. Azoulay, *Phys. Rev. B*, **37** (1988) 4188.
- [444] A.J. Tavendale, S.J. Pearton, A.A. Williams and D. Alexiev, *Appl. Phys. Lett.*, **56** (1990) 1457.
- [445] N.M. Johnson, C. Herring and D. Bour, *Phys. Rev. B*, **48** (1993) 18308.
- [446] M.H. Yuan, L.P. Wang, S.X. Jin, J.J. Chen and G.G. Qin, *Appl. Phys. Lett.*, **58** (1991) 925.
- [447] A.W.R. Leitch, Th. Prescha and J. Weber, *Phys. Rev. B*, **44** (1991) 1375.
- [448] G. Roos, N.M. Johnson, C. Herring and J.S. Harris, *Appl. Phys. Lett.*, **59** (1991) 461.
- [449] E. Truncel, H. Sigg, E. Meier, L. Pavesi, P. Giannozzi, D. Martin, F. Morier-Genoud and F.K. Reinhart, *Mater. Sci. Forum*, **83-87** (1992) 635.
- [450] R.E. Pritchard, B.R. Davidson, R.C. Newman, T.J. Bullough, T.B. Joyce, R. Jones and S. Öberg, *Semicond. Sci. Technol.*, **9** (1994) 140.
- [451] R.E. Pritchard, R.C. Newman, J. Wagner, F. Fuchs, R. Jones and S. Öberg, *Phys. Rev. B*, **50** (1994) 10628.
- [452] W.-S. Hahn, B. Clerjaud, D. Côte, F. Gendron, C. Porte, W. Ulrici, D. Wasik and W. Wilkening, *Mater. Sci. Forum*, **143-147** (1994) 277.
- [453] Y. Cheng, M. Stavola, C.R. Abernathy, S.J. Pearton and W.S. Hobson, *Phys. Rev. B*, **49** (1994) 2469.
- [454] M.D. McCluskey, E.E. Haller, J. Walker and N.M. Johnson, *Appl. Phys. Lett.*, **65** (1994) 2191.
- [455] W.C. Dautremont-Smith, J. Lopata, S.J. Pearton, L.A. Koszi, M. Stavola and V. Swaminathan, *J. Appl. Phys.*, **66** (1989) 1993.
- [456] S. Balasubramanian, V. Kumar, N. Balasubramanian and V. Premachandran, *Appl. Phys. Lett.*, **64** (1994) 2256.
- [457] R. Darwich, B. Pajot, B. Rose, D. Robein, B. Theys, R. Rahbi, C. Porte and F. Gendron, *Phys. Rev. B*, **48** (1993) 17776.
- [458] V.A. Gorbylev, A.A. Chelnii, A.Y. Polyakov, S.J. Pearton, N.B. Smirnov, R.G. Wilson, A.G. Milnes, A.A. Cnokalin, A.V. Govorkov, B.M. Leiferov, O.M. Borodina and A.A. Balmashnov, *J. Appl. Phys.*, **76** (1994) 7390.
- [459] J.I. Pankove, *MRS Proc.*, **162** (1990) 515.
- [460] M.S. Brandt, N.M. Johnson, R.J. Molnar, R. Singh and T.D. Moustakas, *Appl. Phys. Lett.*, **64** (1994) 2264.
- [461] J.M. Zavada, R.G. Wilson, C.R. Abernathy and S.J. Pearton, *Appl. Phys. Lett.*, **64** (1994) 2724.
- [462] S.J. Pearton, private communication.
- [463] J.A. Van Vechten, J.D. Zook, R.D. Horning and B. Goldenberg, *Jpn. J. Appl. Phys.*, **31** (1992) 3662.
- [464] Y.H. Xie, private communication.
- [465] J. Ren, K.A. Bowers, B. Snead, D.L. Dreifus, J.W. Cook, Jr., J.F. Schetzina and R.M. Kolbas, *Appl. Phys. Lett.*, **57** (1990) 1901.
- [466] C.G. Van de Walle, D.B. Laks, G.F. Neumark and S.T. Pantelides, *Phys. Rev. B*, **47** (1993) 9425.

- [467] C.A. Coronado, E. Ho, P.A. Fisher, J.L. House, K. Lu, G.S. Petrich and L.A. Kolodziejski, *J. Electron. Mater.*, **23** (1994) 269.
- [468] E. Ho, P.A. Fisher, J.L. House, G.S. Petrich, L.A. Kolodziejski, J. Walker and N.M. Johnson, *Appl. Phys. Lett.*, **66** (1995) 1062.
- [469] L.A. Kolodziejski, private communication.
- [470] J. Tatarkiewicz, A. Witowski and E. Jahne, *Phys. Status Solidi, (b)*, **142** (1987) K101.
- [471] J. Tatarkiewicz and A. Witowski, *Phys. Status Solidi, (b)*, **145** (1988) K95.
- [472] J. Tatarkiewicz, A. Breitschwerdt, A. Witowski and H. Hartmann, *Solid State Commun.*, **68** (1988) 1081.
- [473] J. Tatarkiewicz, A. Breitschwerdt and A. Witowski, *Phys. Rev. B*, **39** (1989) 3889.
- [474] P. Sana, A. Rohatgi, J. Kalejs and R.O. Bell, *Appl. Phys. Lett.*, **64** (1994) 97.